NASA CR-182139
GARRETT 21-6689

TRANSITION MIXING STUDY EMPIRICAL MODEL REPORT

by
R. SRINIVASAN
C. WHITE

Garrett Engine Division
Allied-Signal Aerospace Company

February 1988

Prepared for

National Aeronautics and Space Administration
NASA-Lewis Research Center

Contract NAS3-24340

TABLE OF CONTENTS

LIST OF FIGURES

LIST OF FIGURES (Contd)

LIST OF FIGURES (Contd)

LIST OF FIGURES (Contd)

LIST OF FIGURES (Contd)

LIST OF TABLES

TRANSITION MIXING STUDY
EMPIRICAL MODEL REPORT
NASA CONTRACT NO. NAS3-24340

SUMMARY

An existing empirical model for predicting temperature distributions downstream of a row of dilution jets injected into a rectangular duct has been extended to model the effects of curvature associated with transition liners. This extension is based on the results of a 3-D numerical model prediction generated in this contract. The temperature field predicted by the empirical model is presented in this report to show the effects of radius of curvature, inner and outer wall injection for single and opposed rows of jets, flow area convergence, injection position, axial staging, and the relationship among injection into a rectangular duct, an annulus, and a can.

1.0 INTRODUCTION

This report presents the technical efforts performed by Garrett Engine Division (GED)* of Allied-Signal Aerospace Company, a unit of Allied-Signal Inc., under the addendum to TMS Contract No. NAS3-24340. In this task, the empirical model developed during the NASA Dilution Jet Mixing (DJM) Program (Contract NAS3-22110) was extended to include the effects of duct radius of curvature, jet injection location, and can or annular combustor geometries. The modifications to the DJM empirical model were made by using the 3-D numerical model results presented in the TMS Final Report[1] (NASA CR-175062, Garrett 21-5723) as a guide.

1.1 Background

GED had developed an empirical model[2-4] to characterize mixing of single or multiple rows of jets injected into a confined cross flow as a part of the NASA Dilution Jet Mixing (DJM) Program (Contract NAS3-22110). This empirical model, limited to mixing in two-dimensional ducts, was based on extensive experimental data obtained during that program. This empirical model serves as a useful first-order dilution zone design tool. Extension of this model to characterize mixing in curved ducts would greatly widen the model applicability, but would require additional information on temperature and velocity field.

The mixing characteristics of jets with a cross flow in curved ducts have been observed[5,6] to be significantly different from those in rectangular ducts. The 3-D numerical computations performed during the TMS program[1] provided more detailed information on these differences. Although the numerical model results were not validated against experimental data, they showed characteristics observed in References 5 and 6, as well as other test cases where experimental data were available. However, it has been shown[7-10] that the numerical model tends to underestimate mixing, but represents the same qualitative trends observed in several experimental measurements. In the absence of extensive experimental data on mixing in transition liners, the 3-D numerical model results can be used as a guide to extend the DJM empirical model. However, care has to be exercised to use the numerical model results only as a guide to evaluate differences in mixing characteristics between curved and rectangular ducts. Such an effort would significantly extend the applicability of the empirical model to reverse-flow combustion systems.

*Formerly Garrett Turbine Engine Company

References appear after Section 4.0
Nomenclature appears after the References

1.2 Objective

The objective of the addendum task to the TMS program is to extend the DJM empirical model to include the following effects on jet mixing:

- Duct radius of curvature
- Inner and outer wall injections
- Single or multiple rows of jets
- Can and annular geometries.

The 3-D TMS numerical model results are to be used as a guide in modifying the empirical model. Details of the modified empirical model are presented in Section 2.0. The empirical model results and its comparison with the numerical model results are presented in Section 3.0. Finally, Section 4.0 provides the conclusions and recommendations.

2.0 EMPIRICAL MODEL DESCRIPTION

The trend toward increased power density in small gas turbines has required these combustion systems to operate at higher temperature levels. Operation at elevated temperatures demands that a higher percentage of air be used to cool hot-section components. Thus, the amount of dilution air available to tailor the combustor exit profile quality is reduced. This situation is more stringent in reverse-flow combustors (which are commonly used in small gas turbines) because of their larger surface area that needs to be cooled. To control the combustor exit temperature profile quality, cost-effective design methods that accurately characterize the exit temperature distribution, in terms of geometric and flow variables upstream, are needed.

Empirical models currently available in literature[2,3,4,11] that are applicable to combustor dilution zones are limited to rectangular ducts without turn sections. The results reported in References 1, 5, and 6 show that the radius of curvature in turn sections has a significant influence on jet penetration and mixing characteristics. In the present program, the NASA/Garrett empirical models developed in References 2, 3, and 4 are modified and extended to be applicable to jet mixing turn sections as well as to annular and can combustors. Detailed description of the TMS empirical model is presented in paragraphs 2.1 and 2.2. The details of the basic empirical model are presented in paragraph 2.1, and the modifications made in this program to extend the model applicability are described in paragraph 2.2.

2.1 NASA/Garrett Empirical Model

The empirical model developed in this program uses the same nomenclature used in References 2, 3, 4, and 11. This nomenclature also applies to single-sided, opposed, or double rows of jets injected into a turn section. The empirical models available in literature are based on experimental data, which are limited to jet configurations in a rectangular duct.

The temperature field in the flow field is described in a nondimensionalized form by:

$$\Theta = \frac{T_m - T}{T_m - T_j} \qquad (1)$$

where:

Θ = Theta, nondimensional temperature difference at a point in the flow field

T_m = Mainstream stagnation temperature

T_j = Jet stagnation temperature

T = Stagnation temperature at a point in the flow field.

Theta is a measure of the temperature suppression in the flow field. The value of theta can vary from one (when measured temperature equals the jet temperature) to zero (when the measured temperature equals the mainstream temperature). The largest values of theta in any profile correspond to the coolest regions of the flow.

If complete mixing of the jet and mainstream flow occurs, the value of theta will be constant and the temperature will everywhere be equal to the ideal equilbrium temperature between jet and mainstream. Thus,

$$\Theta_{EB} = \frac{T_m - T_{EB}}{T_m - T_j} \tag{2}$$

where:

Θ_{EB} is the ideal equilibrium theta.

$$T_{EB} = \frac{\dot{m}_{j_T} T_{j_T} + \dot{m}_{j_B} T_{j_B} + \dot{m}_m T_m}{\dot{m}_{j_T} + \dot{m}_{j_B} + \dot{m}_m} \tag{3}$$

Here, the subscripts T, B, and m represent the top, bottom, and mainstream flows for opposed injections. A similar expression is also valid for single or multiple rows of jets.

The mixing characteristics for opposed injections are similar to those with single-sided injections, with the duct height reduced to an equilvalent height, H_{eq}. For the top row of jets, the equivalent duct height has been obtained by Wittig[12] as

$$(H_{eq})_T = \frac{A_T \sqrt{J_T}}{A_T \sqrt{J_T} + A_B \sqrt{J_B}} \cdot H_0 \tag{4}$$

where:

H_0 = Duct height at the jet injection plane

A_T = Effective area of the top injections

and A_B = Effective area of the bottom injections.

$$(H_{eq})_B = H_0 - (H_{eq})_T \tag{5}$$

The theta distribution in the duct is then defined by

$$\theta = \theta_T \text{ for } 0 \leq Y/H \leq \frac{(H_{eq})_T}{(H_0)} \tag{6}$$

$$\theta = \theta_B \text{ for } \frac{(H_{eq})_T}{H_0} \leq \frac{Y}{H} \leq 1.0 \tag{7}$$

where θ_T and θ_B are the theta distributions in the top and the bottom parts of the duct, which are calculated by the empirical model for the 3-D temperature distribution. These are expressed in nondimensionalized self-similar form as:

$$\theta = \theta^{\pm}_{min} + (\theta_c - \theta^{\pm}_{min}) \exp\left[(-\ln 2)\left(\frac{Y - Y_c}{W^{\pm}_{1/2}}\right)^2\right] \tag{8}$$

This expression is applicable to both top and bottom injections. In this equation, θ_c, $\theta^{\pm}_{min}$, Y_c, and $W^{\pm}_{1/2}$ are scaling parameters as shown in Figure 2-1. θ_c is the maximum temperature difference ratio in the radial (vertical) profile, and Y_c is its location. Y_c represents the position of the jet centerline. Here, θ^{+}_{min} and θ^{-}_{min} are the minimum dimensionless temperature difference beyond and before the jet centerline, respectively.

Since the flow is confined, the entrainment characteristics of the jets are not necessarily symmetrical about the jet centerlines. Thus, the half widths $W^{+}_{1/2}$ and $W^{-}_{1/2}$ are different for top and bottom injections. But, for the temperature profile to be continuous,

$$\left(\theta^{+}_{min}\right)_T = \left(\theta^{+}_{min}\right)_B \tag{9}$$

The correlations describe the scaling parameters as functions of independent variables J, S/D, H_{eq}/D, X/H_{eq}, and Z/S. The scaling parameters are nondimensionalized by using the equivalent duct height (H_{eq}).

Jet Thermal Centerline Trajectory

$$Y_c/H_{eq} = (a_1)(0.3575)(J)^{0.25}(S/D)^{0.14}(H_{eq}/D)^{-0.45} \times (C_d)^{0.155}(X/H_{eq})^{0.17}[\exp(-b)] \tag{10}$$

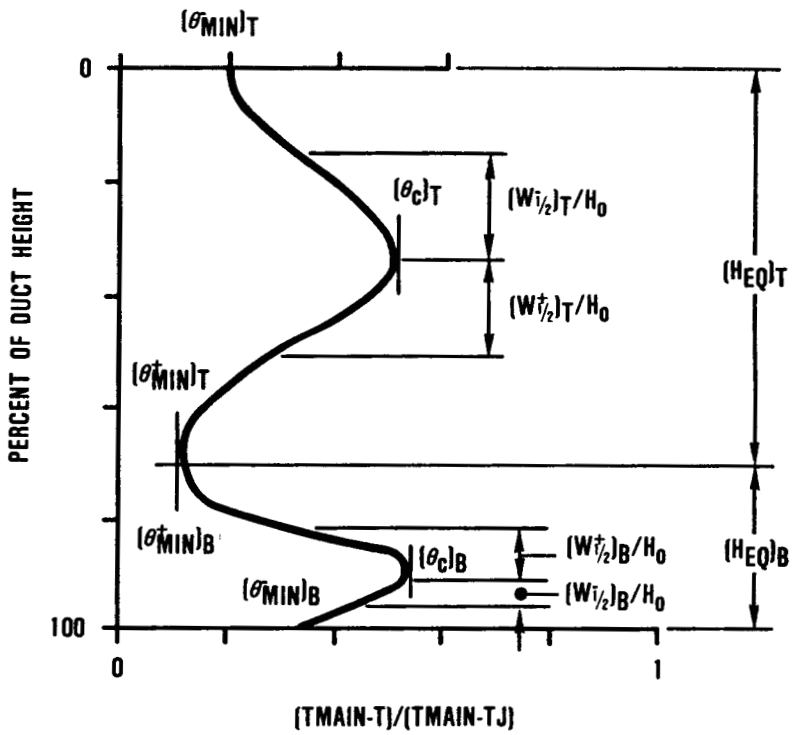

Figure 2-1. Schematic of Typical Radial Temperature Profile.

where:

$$a_1 = \min[1+S/H_{eq}),2]$$

$$b = (0.091)(X/H_{eq})^2[(H_{eq}/S)-(J^{0.5})/3.5)]$$

Centerplane Maximum Temperature Difference Ratio

$$\theta_c = \theta_{EB} + (1 - \theta_{EB})[(a_1)(J)^{-0.35}(C_d)^{0.5}(H_{eq}/D)^{-1} \times (X/H_{eq})^{-1}]^f \quad (11)$$

where:

$$f = 1.15[(S/H_{eq})/(1 + S/H_{eq})]^{0.5}$$

$$\theta_{EB} = W_j/W_T$$

Centerplane Minimum Temperature Difference Ratios

Opposite side of centerline

$$(\theta^+_{min})/(\theta_c) = 1 - \exp(-c^+) \quad (12)$$

where:

$$c^+ = (a_3)(0.038)(J)^{1.62}(S/D)^{1.5}(H_{eq}/D)^{-2.57} \times (C_d)^{0.535}(X/H_{eq})^{1.1} \quad (13)$$

$a_3 = 1$ if $(Y_c/H_{eq} + W^+_{1/2}/H_{eq}) \leq 1$

$a_3 = (H_0/H_{eq})^{3.67}$ if $(Y_c/H_{eq} + W^+_{1/2}/H_{eq}) > 1$

Injection side of centerline

$$(\theta^-_{min})/(\theta_c) = 1 - \exp(-c^-) \quad (14)$$

where:

$$c^- = (Q)\ a_4\ (J)^{-0.3}(S/D)^{-1.4}(H_{eq}/D)^{0.9} \times (C_d)^{0.25}(X/H_{eq})^{0.9} \quad (15)$$

$a_4 = 1.57$

$Q = 1$ if $(Y_c/H_{eq} + W^+_{1/2}/H_{eq}) \leq 1$, or $R_{ci}/H_{eq} < \infty$

$Q = \exp[(0.22)(X/H_{eq})^2((J^{0.5})/5-S/H_{eq})]$

if $(Y_c/H_{eq} + W^+_{1/2}/H_{eq}) > 1$, and $R_{ci}/H_{eq} = \infty$

Centerplane Half-Widths

Opposite side of centerline

$$(W_{1/2}^{+})/H_{eq} = a_5\,(J)^{0.18}(S/D)^{-0.25}(H_0/H_{eq})^{0.5} \times (C_d)^{0.125}(X/H_{eq})^{0.5} \quad (16)$$

$$a_5 = 0.1623$$

Injection side of centerline

$$(W_{1/2}^{-})/H_{eq} = a_6\,(J)^{0.15}(S/D)^{0.27}(H_{eq}/D)^{-0.38} \times (H_0/H_{eq})^{0.5}(C_d)^{0.055}(X/H_{eq})^{0.12} \quad (17)$$

$$a_6 = 0.2$$

Off-Centerplane Thermal Trajectory

$$Y_{c,z}/Y_c = 1 - (4)(Z/S)^2[\exp(-g)] \quad (18)$$

where:

$$g = (0.227)(J)^{0.67}(S/D)^{-1}(H_{eq}/D)^{0.54}(C_d)^{0.23} \times (X/H_{eq})^{0.54} \quad (19)$$

Off-Centerplane Maximum Temperature Difference Ratio

$$\theta_{c,z}/\theta_c = 1 - (4)(Z/S)^2\exp(-d) \quad (20)$$

where:

$$d = (0.452)(J)^{0.53}(S/D)^{-1.53}(H_{eq}/D)^{0.83}(C_d)^{0.35} \times (X/H_{eq})^{0.83} \quad (21)$$

Off-Centerplane Minimum Temperature Difference Ratios

$$\theta_{min,z}^{\pm}/\theta_{c,z} = \theta_{min}^{\pm}/\theta_c \quad (22)$$

Off-Centerplane Half-Widths

$$W_{1/2,z}^{\pm}/H_{eq} = W_{1/2}^{\pm}/H_{eq} \quad (23)$$

The six scaling parameters, Y_c/H_{eq}, θ_c, θ^+_{min}, θ^-_{min}, $W^+_{1/2}/H_{eq}$, and $W^-_{1/2}/H_{eq}$, are used in Equation 8 to define the vertical profile at any x,z location in the flow. For all except the case of opposed rows of jets with centerlines in-line, H_{eq} in the correlation equations is equal to H_0, the height of the duct at the injection location.

Double (Axially Staged) Rows of Jets and Opposed Rows of Jets with Centerlines Staggered

It was shown in Reference 4 that these flows can be satisfactorily modeled by superimposing independent calculations of the separate elements. This is accomplished as follows:

$$\theta = \frac{T_m - T}{T_m - \overline{T}_j} = \left(\frac{\frac{1}{2}\dot{m}_m + \dot{m}_{j_T}}{\dot{m}_m + \dot{m}_{j_T} + \dot{m}_{j_B}} \right) \theta_T + \left(\frac{\frac{1}{2}\dot{m}_m + \dot{m}_{j_B}}{\dot{m}_m + \dot{m}_{j_T} + \dot{m}_{j_B}} \right) \theta_B \qquad (24)$$

Here, the subscript T represents the top row or the lead row of axially staged jets, the subscript B represents the bottom row or the trailing row of the axially staged jets, and the subscript m represents the mainstream flow.

$$\theta_T = \frac{T_m - T_T}{T_m - T_j}, \qquad \theta_B = \frac{T_m - T_B}{T_m - T_j}$$

These two quantities are computed from equation (8) by using the appropriate equilibrium temperatures as shown here:

$$\left(T_{EB}\right)_T = \left(\frac{\frac{1}{2}\dot{m}_m T_m + \dot{m}_{j_T} T_{j_T}}{\frac{1}{2}\dot{m}_m + \dot{m}_{j_T}} \right)$$

$$\left(T_{EB}\right)_B = \left(\frac{\frac{1}{2}\dot{m}_m T_m + \dot{m}_{j_B} T_{j_B}}{\frac{1}{2}\dot{m}_m + \dot{m}_{j_B}} \right)$$

From the definition given in Equation (2), use the appropriate θ_{EB} value in Equation (11).

Flow Area Convergence

This case is modeled by assuming that the accelerating mainstream will act to decrease the effective momentum flux ratio as the flow proceeds downstream; thus,

$$J(x) = (J)[H(x)/H_0]^2 \qquad (25)$$

The trajectory and the jet half-widths are calculated in terms of the duct height at the injection location and so must be scaled by the inverse of the convergence rate, $H_0/H(x)$, to give profiles in terms of the local duct height.

Nonuniform Mainstream Temperature Profiles

The NASA/Garrett empirical model described in this Paragraph was derived for a uniform flow area and a uniform mainstream condition. When a nonuniform mainstream temperature profile exists, the NASA/Garrett model for theta, θ_{NG}, can be assumed to represent the changes in the local mainstream temperature distribution by dilution jets. In other words,

$$\theta_{NG} = (T_m(y) - T) \; / \; (T_m(y) - T_j) \qquad (26)$$

Here, θ_{NG} represents the results from Equation 8.

For flows with nonuniform profiled mainstream, the ratio of actual temperature change to the maximum possible temperature change due to the jets is obtained from the following definition of nondimensionalized temperature difference ratio:

$$\theta = (T_{max} - T) \; / \; (T_{max} - T_j) \qquad (27)$$

where:

T_{max} = Maximum stagnation temperature of the undisturbed mainstream profile

T = Local stagnation temperature

T_j = Jet stagnation temperature.

Using Equation 27, the profiled mainstream theta, $\theta_m(y)$, can be defined as

$$\theta_m(y) = [T_{max} - T_m(y)] \; / \; (T_{max} - T_j) \qquad (28)$$

From Equations 26, 27, and 28, it is seen that

$$\theta = \theta_m(y) + [1 - \theta_m(y)] \; \theta_{NG} \qquad (29)$$

2.2 TMS Empirical Model

In this program, the NASA/Garrett empirical model described in paragraph 2.1 was extended to include the effects of radius of curvature and injection from inner or outer walls of a turn section. The extended model is also applicable to annular or can combustor geometries.

Effects Due to Curvature

The flow in a curved duct develops a free vortex structure caused by flow turning. In such a structure, the local mainstream velocity, V_m, can be expressed in the form $V_m = C/r$, where $C = 2\bar{U}_m/(r_o + r_i)$, and $\bar{U}_m$ is the average velocity in the duct at the jet injection plane. Here, r_i and r_o are the radius of curvature of the inner and the outer walls, respectively. The free vortex structure results in higher mainstream velocity near the inner wall than near the outer wall. The momentum flux ratio, J, of a jet injected into a curved duct becomes

$$J = \frac{\rho_j V_j^2}{\rho_m \bar{U}_m^2} \cdot \frac{4r^2}{(r_i + r_o)^2} \tag{30}$$

From this equation, the effective momentum flux ratio of the outer wall injection, J_{OD}, is defined as the integrated value of Equation 30 over the upper half of the duct. Similarly, the effective momentum flux ratio of the inner wall, J_{ID}, is defined as the integrated value over the lower half of the duct. These effective momentum flux ratios are:

$$J_{OD} = J_o [1 + 2 C_{OD} + 4 (C_{OD})^2]/3 \tag{31}$$

$$J_{ID} = J_o [1 + 2 C_{ID} + 4 (C_{ID})^2]/3 \tag{32}$$

where:

$$C_{OD} = (1 + H_0/RCI)/(2 + H_0/RCI) \tag{33}$$

$$C_{ID} = 1/(2 + H_0/RCI) \tag{34}$$

$$J_o = (\rho_j V_j^2)/(\rho_m \bar{U}_m^2)$$

Here, H_0 is the duct height at the jet injection location and RCI is the inner wall radius of curvature as shown in Figure 3-1. The derivation of Equations 30 and 31 is shown in Appendix I.

By using the effective momentum flux ratios in the NASA/Garrett empirical model described in paragraph 2.1, good agreement with the 3-D numerical model results were obtained for outer wall (OD) injec-

tions. The 3-D numerical model results showed consistently different mixing characteristics for the inner wall (ID) injections from those predicted for OD injections. The empirical model needed the following additional modifications to exhibit mixing characteristics similar to those observed in the 3-D numerical model predictions.

$$\frac{\bar{\theta}_{min}}{\theta_{c,o}} = 1 - e^{-c^-} \tag{35}$$

where:

$$c^- = Q\ a_4\ J^{-0.3}(S/D)^{-1.4}(H_{eq}/D)^{0.9}C_d^{0.25}(x/H_{eq})^{0.9} \tag{36}$$

and

$a_4 = 1.57$ if $R_{ci}/H_{eq} = \infty$ (straight duct)

$= 3.93$ if $R_{ci}/H_{eq} = <\infty$ (curved duct)

$Q = 1$ if $[(y_c/H_{eq})+(W^+_{1/2}/H_{eq}] \leq 1$ or $R_{ci}/H_{eq}<\infty$

$= \exp\{0.22\ (x/H_{eq})^2[(\sqrt{J}/5)-(S/H_{eq})]\}$

if $[(y_c/H_{eq})+(W^+_{1/2}/H_{eq})]>1$ and $R_{ci}/H_{eq} = \infty$

Centerplane Half-Widths

$$W^+_{1/2}/H_{eq} = a_5\ J^{0.18}(S/D)^{-0.25}(H_0/H_{eq})^{0.5}C_d^{0.125}(x/H_{eq})^{0.5} \tag{37}$$

where

$a_5 = 0.1623$ if $R_{ci}/H_{eq} = \infty$ (straight duct)

$= 0.3$ if $R_{ci}/H_{eq}<\infty$ (curved duct)

$$W^-_{1/2}/H_{eq} = a_6\ J^{0.15}(S/D)^{0.27}(H_{eq}/D)^{-0.38}(H_0/H_{eq})^{0.5} \times C_d^{0.055}(x/H_{eq})^{0.12} \tag{38}$$

where

$a_6 = 0.20$ if $R_{ci}/H_{eq} = \infty$ (straight duct)

$= 0.5$ if $R_{ci}/H_{eq}<\infty$ (curved duct)

For opposed in-line injections, the equivalent duct height was obtained from:

$$(H_{eq})_{OD} = H_0 \, A_{OD} \sqrt{J_{OD}} / (A_{OD} \sqrt{J_{OD}} + A_{ID} \sqrt{J_{ID}}) \qquad (39)$$

where:

H_0 = Channel height at injection plane

A_{OD} = Geometric area of OD jets

A_{ID} = Geometric area of ID jets

J_{OD} and J_{ID} are the effective momentum flux ratios for OD and ID jets, respectively (Equations 31 and 32).

These modifications in the NASA/Garrett empirical model resulted in improved agreement with the 3-D numerical model predictions.

For all the TMS test cases, the empirical model shows trends similar to the 3-D numerical model results, but with higher mixing rates. In the NASA Dilution Jet Mixing Program[13], it was demonstrated that the 3-D numerical model consistently underestimates mixing, compared to measurements. Therefore, the empirical model results are expected to be accurate as a design tool. An assessment of the empirical model results, in comparison with those of the 3-D numerical model, is presented in paragraph 3.0.

3.0 EMPIRICAL MODEL ASSESSMENT

The empirical model is assessed by comparing the predicted distribution of a nondimensional temperature field with the 3-D numerical model results. The temperature distributions are presented for each case in the form of contours along the axial and cross-stream planes. The model assessment is presented in this report on the basis of the effects of the following parameters on the thermal mixing:

- o Duct radius of curvature
- o Jet injection side (OD versus ID)
- o Opposed injection
- o Flow area convergence
- o Injection position
- o Axially staged injection
- o Non-uniform profiled mainstream
- o Can, channel, and annular geometries.

There are no directly comparable experimental data available for the geometries considered in this report. However, the empirical model results have been assessed against measurements obtained for jet mixing in rectangular ducts and the corresponding 3-D numerical model results in Reference 13. The basic geometry of the transition liner used is shown in Figure 3-1*. Table 3-1 provides the values of each of the parameters considered. These are also cases for which 3-D numerical model results were reported in Reference 1. The empirical model results are presented for all the cases except test cases 6, 14, 36, 38, and 39. The empirical model results for θ are presented for these cases in Figures 3-2 through 3-38. Most of the test cases evaluated in this program have rectangular cross sections, as shown in Figure 3-2a. For test cases with nonrectangular cross sections, the appropriate geometries are presented in the centerplane plots.

The empirical model results are presented only for nondimensionalized temperature difference, theta. To provide clarity in plotting the theta contours, some assumptions are made on the theta distribution. Upstream of the jet leading edge, theta values were set equal to zero and at the orifice centerline, the theta value was set equal to 1. The contour plotting software was used to blend the interpolated countour values. Furthermore, the accuracy of the empirical model is questionable in regions less than $X/H_0 = 0.25$. Therefore, it is recommended that the contour values in the regions upstream of $X/H_0 = 0.25$ should be used with caution.

3.1 Effects of Duct Radius of Curvature

Table 3-2 lists the relevant test cases with the corresponding configurations and figure numbers. The first comparison consists of

*Figures are at the end of this section.

Table 3-1. Numerical Experiment Test Cases.

PARAMETER	DESCRIPTION	UNITS	CASE 1	CASE 2	CASE 3	CASE 4	CASE 5	CASE 6	CASE 7	CASE 8
Rci/H0	Curvature Ratio	---	0.5	0.25	0.5	0.5	0.5	0.5	0.5	0.5
AR	Ref. Area Ratio	---	1	1	1	1	3	3 (Cir)	1	3
J	Mom. Flux Ratio	---	26.4	26.4	26.4	26.4	26.4	26.4	6.6	6.6
D/H0	Jet Dia. Ratio	---	0.25	0.25	0.125	0.125	0.25	0.25	0.25	0.25
S/H0	Spacing Ratio	---	0.5	0.5	0.5	0.5	0.5	0.5	0.5	0.5
Iside	Injection Side	---	OD	OD	OD	ID	OD	OD	OD	OD
Type	Injection Type	---	Single	Single	Single	Single	Single	Single	Single	Single
Tprof	Inlet Profile	---	Uniform	Uniform	Uniform	Uniform	Uniform	Uniform	Uniform	Uniform
Rt	Liner Radius	Meters	Inf.	Inf.	Inf.	Inf.	Inf.	0.2821	Inf.	Inf.
Phi	Inj. Position	Deg's	0	0	0	0	0	0	0	0
H0	Duct Height	Meters	0.1016	0.1016	0.1016	0.1016	0.1016	0.1016	0.1016	0.1016

PARAMETER	DESCRIPTION	UNITS	CASE 9	CASE 10	CASE 11	CASE 12	CASE 13	CASE 14	CASE 15	CASE 16
Rci/H0	Curvature Ratio	---	0.5	0.5	0.5	Inf	0.5	0.5	0.5	0.5
AR	Ref. Area Ratio	---	1	1	3	1	1	1	1	1
J	Mom. Flux Ratio	---	26.4	6.6	6.6	26.4	26.4	---	6.6	6.6
D/H0	Jet Dia. Ratio	---	0.25	0.25	0.25	0.25	0.25	---	0.25	0.25
S/H0	Spacing Ratio	---	0.5	0.5	0.5	0.5	0.5	---	0.5	0.5
Iside	Injection Side	---	ID	OD/ID	OD/ID	OD	OD	---	ID	OD
Type	Injection Type	---	Single	Opposed	Opposed	Single	Single	---	Single	Single
Tprof	Inlet Profile	---	Uniform	Uniform	Uniform	Uniform	Uniform	OD Peak.	Uniform	OD Peak.
Rt	Liner Radius	Meters	Inf.	Inf.	Inf.	Inf.	Inf.	Inf.	Inf.	Inf.
Phi	Inj. Position	Deg's	0	0	0	---	20	---	0	0
H0	Duct Height	Meters	0.1016	0.1016	0.1016	0.1016	0.1016	0.1016	0.1016	0.1016

PARAMETER	DESCRIPTION	UNITS	CASE 17	CASE 18	CASE 19	CASE 20	CASE 21	CASE 22	CASE 23	CASE 24
Rci/H0	Curvature Ratio	---	0.5	0.5	0.5	0.5	Inf	Inf	Inf	0.5
AR	Ref. Area Ratio	---	1	1	1	1	1	1	1	1
J	Mom. Flux Ratio	---	26.4	26.4	26.4	105.6	6.6	26.4	26.4	26.4
D/H0	Jet Dia. Ratio	---	0.1768	0.25	0.125	0.125	0.25	0.1768	0.125	0.125
S/H0	Spacing Ratio	---	0.5	1	0.25	0.5	0.5*	0.3535*	0.25*	0.5
Iside	Injection Side	---	OD	OD/ID	OD	ID	OD/ID	OD	OD	ID
Type	Injection Type	---	Double	Staggard	Single	Single	Double	Single	Single	Single
Tprof	Inlet Profile	---	Uniform	Uniform	Uniform	Uniform	Uniform	Uniform	Uniform	Uniform
Rt	Liner Radius	Meters	Inf.	Inf.	Inf.	Inf	0.1016	0.1016	0	Inf.
Phi	Inj. Position	Deg's	0/20	0	0	0	---	---	---	60
H0	Duct Height	Meters	0.1016	0.1016	0.1016	0.1016	0.1016	0.1437	0.2032	0.1016

*Value at the injection wall

Table 3-1. Numerical Experiment Test Cases (Contd).

PARAMETER	DESCRIPTION	UNITS	CASE 25	CASE 26	CASE 27	CASE 28	CASE 29	CASE 30	CASE 31	CASE 32
Rci/H0	Curvature Ratio	---	0.5	0.25	0.25	0.25	0.25	Inf	Inf	0.25
AR	Ref. Area Ratio	---	1	1	1	1	1	1	3	3
J	Mom. Flux Ratio	---	26.4	26.4	6.6	6.6	6.6	6.6	6.6	6.6
D/H0	Jet Dia. Ratio	---	0.1768	0.25	0.25	0.25	0.25	0.25	0.25	0.25
S/H0	Spacing Ratio	---	0.5	0.5	0.5	0.5	0.5	0.5	0.5	0.5
Iside	Injection Side	---	OD	ID	ID	OD	OD/ID	OD/ID	OD/ID	OD
Type	Injection Type	---	Dou/Off	Single	Single	Single	Opposed	Opposed	Opposed	Single
Tprof	Inlet Profile	---	Uniform	Uniform	Uniform	Uniform	Uniform	Uniform	Uniform	Uniform
Rt	Liner Radius	Meters	Inf.	Inf.	Inf.	Inf.	Inf.	Inf.	Inf.	Inf.
Phi	Inj. Position	Deg's	0/20	0	0	0	0	---	---	0
H0	Duct Height	Meters	0.1016	0.1016	0.1016	0.1016	0.1016	0.1016	0.1016	0.1016

PARAMETER	DESCRIPTION	UNITS	CASE 33	CASE 34	CASE 35	CASE 36	CASE 37	CASE 38	CASE 39	CASE 40
Rci/H0	Curvature Ratio	---	0.25	0.25	0.25	0.25	0.5	Inf	Inf	Inf
AR	Ref. Area Ratio	---	3	3	3 (Cir)	3 (Comb)	1	1	1	1
J	Mom. Flux Ratio	---	6.6	6.6	6.6	6.6	26.4	6.6	6.6	26.4
D/H0	Jet Dia. Ratio	---	0.25	0.25	0.25	0.25	0.125	Slot	Slot	0.25
S/H0	Spacing Ratio	---	0.5	0.5	0.5	0.5	0.25	0.5	0.5	1*
Iside	Injection Side	---	OD/ID	ID	OD/ID	OD/ID	OD/ID	OD/ID	OD/ID	OD
Type	Injection Type	---	Opposed	Single	Opposed	Opposed	Opposed	Opp/Align	Opp/Cross	Single
Tprof	Inlet Profile	---	Uniform	Uniform	Uniform	Uniform	Uniform	Uniform	Uniform	Uniform
Rt	Liner Radius	Meters	Inf.	Inf.	0.2208	0.3623	Inf.	Inf	Inf	0
Phi	Inj. Position	Deg's	0	0	0	0	0	---	---	---
H0	Duct Height	Meters	0.1016	0.1016	0.1016	0.1016	0.1016	0.1016	0.1016	0.1016

PARAMETER	DESCRIPTION	UNITS	CASE 41	CASE 42
Rci/H0	Curvature Ratio	---	Inf	Inf
AR	Ref. Area Ratio	---	1	1
J	Mom. Flux Ratio	---	26.4	6.6
D/H0	Jet Dia. Ratio	---	0.25	0.25
S/H0	Spacing Ratio	---	0.707*	0.5
Iside	Injection Side	---	OD	OD
Type	Injection Type	---	Single	Single
Tprof	Inlet Profile	---	Uniform	Uniform
Rt	Liner Radius	Meters	0	Inf.
Phi	Inj. Position	Deg's	---	---
H0	Duct Height	Meters	0.1016	0.1016

*Value at the injection wall

Table 3-2. Test Cases Comparing Curvature Effects.

			Comparison 1			Comparison 2		
PARAMETER	DESCRIPTION	UNITS	CASE 1	CASE 2	CASE 12	CASE 7	CASE 28	CASE 42
Rci/H0	Curvature Ratio	---	0.5	0.25	Inf	0.5	0.25	Inf
AR	Ref. Area Ratio	---	1	1	1	1	1	1
J	Mom. Flux Ratio	---	26.4	26.4	26.4	6.6	6.6	6.6
D/H0	Jet Dia. Ratio	---	0.25	0.25	0.25	0.25	0.25	0.25
S/H0	Spacing Ratio	---	0.5	0.5	0.5	0.5	0.5	0.5
Iside	Injection Side	---	OD	OD	OD	OD	OD	OD
Type	Injection Type	---	Single	Single	Single	Single	Single	Single
Iprof	Inlet Profile	---	Uniform	Uniform	Uniform	Uniform	Uniform	Uniform
Rt	Liner Radius	Meters	Inf.	Inf.	Inf.	Inf.	Inf.	Inf.
Phi	Inj. Position	Deg's	0	0	---	0	0	---
H0	Duct Height	Meters	0.1016	0.1016	0.1016	0.1016	0.1016	0.1016
	Figure Number	---	3-2	3-3	3-12	3-7	3-27	3-38

test cases 1, 2, and 12 at a momentum flux ratio (J) of 26.4. The results are presented in Figures 3-2, 3-3, and 3-13, respectively. Test case 12 represents a straight duct, while cases 1 and 2 represent ducts with nondimensional inner wall radius of curvature (R_{ci}/H_0) of 0.5 and 0.25, respectively. For each of these cases, contour plots of θ are presented in the longitudinal plane along the jet centerline and in the transverse plane at ϕ = 30 degrees into the turn section. For straight duct cases, the transverse plane contours are presented at x/H_0 = 1.0.

The empirical model predicts deeper jet penetration and increased mixing in curved ducts (Figures 3-2 and 3-3), compared to straight ducts (Figure 3-12). Decreasing the curvature ratio (R_{ci}/H_0) from 0.5 to 0.25 results in a slightly higher mixing rate, as seen in Figures 3-2 and 3-3.

The second comparison comprises cases 7, 28, and 42, which show the effects of curvature at a momentum flux ratio (J) of 6.6. The empirical model results for these cases are presented in Figures 3-7, 3-27, and 3-38. These figures also show increased jet penetration in a curved duct, similar to that observed for J = 26.4.

Comparison of the empirical model results and the 3-D numerical model predictions (Reference 1) shows good agreement. The empirical model, however, shows higher mixing than does the 3-D numerical model for all the test cases evaluated. It has been shown (Reference 13) that the numerical model consistently underestimates mixing, compared to measurements. In view of these factors, the empirical model results are expected to be accurate within most engineering design accuracy requirements.

3.2 Effects of OD and ID Injections Into a Curved Duct

The relevant test cases and their defining parameters needed to discuss the effect of outer wall (OD) and inner wall (ID) injections are listed in Table 3-3.

The first two cases (1 and 9) compare the temperature field for a curvature ratio of 0.5 at J = 26.4. Case 1 (Figure 3-2) represents OD injection and case 9 (Figure 3-9) represents ID injection. The jet penetration for OD wall injection is deeper than that for ID injection for the same orifice configuration and momentum flux ratio. This effect is caused by the free vortex structure associated with flow in turn sections. Furthermore, the jet structure, as seen in the transverse plane contour plots, shows significant differences. The OD injection (Figure 3-2b) exhibits the familiar kidney-shaped vortex structure, which is not evident in ID injection (Figure 3-9b). For OD injections, the process of mainstream entrainment by the jets through the pair of shed vortices is augmented by the free vortex structure caused by flow turning. For ID injections, however, the entrainment of mainstream is against the

Table 3-3. Test Cases Comparing OD and ID Injection Effects.

			Comparison 1		Comparison 2		Comparison 3	
PARAMETER	DESCRIPTION	UNITS	CASE 1	CASE 9	CASE 3	CASE 4	CASE 7	CASE 15
Iside	Injection Side	---	OD	ID	OD	ID	OD	ID
Rci/HO	Curvature Ratio	---	0.5	0.5	0.5	0.5	0.5	0.5
AR	Ref. Area Ratio	---	1	1	1	1	1	1
J	Mom. Flux Ratio	---	26.4	26.4	26.4	26.4	6.6	6.6
D/HO	Jet Dia. Ratio	---	0.25	0.25	0.125	0.125	0.25	0.25
S/HO	Spacing Ratio	---	0.5	0.5	0.5	0.5	0.5	0.5
Type	Injection Type	---	Single	Single	Single	Single	Single	Single
Tprof	Inlet Profile	---	Uniform	Uniform	Uniform	Uniform	Uniform	Uniform
Rt	Liner Radius	Meters	Inf.	Inf.	Inf.	Inf.	Inf.	Inf.
Phi	Inj. Position	Deg's	0	0	0	0	0	0
HO	Duct Height	Meters	0.1016	0.1016	0.1016	0.1016	0.1016	0.1016
	Figure Number	---	3-2	3-9	3-4	3-5	3-7	3-14

direction of the free vortex in turn sections. This difference between the two vortex interactions accounts for the jet structural differences between OD and ID injections.

The next two cases, 3 and 4, show similar OD and ID injection comparison for D/H_0 = 0.125 at the same values of R_{ci}/H_0 = 0.5 and J = 26.4. Case 3 (Figure 3-4) represents OD injection, case 4 (Figure 3-5) corresponds to ID injection. These figures also show the reduced jet penetration and mixing for ID injections compared to OD injections. These figures also show the reduction in jet penetration, compared to cases 1 and 9, associated with reduced jet diameter.

The next test cases, 7 and 15, compare OD and ID injections with the same configuration as cases 1 and 9, but at a reduced momentum flux ratio of 6.6. Case 7 (Figure 3-7) represents OD injection; case 15 (Figure 3-14) corresponds to ID injection. At J = 6.6, the OD jets penetrate to approximately 45 percent of duct height at 30 degrees into the turn section (compared to 70 percent at J = 26.4). At the same location, the ID jets penetrate only approximately 30 percent of the duct height at J = 6.6 (compared to 60 percent at J = 26.4). Apart from the differences in the jet penetration, these cases exhibit similar characteristics observed for OD and ID injections.

The next cases, 27 and 28, provide a similar comparison at J = 6.6 for R_{ci}/H_0 = 0.25. Case 27 (Figure 3-26) corresponds to ID injection, while case 28 (Figure 3-27) represents OD injection. Reduced jet penetration and non-kidney-shaped structure for ID jets are also seen in these cases. Similar differences in jet mixing characteristics were observed in the 3-D numerical model predictions reported in Reference 1.

3.3 Effects of Opposed Injection

The relevant cases for discussing the effects of opposed injection in a curved duct are listed in Table 3-4.

The first test case in this table, case 30 (Figure 29), corresponds to opposed injection in a straight duct with J = 6.6, which provides a baseline for comparison. For this case, the opposing jets impinge at the center of the duct, exhibiting identical mixing characteristics.

Test case 10 (Figure 3-10) corresponds to opposed jet injection in a curved duct with R_{ci}/H_0 = 0.5 and J = 6.6. For this case, the OD jets penetrate farther than the ID jets, thus the jet impingement occurs closer to the inner wall. In addition, the difference in the structure of jets for OD and ID injections are also evident. The total jet mass flow rate in this case is the same as that in cases 1 (OD jets) and 9 (ID jets), but the opposed jet configuration results

Table 3-4. Test Cases Comparing Opposed Injection Effects In a Curved Duct.

			Comparison 1				
PARAMETER	DESCRIPTION	UNITS	CASE 30	CASE 10	CASE 29	CASE 37	CASE 18
Iside	Injection Side	---	OD/ID	OD/ID	OD/ID	OD/ID	OD/ID
Rci/H0	Curvature Ratio	---	Inf	0.5	0.25	0.5	0.5
AR	Ref. Area Ratio	---	1	1	1	1	1
J	Mom. Flux Ratio	---	6.6	6.6	6.6	26.4	26.4
S/H0	Spacing Ratio	---	0.5	0.5	0.5	0.25	1.0
D/H0	Jet Dia. Ratio	---	0.25	0.25	0.25	0.125	0.25
Type	Injection Type	---	Opposed	Opposed	Opposed	Opposed	Staggered
Tprof	Inlet Profile	---	Uniform	Uniform	Uniform	Uniform	Uniform
Rt	Liner Radius	Meters	Inf.	Inf.	Inf.	Inf.	Inf.
Phi	Inj. Position	Deg's	---	0	0	0	0
H0	Duct Height	Meters	0.1016	0.1016	0.1016	0.1016	0.1016
	Figure Number	---	3-29	3-10	3-28	3-35	3-17

in enhanced mixing, compared to single-sided injection for the same jet mass flow rate. The same effect was also seen in the 3-D numerical results.

It was concluded in References 11, 14, and 15 that the most significant flow and geometric variables affecting the penetration and mixing of a row of jets injected into a confined cross flow were the jet-to-mainstream momentum flux ratio and the ratio of jet spacing to the height of the duct. That is, the mixing is similar if these parameters are coupled such that:

$$C = (S/H_0) \sqrt{J}$$

It was shown in Reference 16 that optimum mixing was obtained in a rectangular duct for C = 2.5, and that values of C that were a factor of two larger or smaller corresponded to over- and under-penetration.

For opposed jets in a straight duct, optimum mixing was obtained in Reference 16 for C = 1.25. This implies that the equivalent duct height for opposed injection is 0.5 H_0. For opposed jets in a curved duct, the equivalent duct height would be slightly different from 0.5 H_0 because of the curvature effects on jet penetration. However, the optimum value of C for curved ducts is the same as that for straight ducts.

Test Case 29 (Figure 3-28) corresponds to opposed jet injection in a curved duct with R_{ci}/H_0 = 0.25 and J = 6.6. For this case, the drift of the jets toward the inner wall is evident. Comparing this to equivalent single-sided injections, namely, cases 2 (Figure 3-3) and 26 (Figure 3-25) show enhanced mixing with opposed injections.

Test case 37 (Figure 3-35) represents opposed jet injection in a curved duct with R_{ci}/H_0 = 0.5, J = 26.4, and D/H_0 = 0.125. This case has twice as many as jets as test cases 7 (Figure 3-7) and 15 (Figure 3-14), but has half the diameter. These three cases all have the same total jet flow rate. Comparison of theta distributions for these cases clearly shows the enhanced mixing associated with opposed injection.

It was also reported in References 14 and 16 that enhanced mixing was obtained when alternate jets for "optimum" one-side injection were moved to the opposite wall, creating opposed rows of jets with centerlines staggered. The analogous situation in a turning duct is shown in Figure 3-17a for case 18. Figure 3-17a shows theta contours along the plane containing OD jet centerline, and Figure 3-17b shows theta contours along the ID jet centerline. Figure 3-17c shows the theta contours on the transverse plane. The equivalent single-sided injection results are presented in Figure 3-2 (for case 1) and in Figure 3-9 (case 9) for OD and ID injections, respectively.

These contours show that both the OD and ID jets in the opposed row/staggered jets configuration penetrate farther than those in the comparable single-side case, as was also observed in the straight duct case in Reference 16.

3.4 Effects of Convergence

The relevant test cases that show the effects of convergence are listed in Table 3-5. This table includes convergence effects with single-sided injections from OD as well as ID in addition to opposed injection in both rectangular and curved ducts. For these cases, the inlet-to-exit area ratio is maintained at 3.0. For one of these cases, the convergence in turning duct is achieved through reduction in flow passage in the circumferential direction, while a constant channel height is maintained.

The first comparison consists of case 1 (Figure 3-2), with an area ratio (AR) of 1.0, and case 5 (Figure 3-6), with an area ratio of 3.0 for the same orifice geometry and flow conditions.

Test cases 7 (Figure 3-7) and 8 (Figure 3-8) provide a similar comparison at J = 6.6. The reduction in flow area in the turning duct increases the migration of the jets toward the inner wall and causes a small increase in the mixing rate.

Cases 27 (Figure 3-26) and 34 (Figure 3-33) provide a comparison of convergence effects for ID jets with J = 6.6 and R_{ci}/H_0 = 0.25. For these cases, the nondimensional temperature distributions show little difference, which implies negligible effects of convergence for ID injections.

The next set of cases, 29, 33, and 35, show the convergence effects for opposed jet injection. Case 29 (Figure 3-28) corresponds to AR = 1.0; case 33 (Figure 3-32) shows the results for convergence in the radial direction (AR = 3.0), and case 35 (Figure 3-34) shows the results for convergence in the circumferential direction. These figures also show minimal influence of convergence on mixing.

Test cases 30 (Figure 3-29) and 31 (Figure 3-30) show the convergence effects in a rectangular duct. Convergence apparently reduces the gradients in the theta distribution, and the effects are similar to those observed for curved ducts.

3.5 Effects of Jet Injection Position

The relevant test cases that show the effects of injection position are listed in Table 3-6. The first pair of cases compares the effects of change in the injection position from 0 degrees (case 1, Figure 3-2), or the start of the turning section of the duct to 20 degrees into the turning section (case 13, Figure 3-13). The jet

Table 3-5. Test Cases Comparing Convergence Effects.

PARAMETER	DESCRIPTION	UNITS	Comparison 1		Comparison 2		Comparison 3	
			CASE 1	CASE 5	CASE 7	CASE 8	CASE 10	CASE 11
AR	Ref. Area Ratio	---	1	3	1	3	1	3
Rci/H0	Curvature Ratio	---	0.5	0.5	0.5	0.5	0.5	0.5
J	Mom. Flux Ratio	---	26.4	26.4	6.6	6.6	6.6	6.6
D/H0	Jet Dia. Ratio	---	0.25	0.25	0.25	0.25	0.25	0.25
S/H0	Spacing Ratio	---	0.5	0.5	0.5	0.5	0.5	0.5
Iside	Injection Side	---	OD	OD	OD	OD	OD/ID	OD/ID
Type	Injection Type	---	Single	Single	Single	Single	Opposed	Opposed
Tprof	Inlet Profile	---	Uniform	Uniform	Uniform	Uniform	Uniform	Uniform
Rt	Liner Radius	Meters	Inf.	Inf.	Inf.	Inf.	Inf.	Inf.
Phi	Inj. Position	Deg's	0	0	0	0	0	0
H0	Duct Height	Meters	0.1016	0.1016	0.1016	0.1016	0.1016	0.1016
	Figure Number	---	3-2	3-6	3-7	3-8	3-10	3-11

PARAMETER	DESCRIPTION	UNITS	Comparison 4		Comparison 5			Comparison 6	
			CASE 27	CASE 34	CASE 29	CASE 33	CASE 35	CASE 30	CASE 31
AR	Ref. Area Ratio	---	1	3	1	3	3 (Cir)	1	3
Rci/H0	Curvature Ratio	---	0.25	0.25	0.25	0.25	0.25	Inf	Inf
J	Mom. Flux Ratio	---	6.6	6.6	6.6	6.6	6.6	6.6	6.6
D/H0	Jet Dia. Ratio	---	0.25	0.25	0.25	0.25	0.25	0.25	0.25
S/H0	Spacing Ratio	---	0.5	0.5	0.5	0.5	0.5	0.5	0.5
Iside	Injection Side	---	ID	ID	OD/ID	OD/ID	OD/ID	OD/ID	OD/ID
Type	Injection Type	---	Single	Single	Opposed	Opposed	Opposed	Opposed	Opposed
Tprof	Inlet Profile	---	Uniform	Uniform	Uniform	Uniform	Uniform	Uniform	Uniform
Rt	Liner Radius	Meters	Inf.	Inf.	Inf.	Inf.	0.2208	Inf.	Inf.
Phi	Inj. Position	Deg's	0	0	0	0	0	---	---
H0	Duct Height	Meters	0.1016	0.1016	0.1016	0.1016	0.1016	0.1016	0.1016
	Figure Number	---	3-26	3-33	3-28	3-32	3-34	3-29	3-30

Table 3-6. Test Cases Comparing Injection Position Effects.

			Comparison 1		Comparison 2	
PARAMETER	DESCRIPTION	UNITS	CASE 1	CASE 13	CASE 4	CASE 24
Phi	Inj. Position	Deg's	0	20	0	60
Rci/H0	Curvature Ratio	---	0.5	0.5	0.5	0.5
AR	Ref. Area Ratio	---	1	1	1	1
J	Mom. Flux Ratio	---	26.4	26.4	26.4	26.4
D/H0	Jet Dia. Ratio	---	0.25	0.25	0.125	0.125
S/H0	Spacing Ratio	---	0.5	0.5	0.5	0.5
Iside	Injection Side	---	OD	OD	ID	ID
Type	Injection Type	---	Single	Single	Single	Single
Tprof	Inlet Profile	---	Uniform	Uniform	Uniform	Uniform
Rt	Liner Radius	Meters	Inf.	Inf.	Inf.	Inf.
H0	Duct Height	Meters	0.1016	0.1016	0.1016	0.1016
	Figure Number	---	3-2	3-13	3-5	3-23

injection position of 20 degrees also corresponds to the downstream jet location in cases 17 and 25 for a double row of axially staged jets. The results for cases 1 and 13 are similar.

The second pair of cases, 4 (Figure 3-5) and 24 (Figure 3-23), compares the empirical model results for ID injections when the injection position is moved from 0 to 60 degrees in the turn section. The pressure gradient caused by the turn section at the 60 degree position is significantly different from that at the 0 degree position. This causes increased jet spreading for case 24 (Figure 3-23b), compared to case 4 (Figure 3-5b).

3.6 Effects of Axially Staged Injection

The effects of axial staging are presented from the relevant test cases shown in Table 3-7. Case 1 (Figure 3-2) provides a baseline configuration. Test case 17 (Figure 3-17) corresponds to a double row of orifices with $D/H_0 = 0.1768$, with the trailing row positioned at 20 degrees into the turn section. The empirical model predicts increased mixing for this configuration, compared to case 1, even though the jet penetrations are comparable. This is primarily because of the added mixing caused by the wake of the lead row of jets.

In test case 25 (Figure 3-24), the double row of orifices used in case 17 is positioned in a staggered configuration. The contours shown in Figure 3-24a correspond to the results along the lead-row centerplane. Figure 3-24b shows the results along the trailing-row centerplane. These figures show contours similar to those obtained for case 17. However, the transverse plane contours (Figure 3-24c) show a substantially uniform theta distribution in the cross-stream direction. This effect was not predicted by the 3-D numerical model. The results reported in Reference 13 show that the experimental data were in better agreement with the empirical model results than with the 3-D numerical predictions.

3.7 Effects of Mainstream Inlet Temperature Profile

The effect of mainstream inlet temperature profile is seen by comparing the results for the test cases shown in Table 3-8. Case 7 (Figure 3-7) provides the baseline case with a uniform mainstream inlet profile. Case 16 corresponds to single-sided (OD) injection with a non-uniform inlet temperature profile. Figure 3-39 shows the nondimensionalized mainstream inlet temperature profile (an OD peaked temperature profile with peak value at 80 percent of duct height). For this case, the empirical model results were obtained by superimposing the results obtained for case 7 and the inlet theta distribution. Figure 3-15 shows good agreement with the numerical model results reported in Reference 1.

Table 3-7. Test Cases Comparing Axially Staged Injection Effects.

			Comparison 1		
PARAMETER	DESCRIPTION	UNITS	CASE 1	CASE 17	CASE 25
Type	Injection Type	---	Single	Double	Dou/Off
Rci/H0	Curvature Ratio	---	0.5	0.5	0.5
AR	Ref. Area Ratio	---	1	1	1
J	Mom. Flux Ratio	---	26.4	26.4	26.4
D/H0	Jet Dia. Ratio	---	0.25	0.1768	0.1768
S/H0	Spacing Ratio	---	0.5	0.5	0.5
Iside	Injection Side	---	OD	OD	OD
Tprof	Inlet Profile	---	Uniform	Uniform	Uniform
Rt	Liner Radius	Meters	Inf.	Inf.	Inf.
Phi	Inj. Position	Deg's	0	0/20	0/20
H0	Duct Height	Meters	0.1016	0.1016	0.1016
	Figure Number	---	3-2	3-17	3-24

Table 3-8. Test Cases Comparing Mainstream Inlet Profile Effects.

PARAMETER	DESCRIPTION	UNITS	CASE 7	CASE 16
Tprof	Inlet Profile	---	Uniform	OD Peak.
Rci/HO	Curvature Ratio	---	0.5	0.5
AR	Ref. Area Ratio	---	1	1
J	Mom. Flux Ratio	---	6.6	6.6
D/HO	Jet Dia. Ratio	---	0.25	0.25
S/HO	Spacing Ratio	---	0.5	0.5
Iside	Injection Side	---	OD	OD
Type	Injection Type	---	Single	Single
Rt	Liner Radius	Meters	Inf.	Inf.
Phi	Inj. Position	Deg's	0	0
HO	Duct Height	Meters	0.1016	0.1016
	Figure Number	---	3-7	3-15

3.8 Mixing of Jets in a Can, Rectangular, and Annular Duct

Table 3-9 lists the relevent test cases comparing jet mixing in can, rectangular, and annular ducts. The first set of cases are 12, 22, and 23. Case 12 (Figure 3-12) represents single-sided injection into a rectangular duct. Case 22 (Figure 3-21) represents injection into an equivalent-area annular duct using the same orifice configuration. Case 23 (Figure 3-22) corresponds to injection into a straight can having the same volume as the rectangular duct. The jet penetration into an annular duct is comparable to that in a rectangular duct even though S/H_0 values are different. At $x/H_0 = 1$, the jet penetration is approximately 50 percent of the duct height in cases 12 and 22. For the case of injection in a can, however, the jet penetration is about 40 percent of the can radius.

The next pair of cases, 21 and 30, compares the effects of opposed injection into an annulus and an equivalent-area rectangular duct. Figure 3-29 (case 30) shows the empirical model results for injection into a rectangular duct. The jets impinge at mid-channel, followed by enhanced mixing with theta contours similar to those obtained in case 12. The total jet flow rates in cases 30 and 12 are the same.

Figure 3-20 (case 21) shows the results for opposed injection into an annulus. The values of J, S/H_0, and D/H_0, were maintained the same as in Case 30, but the channel height was varied in order to maintain the same flow area. The resulting value of the jet-to-mainstream flow rate ratio for case 21 is 0.3195, compared to 0.3082 for case 30. The jet penetration and mixing for these two cases are comparable. However, the structure of the inner jet into the annulus is different from that in a straight duct because of the inner wall radius effects. This effect was also observed in the 3-D numerical model results.

The last set of cases (12, 40, and 41) shows the equivalency between injection in a rectangular duct and in a can. Case 12 (Figure 3-12) represents a rectangular duct geometry. In case 40, a can with the same spacing ratio and with a radius equal to the duct height in case 12 was used, but the spacing was based on the sector arc length at half the can radius. Case 41 also uses a can of the same radius and spacing, but the spacing was based on the sector arc length at the radius which divided the cross sectional area of the can into two equal parts. Streamwise contours for these cans can be seen in Figures 3-36 and 3-37. The trajectory of the jet in case 41 almost duplicates that of case 12, while case 40 over-penetrates. The equivalency of uses 12 and 41 can also be seen in the cross-stream contours shown in Figures 3-36b and 3-37b.

Table 3-9. Test Cases Comparing Can, Annular/Channel Geometry Effects.

			Comparison 1			Comparison 2		Comparison 3		
PARAMETER	DESCRIPTION	UNITS	CASE 12	CASE 22	CASE 23	CASE 21	CASE 30	CASE 12	CASE 40	CASE 41
Rt	Liner Radius	Meters	Inf.	0.1016	0	0.1016	Inf.	Inf.	0	0
Rci/H0	Curvature Ratio	---	Inf	Inf	Inf	Inf	Inf	Inf	Inf	Inf
AR	Ref. Area Ratio	---	1	1	1	1	1	1	1	1
J	Mom. Flux Ratio	---	26.4	26.4	26.4	6.6	6.6	26.4	26.4	26.4
D/H0	Jet Dia. Ratio	---	0.25	0.1768	0.125	0.25	0.25	0.25	0.25	0.25
S/H0	Spacing Ratio	---	0.5	0.3535	0.25	0.5	0.5	0.5	1	0.707
Iside	Injection Side	---	OD	OD	OD	OD/ID	OD/ID	OD	OD	OD
Type	Injection Type	---	Single	Single	Single	Double	Opposed	Single	Single	Single
Tprof	Inlet Profile	---	Uniform	Uniform	Uniform	Uniform	Uniform	Uniform	Uniform	Uniform
Phi	Inj. Position	Deg's	---	---	---	---	---	---	---	---
H0	Duct Height	Meters	0.1016	0.1437	0.2032	0.1016	0.1016	0.1016	0.1016	0.1016
	Figure Number	---	3-12	3-21	3-22	3-20	3-29	3-12	3-36	3-37

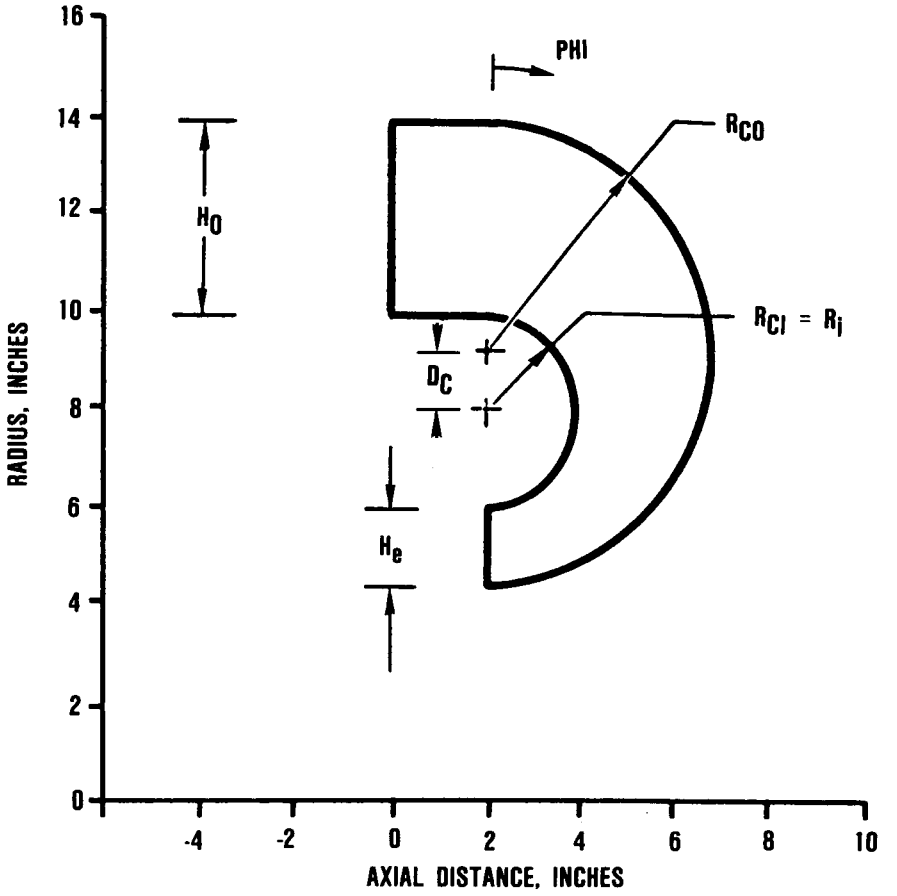

Figure 3-1. Basic Geometry of the Transition Liner.

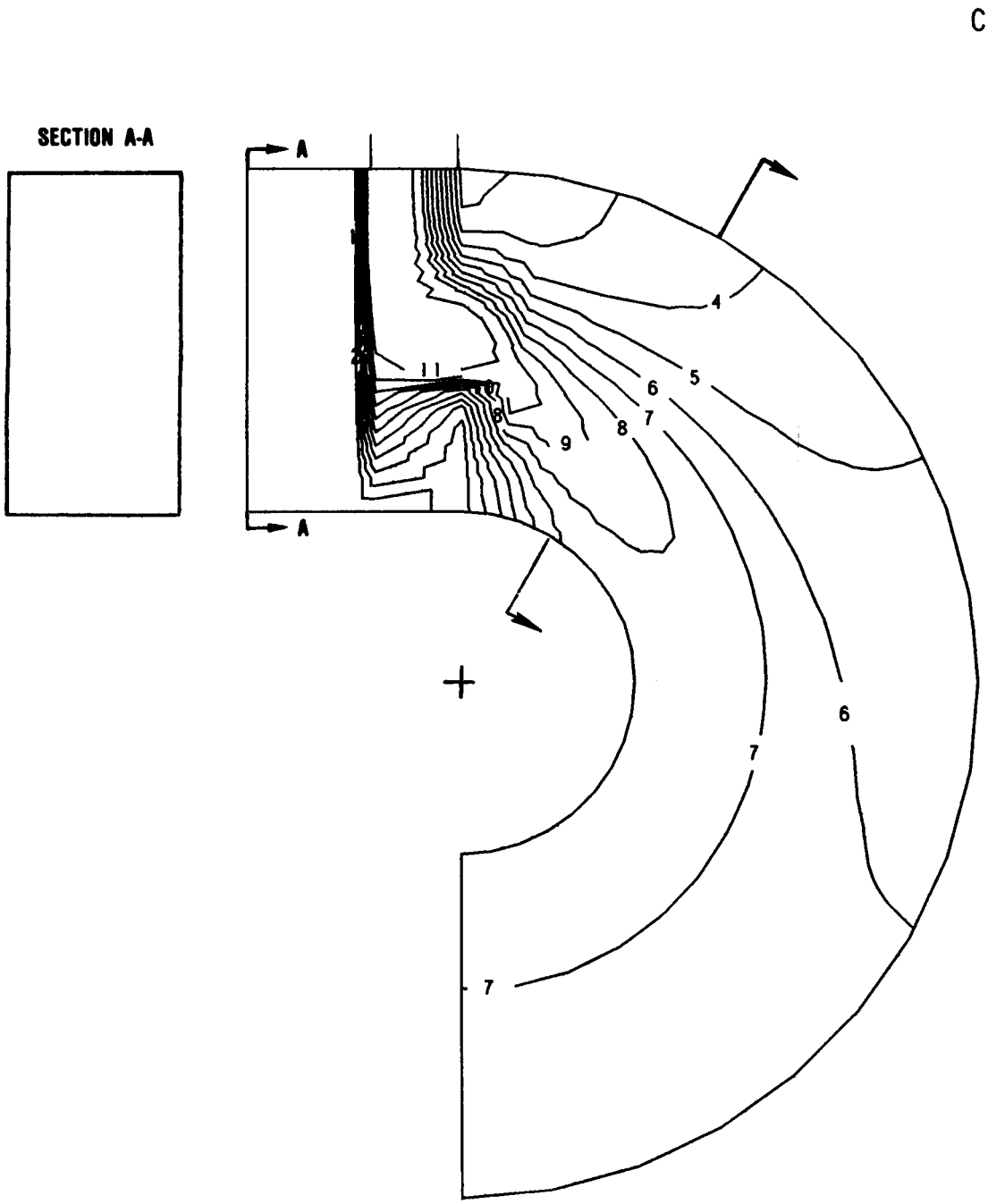

TMS CASE 1 ØD JETS, J=26.7, S/HØ=0.50, D/HØ=.25, RCI/HØ=0.5, AR=1.0

Figure 3-2a. Streamwise Theta Contours for Case 1.

CONTOUR	VALUE
1	0.0500
2	0.1000
3	0.1500
4	0.2000
5	0.2500
6	0.3000
7	0.3500
8	0.4000
9	0.4500
10	0.5000
11	0.6000

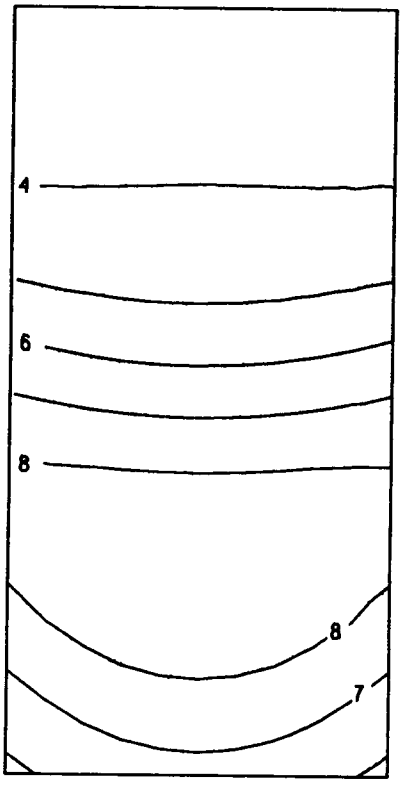

TMS CASE 1 OD JETS, J=26.4, S/HO=.5, RCI/HO=.5, D/HO=.25, AR=1.0

Figure 3-2b. Cross-Stream Theta Contours at Phi = 30 Degrees for Case 1.

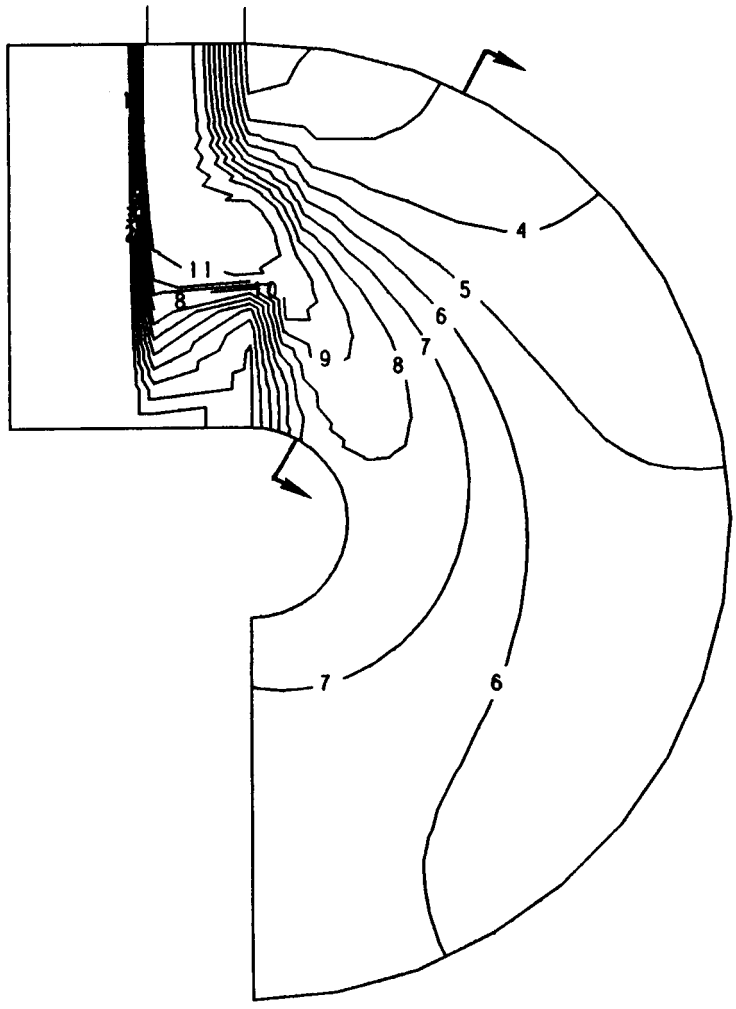

TMS CASE 2 ØD JETS, J=26.7, S/HØ=.50, RCI/HØ=.25, D/HØ=.25, AR=1.0

Figure 3-3a. Streamwise Theta Contours for Case 2.

CONTOUR	VALUE
1	0.0500
2	0.1000
3	0.1500
4	0.2000
5	0.2500
6	0.3000
7	0.3500
8	0.4000
9	0.4500
10	0.5000
11	0.6000

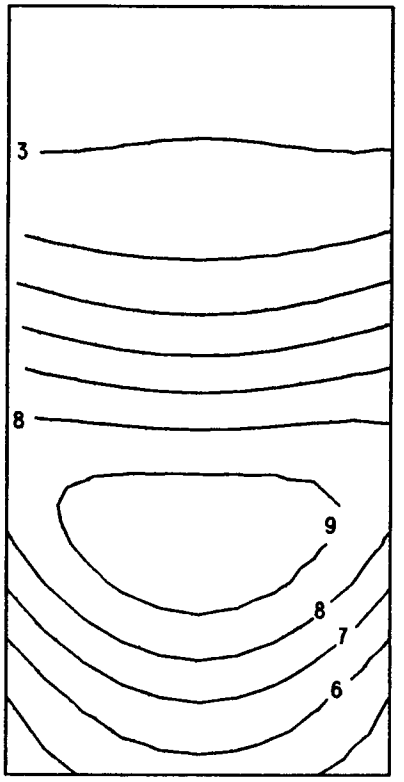

TMS CASE 2-OD JETS, J=26.4, S/HO=0.5, D/HO=0.25, RCI/HO=0.25, AR=1.0

Figure 3-3b. Cross-Stream Theta Contours at Phi = 30 Degrees for Case 2.

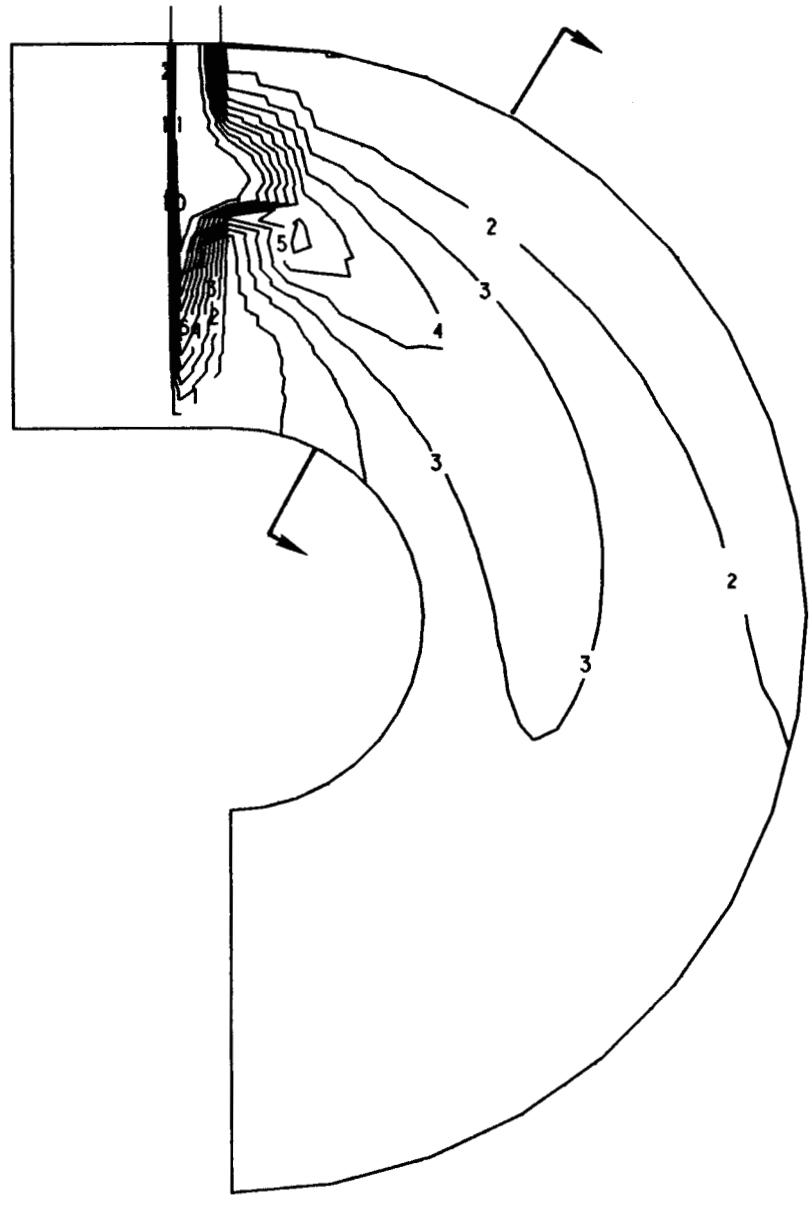

TMS CASE 3-0D JETS, J=26.4, S/H0=0.5, D/H0=0.125, RCI/H0=0.5, AR=1.0

Figure 3-4a. Streamwise Theta Contours for Case 3.

CONTOUR	VALUE
1	0.0500
2	0.1000
3	0.1500
4	0.2000
5	0.2500
6	0.3000
7	0.3500
8	0.4000
9	0.4500
10	0.5000
11	0.6000

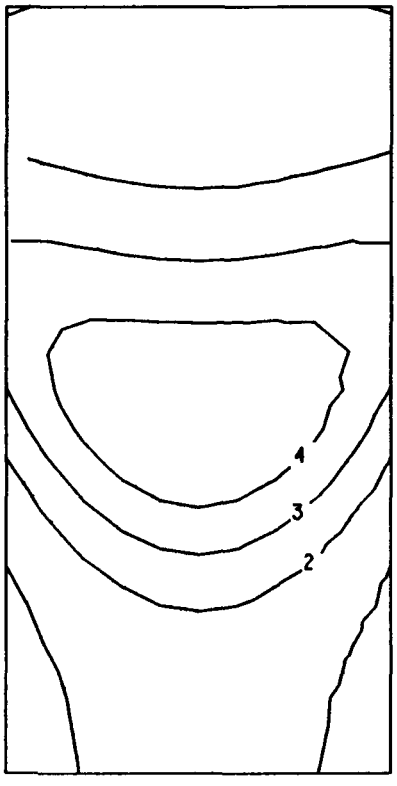

TMS CASE 3-0D JETS, J=26.4, S/H0=0.5, D/H0=0.125, RCI/H0=0.5, AR=1.0

Figure 3-4b. Cross-Stream Theta Contours at Phi = 30 Degrees for Case 3.

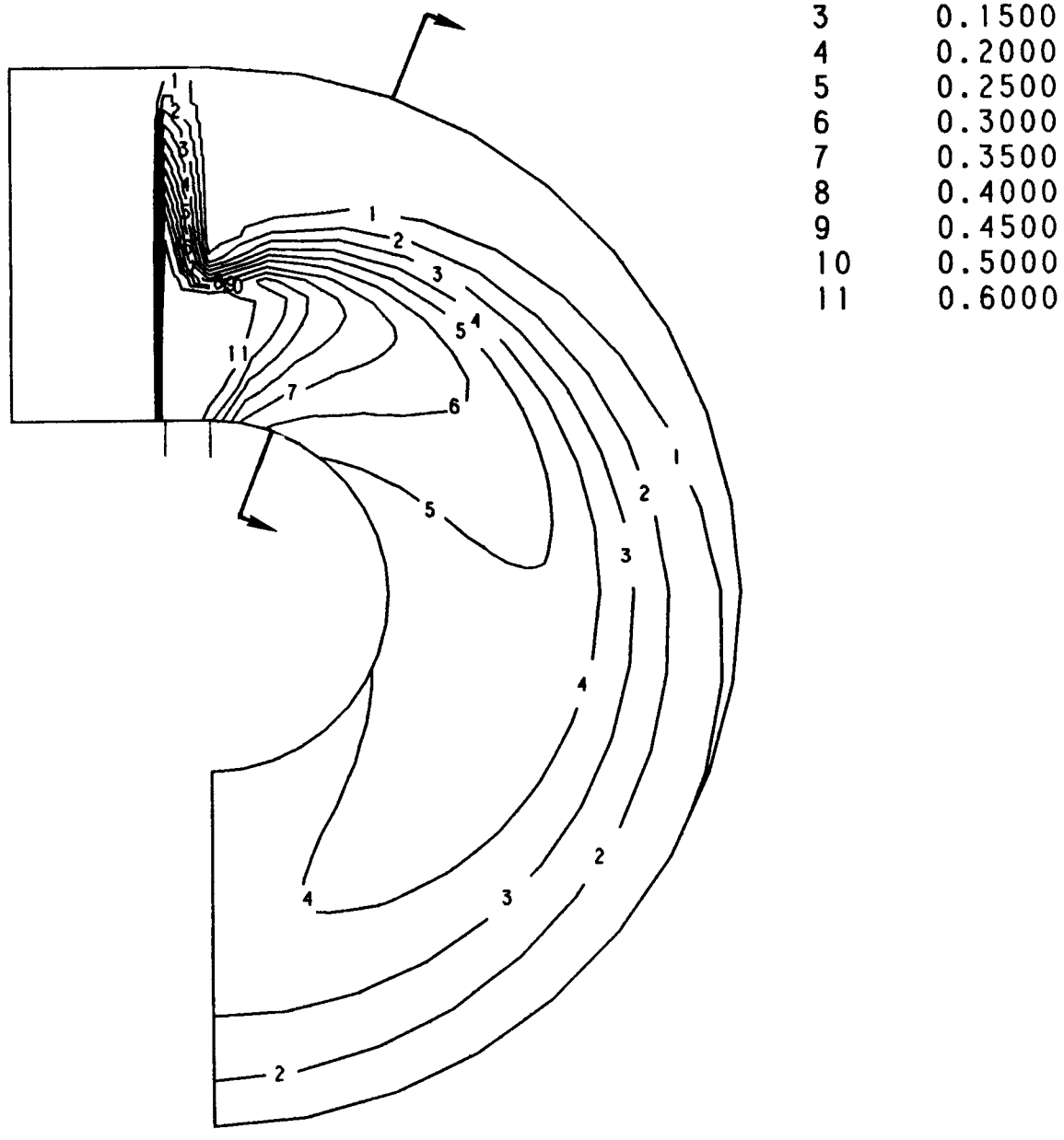

TMS CASE 4-ID JETS, J=26.4, S/HO=0.5, D/HO=0.125, RCI/HO=0.5, AR=1.0

Figure 3-5a. Streamwise Theta Contours for Case 4.

CONTOUR	VALUE
1	0.0500
2	0.1000
3	0.1500
4	0.2000
5	0.2500
6	0.3000
7	0.3500
8	0.4000
9	0.4500
10	0.5000
11	0.6000

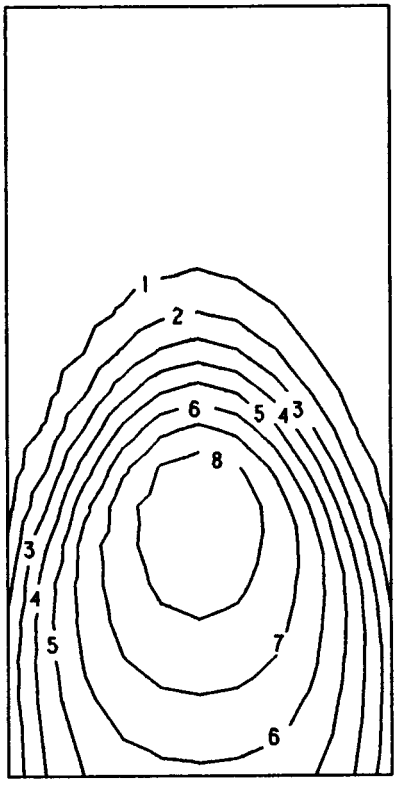

TMS CASE 4-ID JETS, J=26.4, S/H0=0.5, D/H0=0.125, RCI/H0=0.5, AR=1.0

Figure 3-5b. Cross-Stream Theta Contours at Phi = 20 Degrees for Case 4.

CONTOUR	VALUE
1	0.0500
2	0.1000
3	0.1500
4	0.2000
5	0.2500
6	0.3000
7	0.3500
8	0.4000
9	0.4500
10	0.5000
11	0.6000

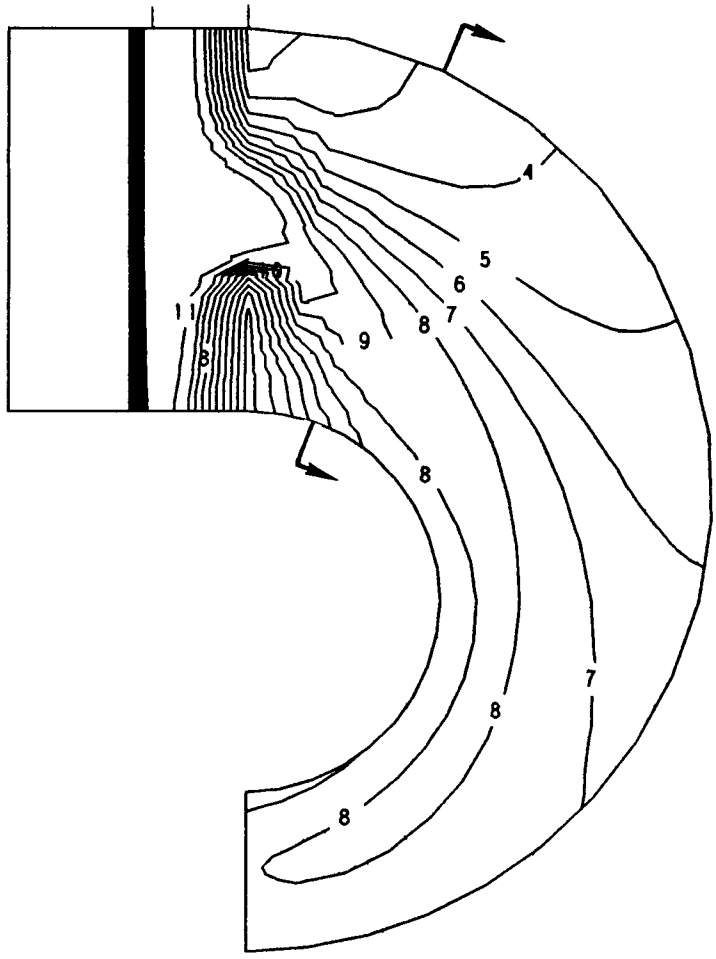

TMS CASE 5-0D JETS, J=26.4, S/H0=0.5, D/H0=0.25, RCI/H0=0.50, AR=3.0

Figure 3-6a. Streamwise Theta Contours for Case 5.

CONTOUR	VALUE
1	0.0500
2	0.1000
3	0.1500
4	0.2000
5	0.2500
6	0.3000
7	0.3500
8	0.4000
9	0.4500
10	0.5000
11	0.6000

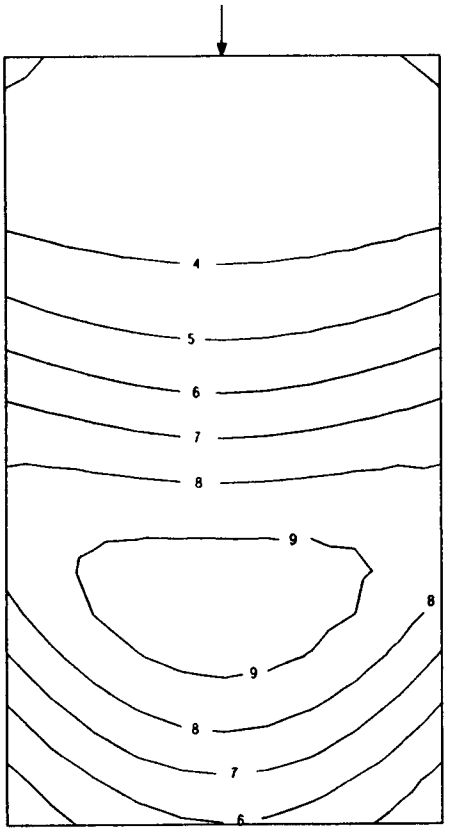

TMS CASE 5-OD JETS, J=26.4, S/HO=0.5, D/HO=0.25, RCI/HO=0.50, AR=3.0

Figure 3-6b. Cross-Stream Theta Contours at Phi = 20 Degrees for Case 5.

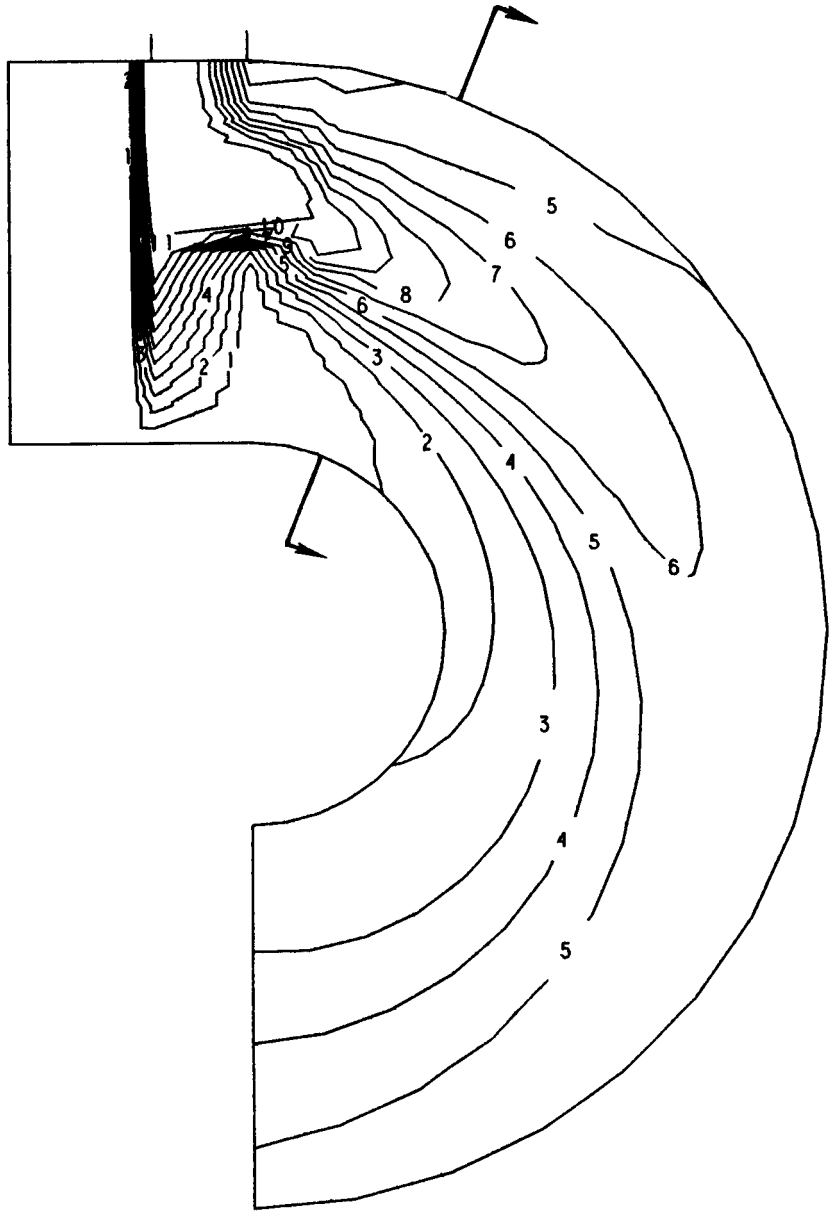

CONTOUR	VALUE
1	0.0500
2	0.1000
3	0.1500
4	0.2000
5	0.2500
6	0.3000
7	0.3500
8	0.4000
9	0.4500
10	0.5000
11	0.6000

TMS CASE 7-0D JETS, J=6.6, S/H0=0.5, D/H0=0.25, RC1/H0=0.50, AR=1.0

Figure 3-7a. Streamwise Theta Contours for Case 7.

CONTOUR	VALUE
1	0.0500
2	0.1000
3	0.1500
4	0.2000
5	0.2500
6	0.3000
7	0.3500
8	0.4000
9	0.4500
10	0.5000
11	0.6000

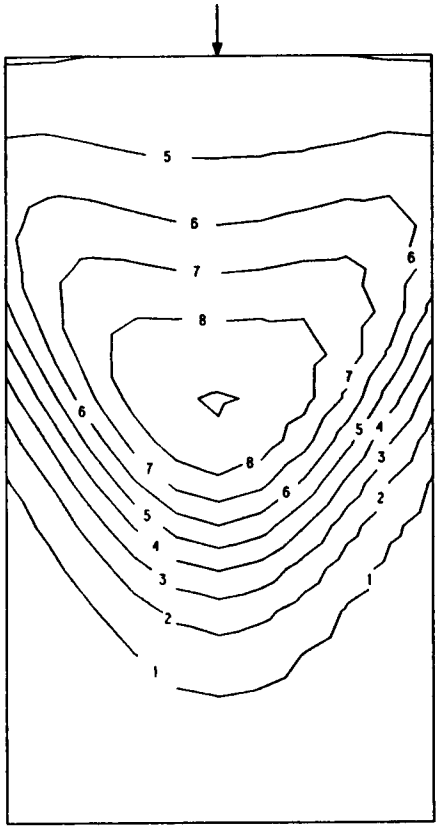

TMS CASE 7-0D JETS, J=6.6, S/H0=0.5, D/H0=0.25, RCI/H0=0.50, AR=1.0

Figure 3-7b. Cross-Stream Theta Contours at Phi = 20 Degrees for Case 7.

CONTOUR	VALUE
1	0.0500
2	0.1000
3	0.1500
4	0.2000
5	0.2500
6	0.3000
7	0.3500
8	0.4000
9	0.4500
10	0.5000
11	0.6000

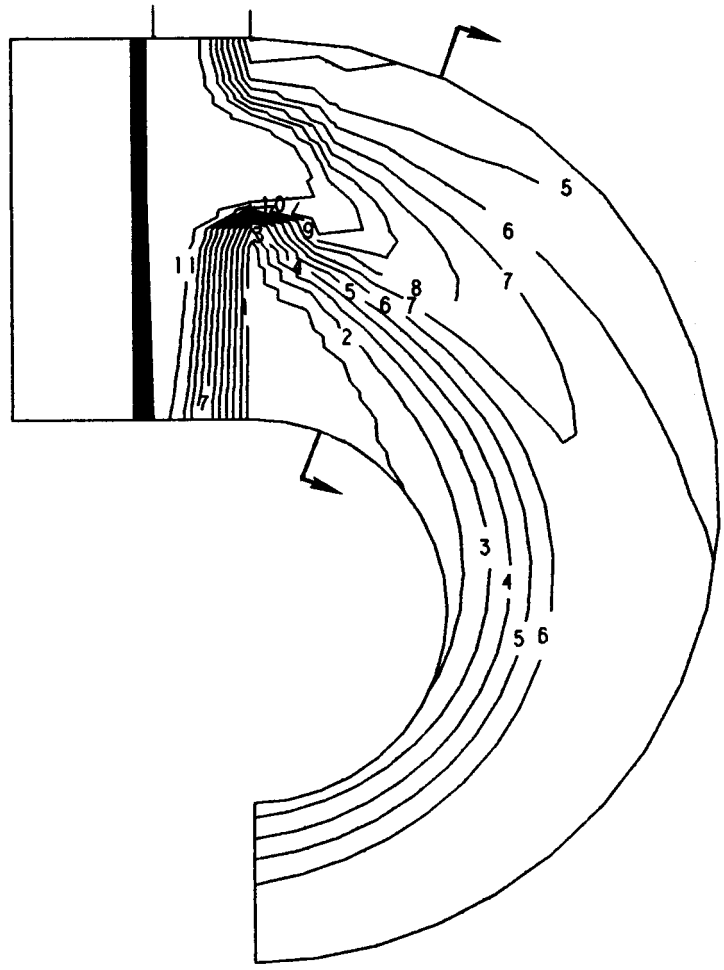

TMS CASE 8-0D JETS, J=6.6, S/H0=0.5, D/H0=0.25, RCI/H0=0.50, AR=3.0

Figure 3-8a. Streamwise Theta Contours for Case 8.

CONTOUR	VALUE
1	0.0500
2	0.1000
3	0.1500
4	0.2000
5	0.2500
6	0.3000
7	0.3500
8	0.4000
9	0.4500
10	0.5000
11	0.6000

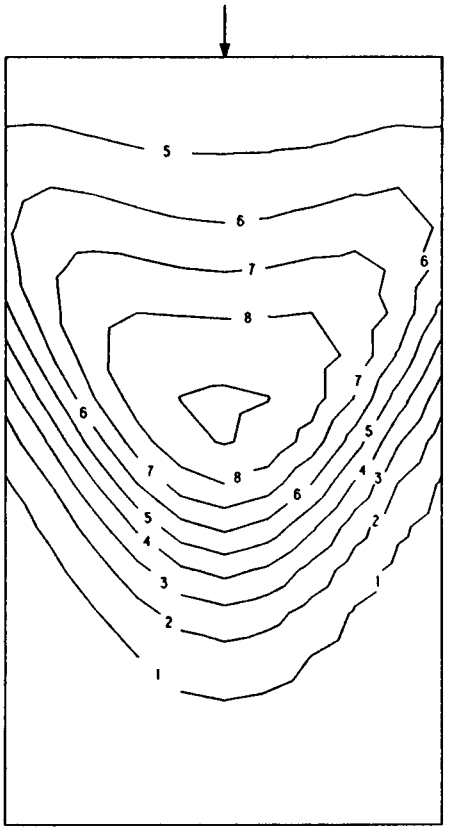

TMS CASE 8-0D JETS, J=6.6, S/H0=0.5, D/H0=0.25, RCI/H0=0.50, AR=3.0

Figure 3-8b. Cross-Stream Theta Contours at Phi = 20 Degrees for Case 8.

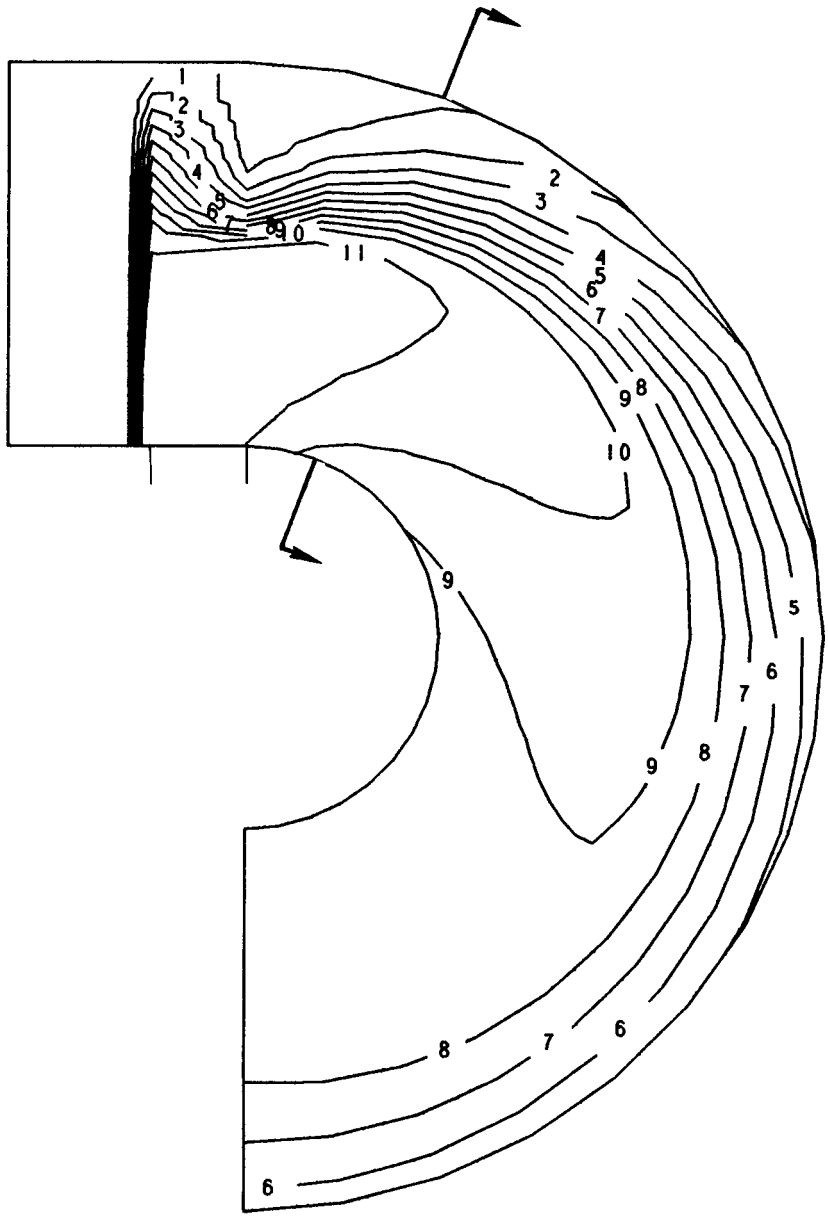

CONTOUR	VALUE
1	0.0500
2	0.1000
3	0.1500
4	0.2000
5	0.2500
6	0.3000
7	0.3500
8	0.4000
9	0.4500
10	0.5000
11	0.6000

TMS CASE 9 ID JETS, J=26.4, S/HO=.50, RCI/HO=.50, D/HO=.25, AR=1.0

Figure 3-9a. Streamwise Theta Contours for Case 9.

CONTOUR	VALUE
1	0.0500
2	0.1000
3	0.1500
4	0.2000
5	0.2500
6	0.3000
7	0.3500
8	0.4000
9	0.4500
10	0.5000
11	0.6000

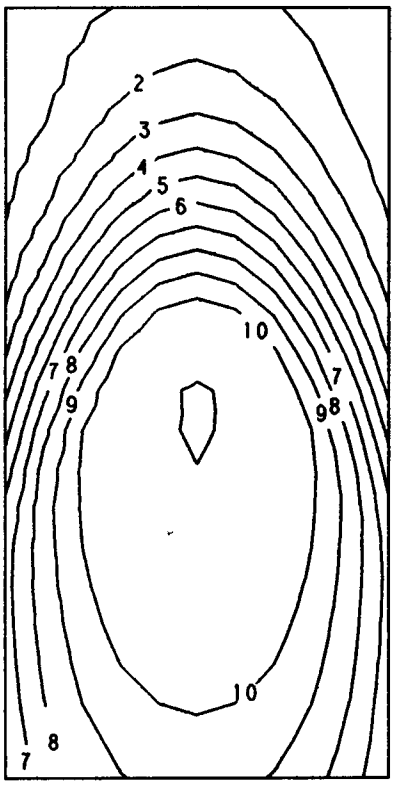

TMS CASE 9 ID JETS, J=26.4, S/H0=.50, RCI/H0=.50, D/H0=.25, AR=1.0

Figure 3-9b. Cross-Stream Theta Contours at Phi = 30 Degrees for Case 9.

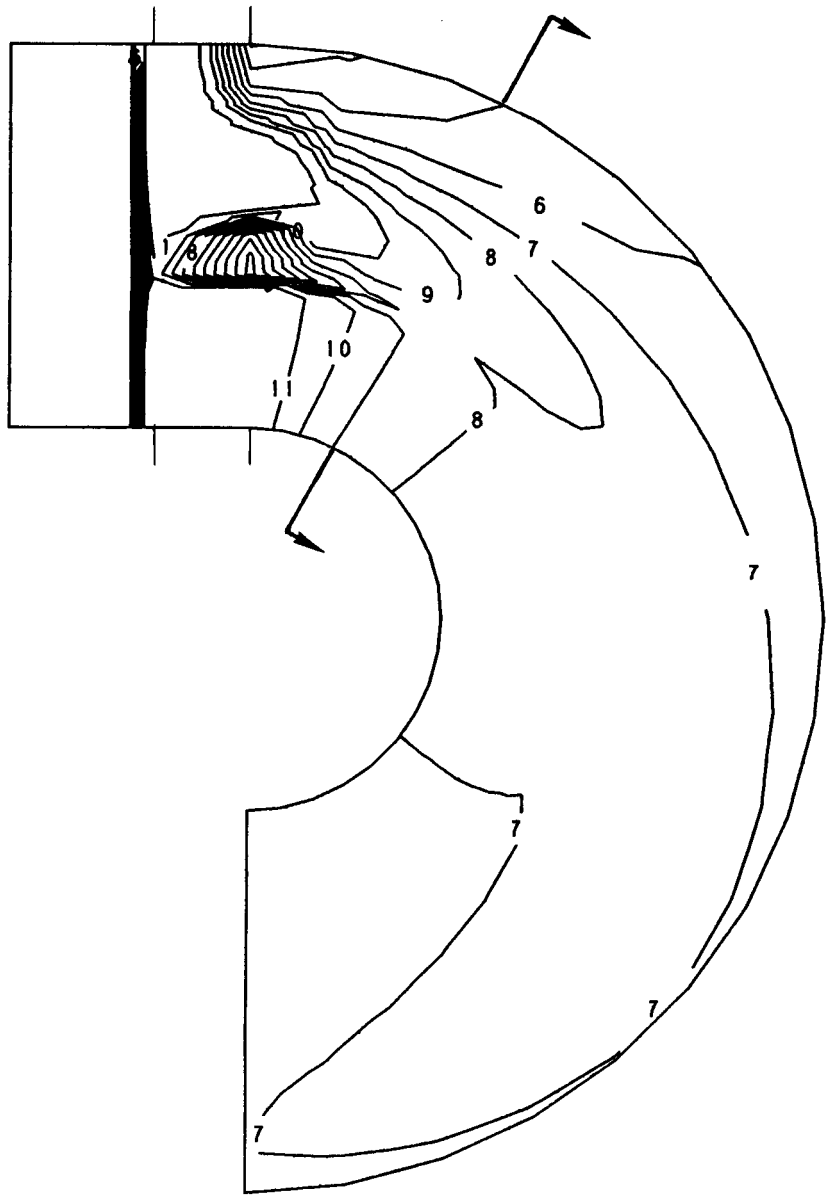

TMS CASE 10-OD/ID JETS (INL), J=6.6, S/HO=.5, RCI/HO=.5, D/HO=.25,AR=1.0

Figure 3-10a. Streamwise Theta Contours for Case 10.

CONTOUR	VALUE
1	0.0500
2	0.1000
3	0.1500
4	0.2000
5	0.2500
6	0.3000
7	0.3500
8	0.4000
9	0.4500
10	0.5000
11	0.6000

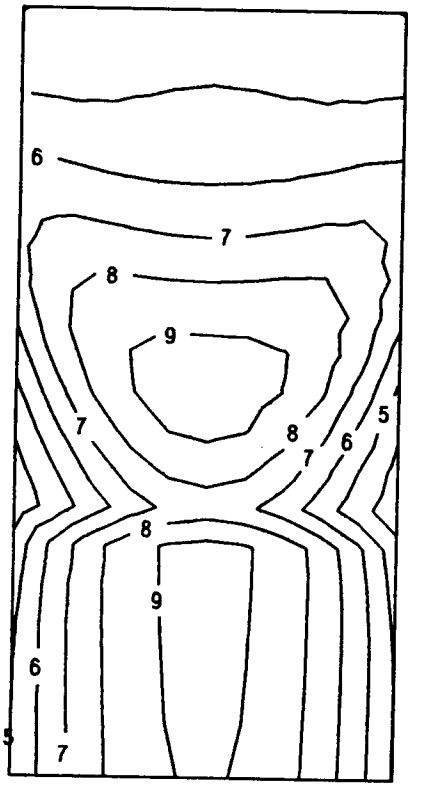

TMS CASE 10-OD/ID JETS (INL), J=6.6, S/HO=.5, RCI/HO=.5, D/HO=.25, AR=1.0

Figure 3-10b. Cross-Stream Theta Contours at Phi = 30 Degrees for Case 10.

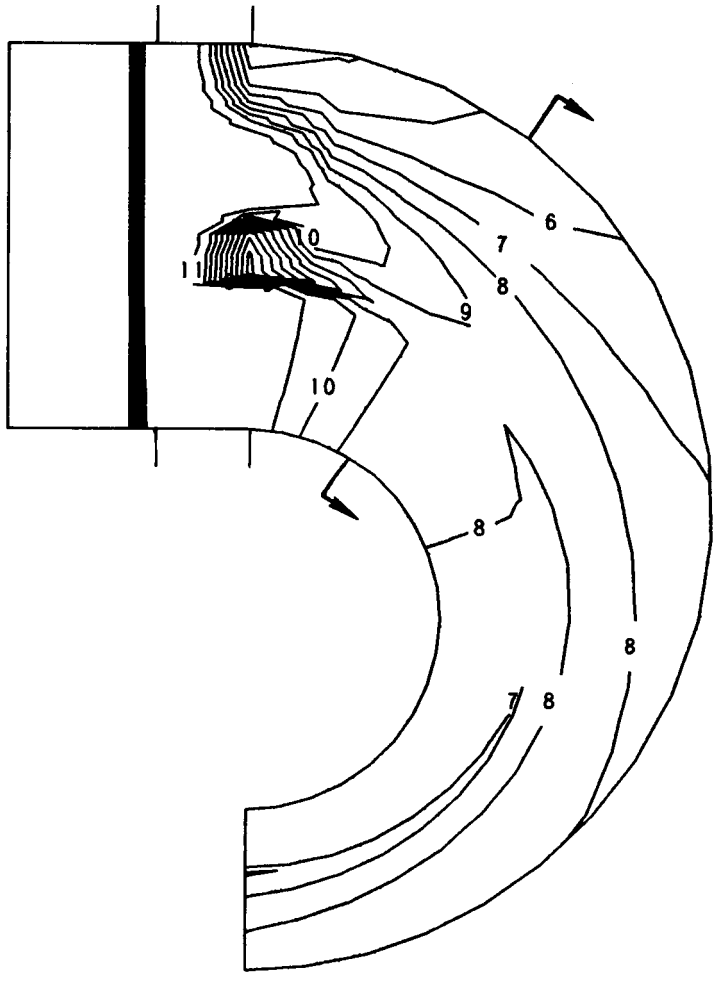

TMS CASE 11-OD/ID JETS (INL), J=6.6, S/HO=.5, RCI/HO=.5, D/HO=.25, AR=3.0

Figure 3-11a. Streamwise Theta Contours for Case 11.

CONTOUR	VALUE
1	0.0500
2	0.1000
3	0.1500
4	0.2000
5	0.2500
6	0.3000
7	0.3500
8	0.4000
9	0.4500
10	0.5000
11	0.6000

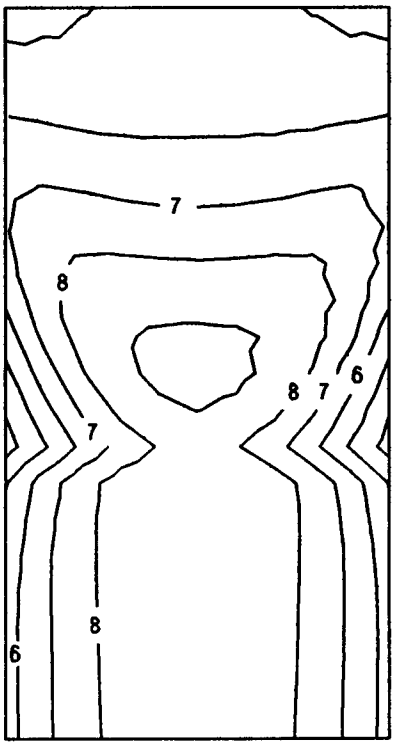

TMS CASE 11-OD/ID JETS(INL), J=6.6, S/HO=.5, D/HO=.25, RCI/HO=.5, AR=3.0

Figure 3-11b. Cross-Stream Theta Contours at Phi = 30 Degrees for Case 11.

CONTOUR	VALUE
1	0.0500
2	0.1000
3	0.1500
4	0.2000
5	0.2500
6	0.3000
7	0.3500
8	0.4000
9	0.4500
10	0.5000
11	0.6000

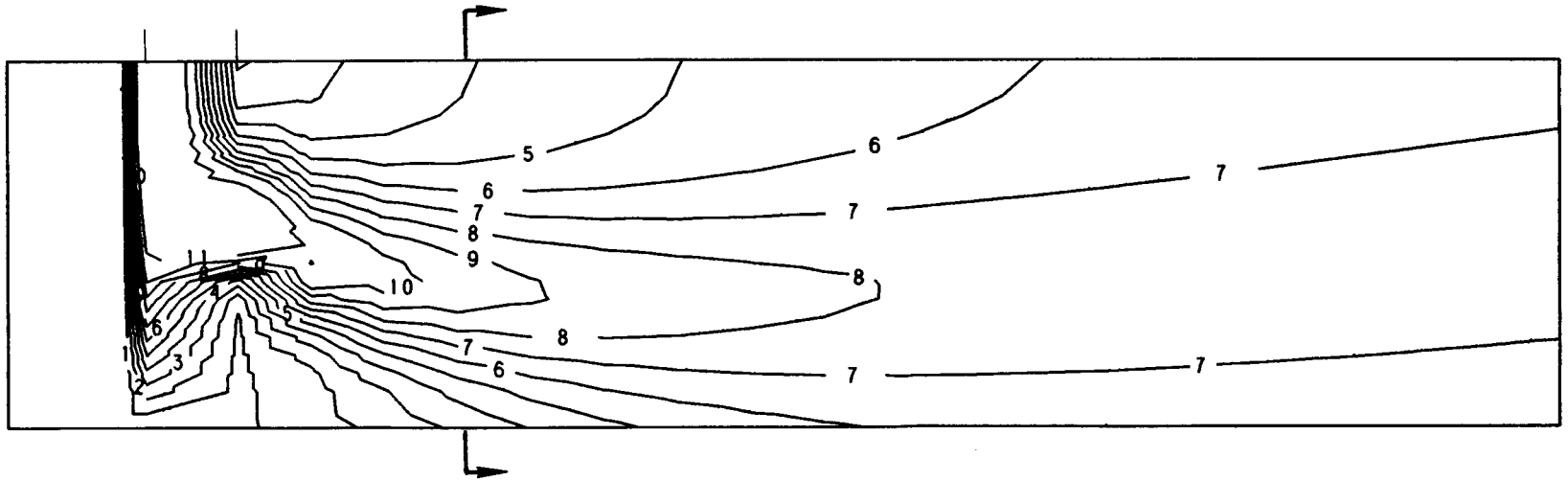

TMS CASE 12-0D JETS (STRAIGHT DUCT), J=26.4, S/H0=0.50, D/H0=.25, AR=1.0

Figure 3-12a. Streamwise Theta Contours for Case 12.

CONTOUR	VALUE
1	0.0500
2	0.1000
3	0.1500
4	0.2000
5	0.2500
6	0.3000
7	0.3500
8	0.4000
9	0.4500
10	0.5000
11	0.6000

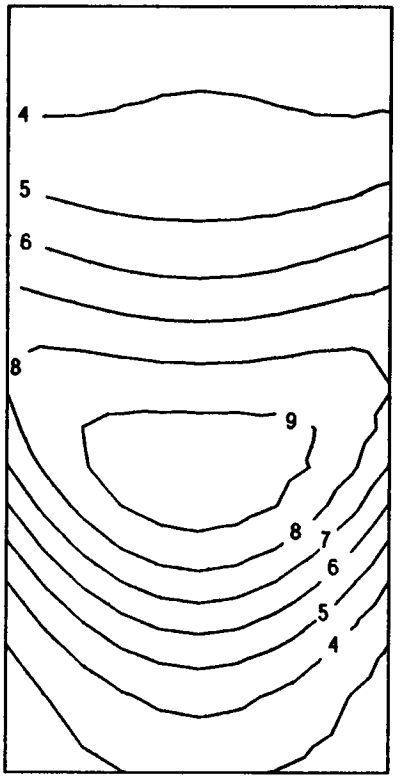

TMS CASE 12 OD JETS (STRAIGHT DUCT), J=26.4, S/HO=.5, D/HO=.25, AR=1.0

Figure 3-12b. Cross-Stream Theta Contours at x/H_0 = 0.75 for Case 12.

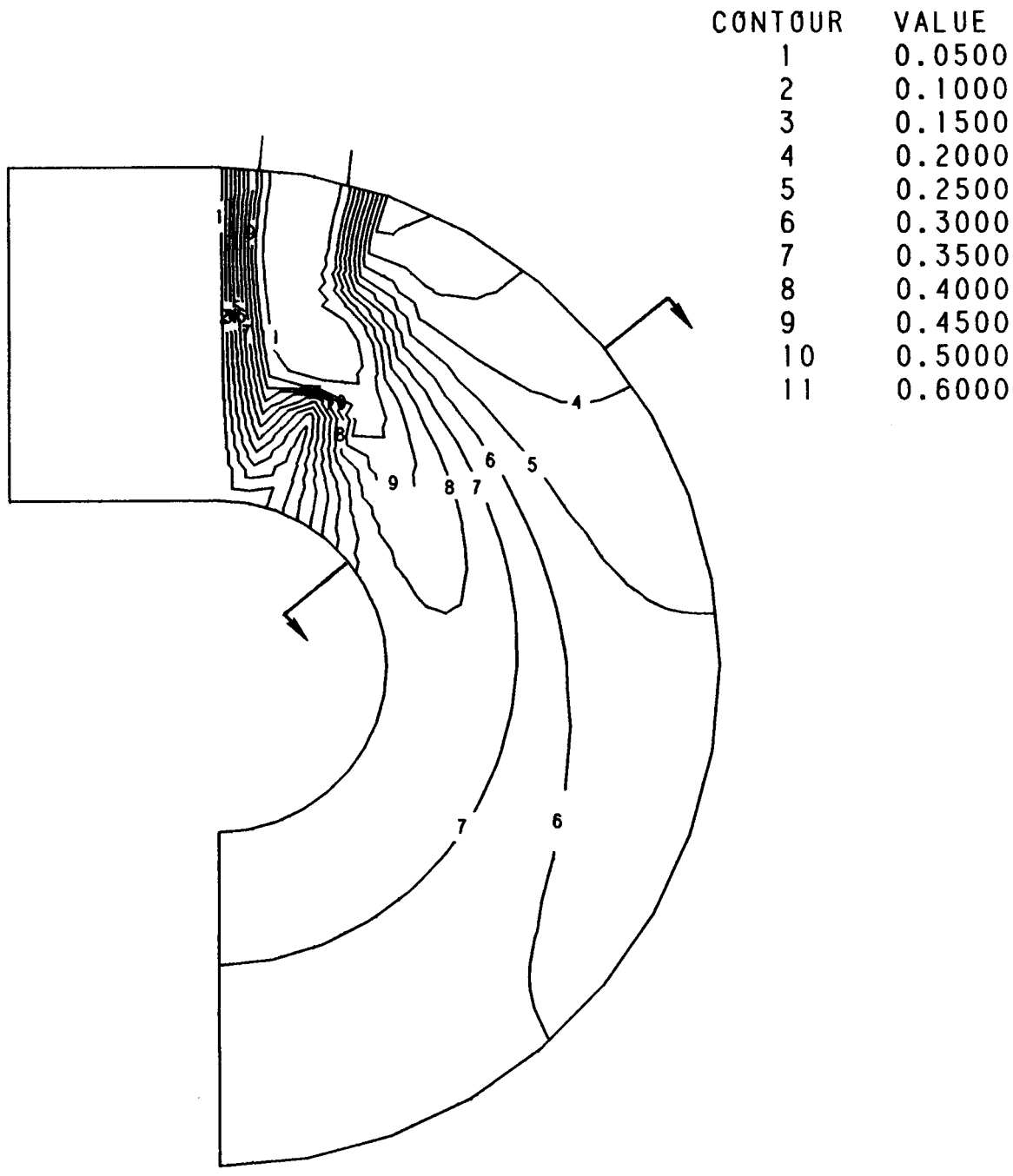

TMS CASE 13-0D JETS-20 DEG, J=26.4, S/H0=.5, D/H0=.25, RCI/H0=.5, AR=1.0

Figure 3-13a. Streamwise Theta Contours for Case 13.

CONTOUR	VALUE
1	0.0500
2	0.1000
3	0.1500
4	0.2000
5	0.2500
6	0.3000
7	0.3500
8	0.4000
9	0.4500
10	0.5000
11	0.6000

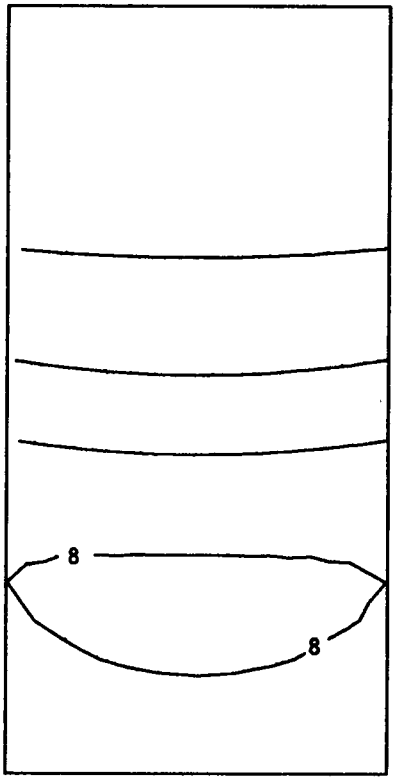

TMS CASE 13-0D JETS-20 DEG, J=26.4, S/H0=.5, D/H0=.25, RCI/H0=.5, AR=1.0

Figure 3-13b. Cross-Stream Theta Contours at Phi = 50 Degrees for Case 13.

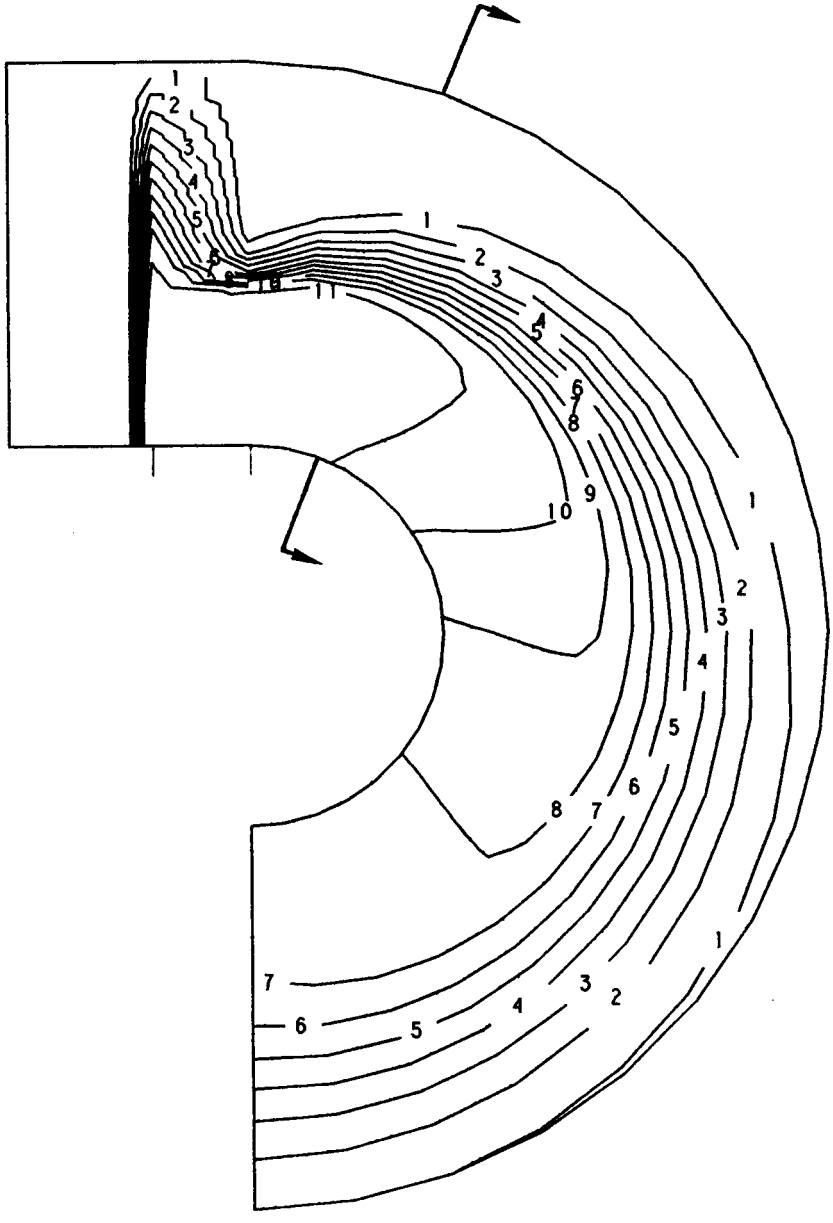

CONTOUR	VALUE
1	0.0500
2	0.1000
3	0.1500
4	0.2000
5	0.2500
6	0.3000
7	0.3500
8	0.4000
9	0.4500
10	0.5000
11	0.6000

TMS CASE 15-ID JETS, J=6.6, S/H0=0.5, D/H0=0.25, RCI/H0=0.50, AR=1.0

Figure 3-14a. Streamwise Theta Contours for Case 15.

CONTOUR	VALUE
1	0.0500
2	0.1000
3	0.1500
4	0.2000
5	0.2500
6	0.3000
7	0.3500
8	0.4000
9	0.4500
10	0.5000
11	0.6000

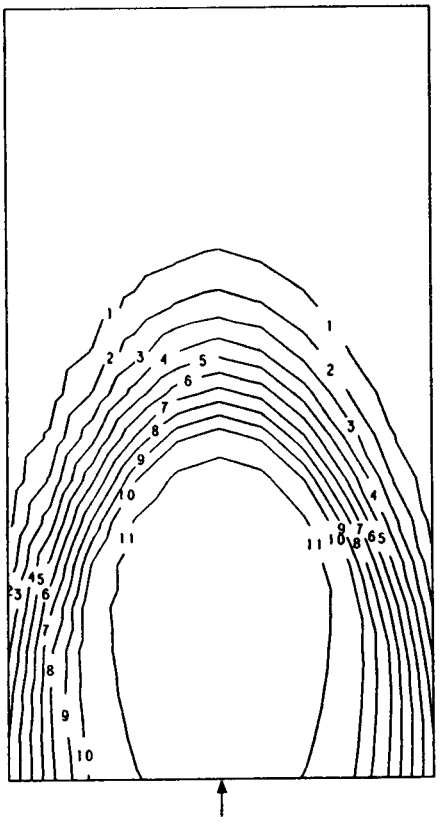

TMS CASE 15-ID JETS, J=6.6, S/HO=0.5, D/HO=0.25, RCI/HO=0.5, AR=1.0

Figure 3-14b. Cross-Stream Theta Contours at Phi = 20 Degrees for Case 15.

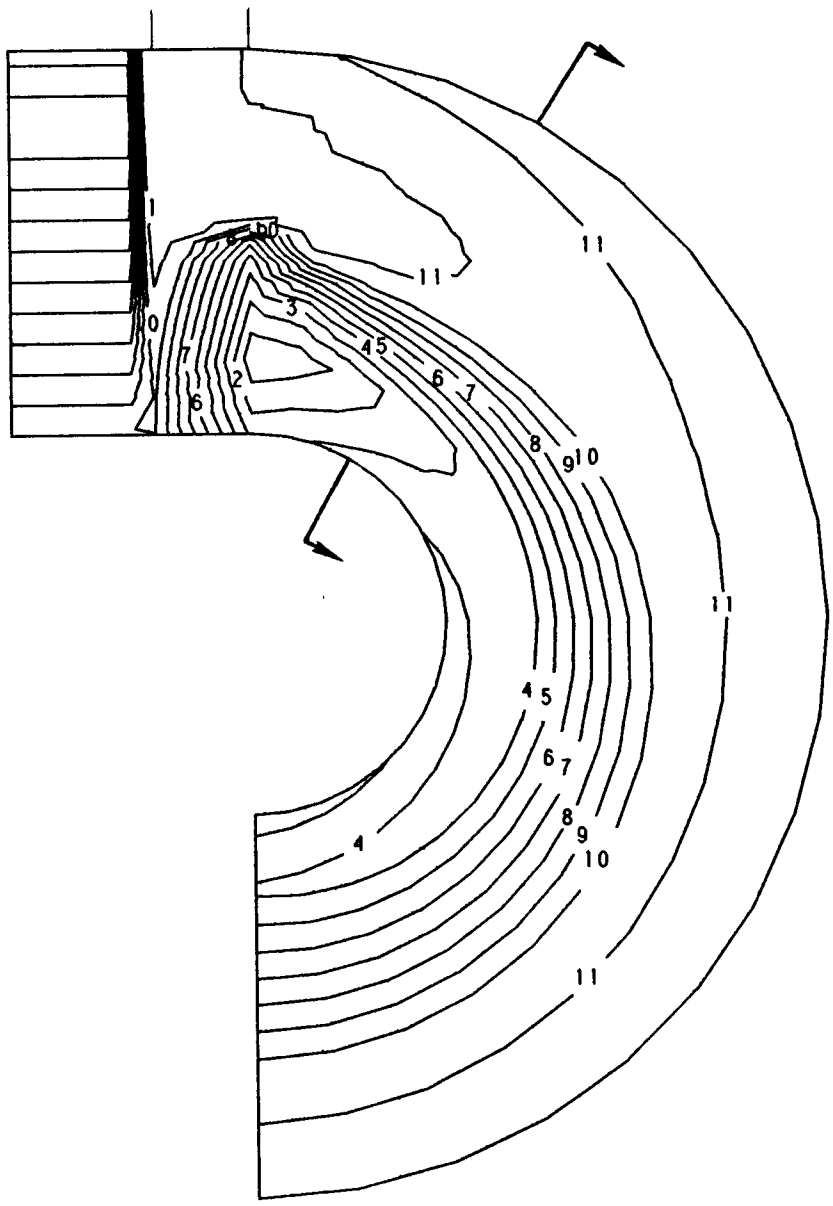

TMS CASE 16-0D JETS(PROFILED), J=6.6, S/H0=0.5, D/H0=0.25 , RCI/H0=.5, AR=1.0

Figure 3-15a. Streamwise Theta Contours for Case 16.

CONTOUR	VALUE
1	0.0500
2	0.1000
3	0.1500
4	0.2000
5	0.2500
6	0.3000
7	0.3500
8	0.4000
9	0.4500
10	0.5000
11	0.6000

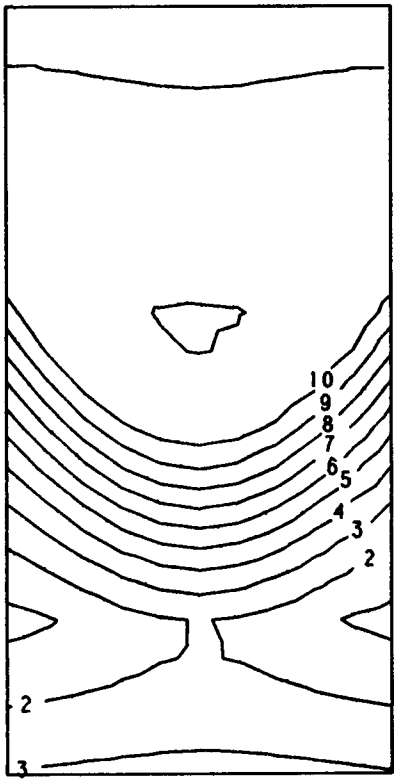

TMS CASE 16-0D JETS(PROFILED), J=6.6, S/H0=0.5, D/H0=0.25 , RCI/H0=.5, AR=1.0

Figure 3-15b. Cross-Stream Theta Contours at Phi = 30 Degrees for Case 16.

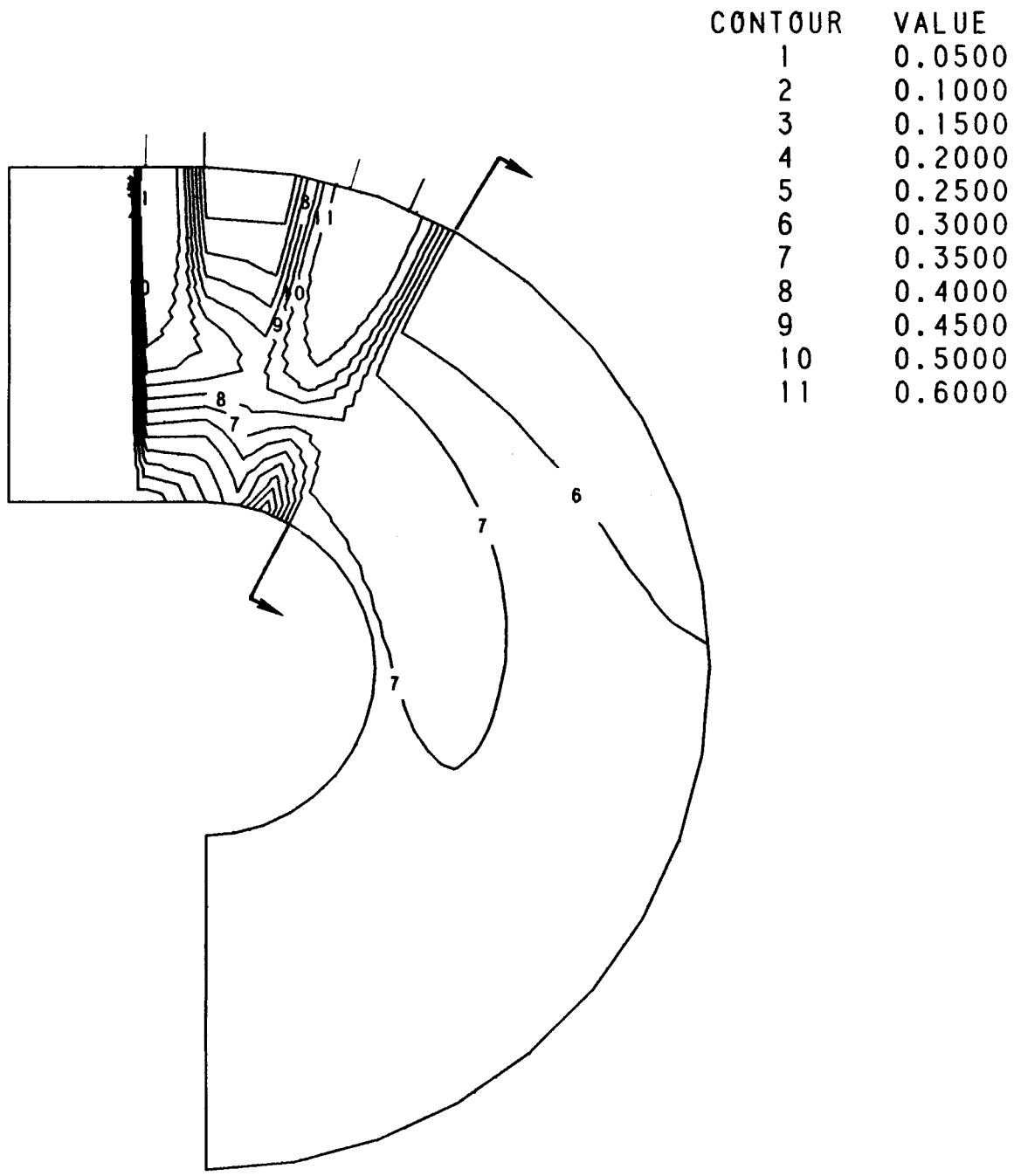

TMS CASE 17-0D STAGED JETS, J=26.4, S/H0=.5, D/H0=.1768, RC1/H0=.5, AR=1.0

Figure 3-16a. Streamwise Theta Contours for Case 17.

CONTOUR	VALUE
1	0.0500
2	0.1000
3	0.1500
4	0.2000
5	0.2500
6	0.3000
7	0.3500
8	0.4000
9	0.4500
10	0.5000
11	0.6000

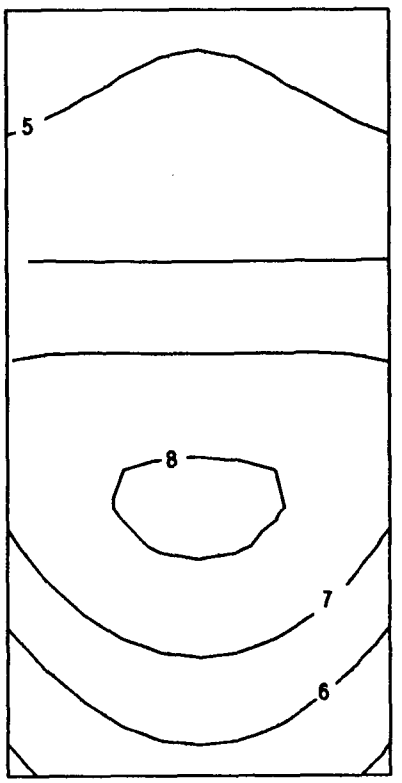

TMS CASE 17-OD STAGED JETS, J=26.4, S/HO=.5, D/HO=.1768, RCI/HO=.5, AR=1.0

Figure 3-16b. Cross-Stream Theta Contours at Phi = 30 Degrees for Case 17.

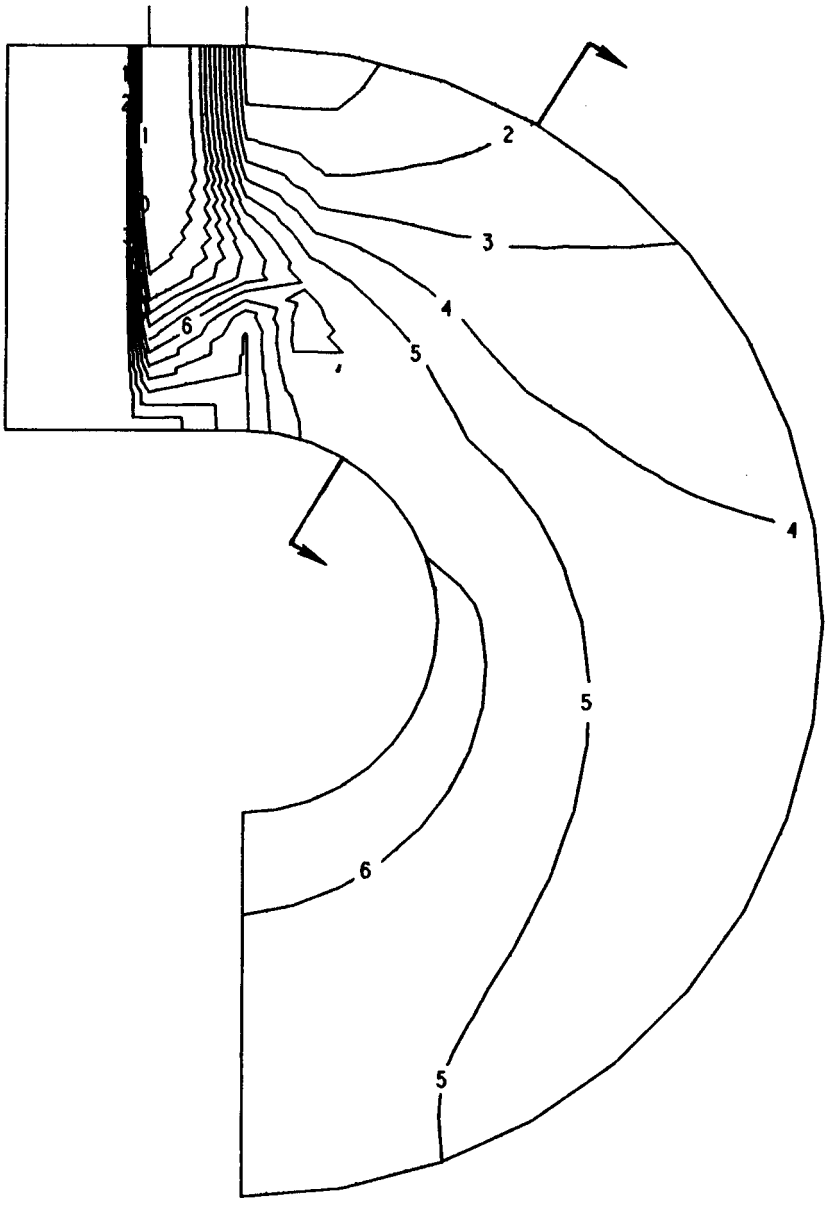

TMS CASE 18-ID/OD JETS(STG), J=26.4, S/HO=1.0, D/HO=.25, RCI/HO=.5, AR=1.0

Figure 3-17a. Streamwise Theta Contours Along the Top Jet Centerplane for Case 18.

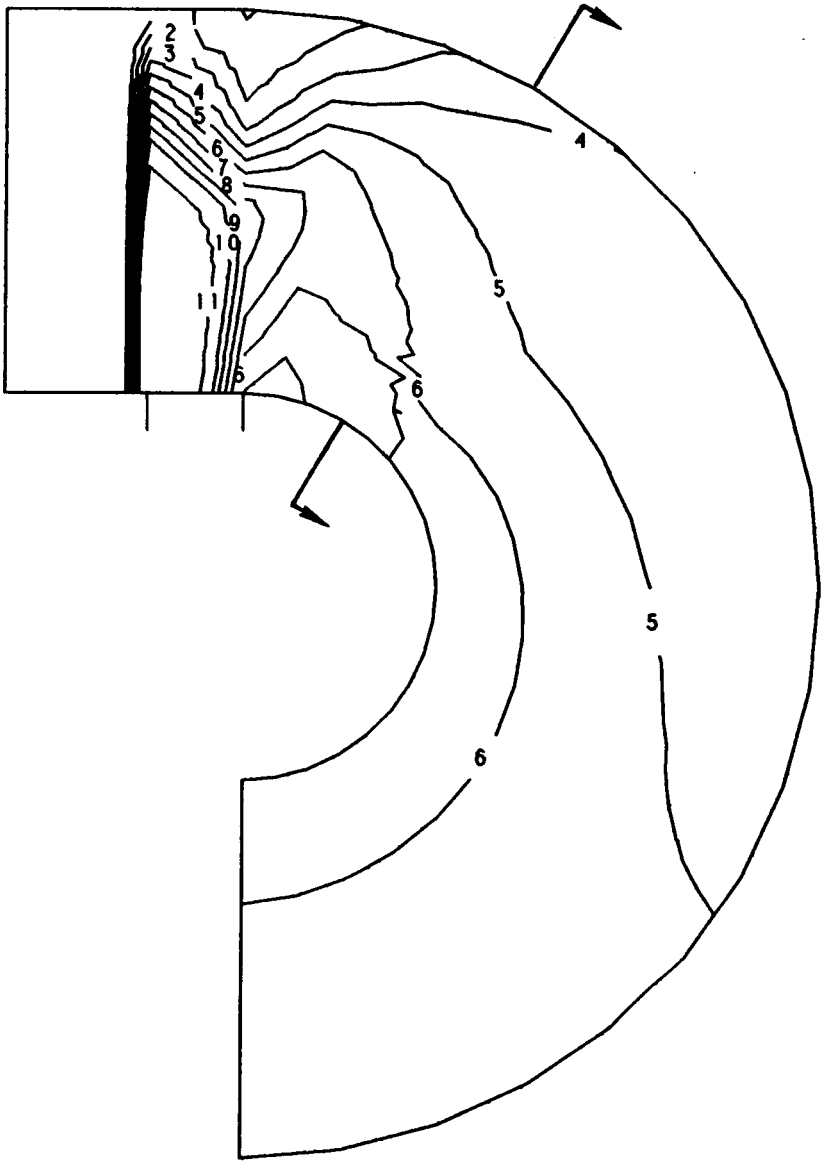

Figure 3-17b. Streamwise Theta Contours Along the Bottom Jet Centerplane for Case 18.

CONTOUR	VALUE
1	0.0500
2	0.1000
3	0.1500
4	0.2000
5	0.2500
6	0.3000
7	0.3500
8	0.4000
9	0.4500
10	0.5000
11	0.6000

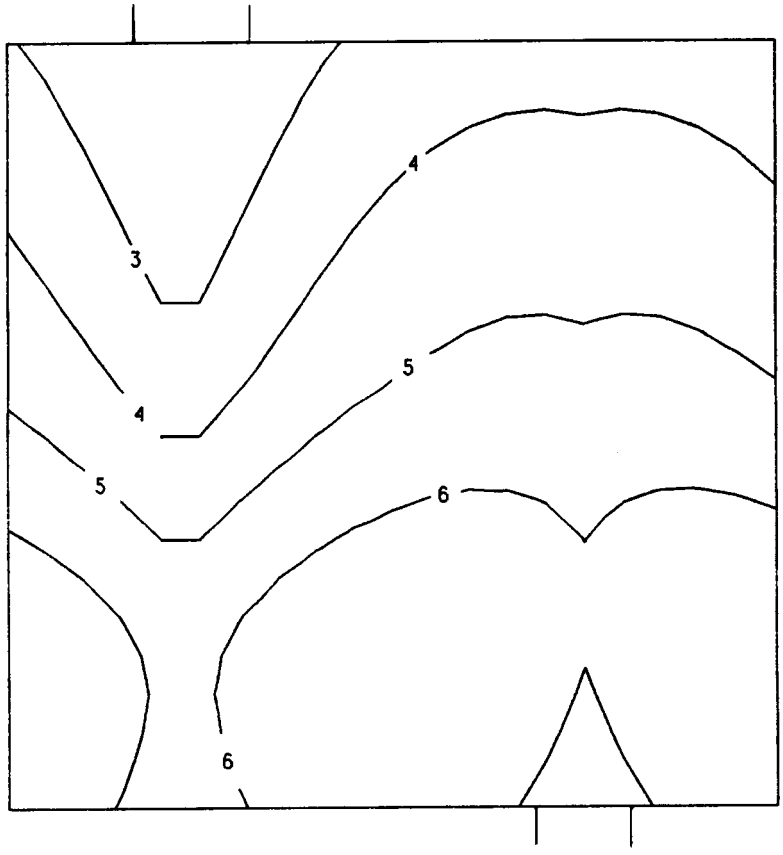

TMS CASE 18-ID/OD JETS(STG), J=26.4, S/HO=1.0, D/HO=.25, RCI/HO=.5, AR=1.0

Figure 3-17c. Cross-Stream Theta Contours at Phi = 30 Degrees for Case 18.

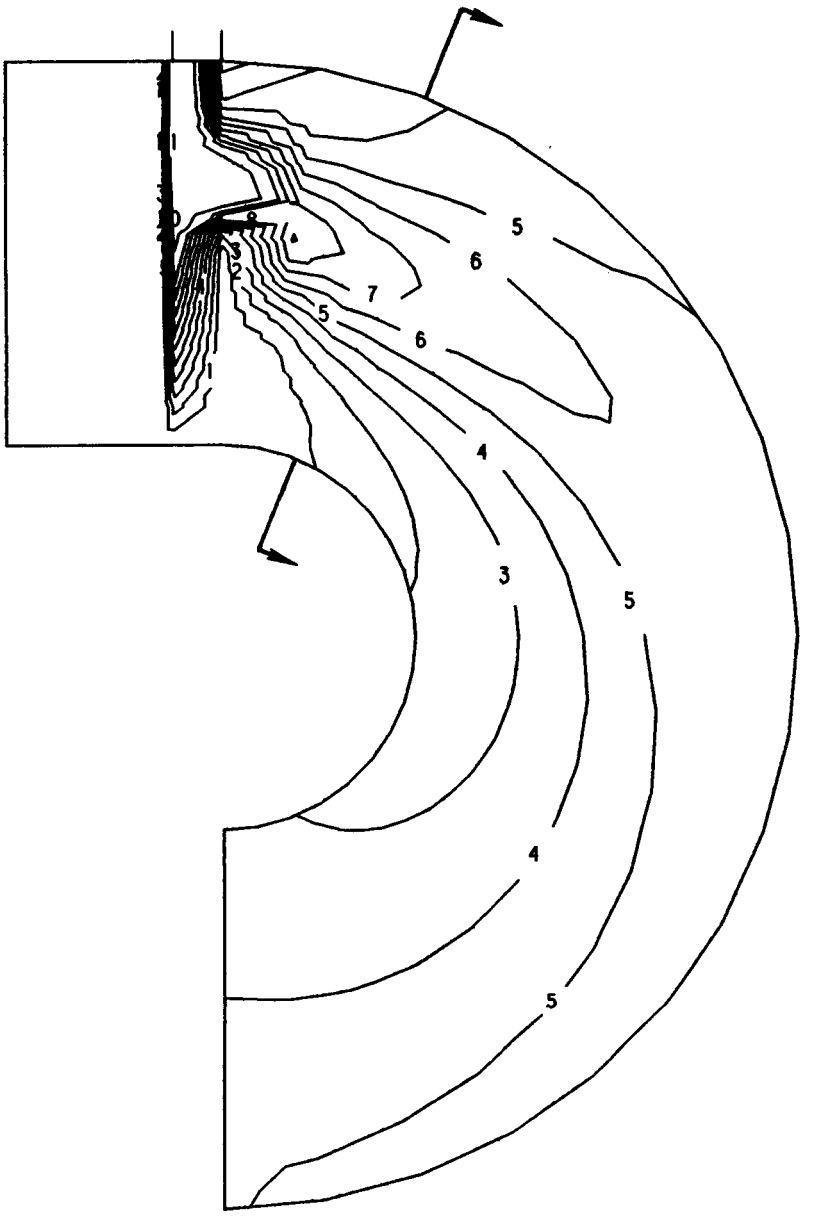

TMS CASE 19-0D JETS, J=26.4, S/H0=0.25, D/H0=0.125, RC1/H0=0.5, AR=1.0

Figure 3-18a. Streamwise Theta Contours for Case 19.

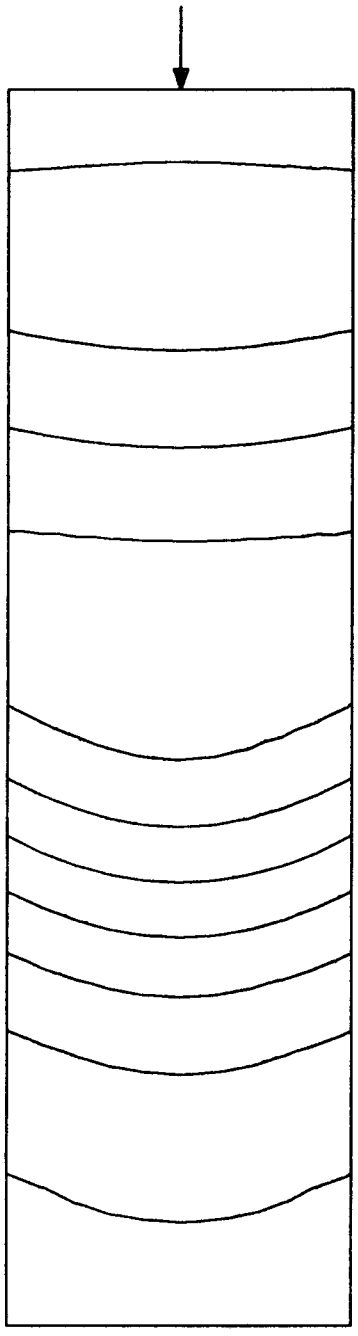

CONTOUR	VALUE
1	0.0500
2	0.1000
3	0.1500
4	0.2000
5	0.2500
6	0.3000
7	0.3500
8	0.4000
9	0.4500
10	0.5000
11	0.6000

TMS CASE 19-0D JETS, J=26.4, S/H0=0.25, D/H0=0.125, RCI/H0=0.5, AR=1.0

Figure 3-18b. Cross-Stream Theta Contours at Phi = 20 Degrees for Case 19.

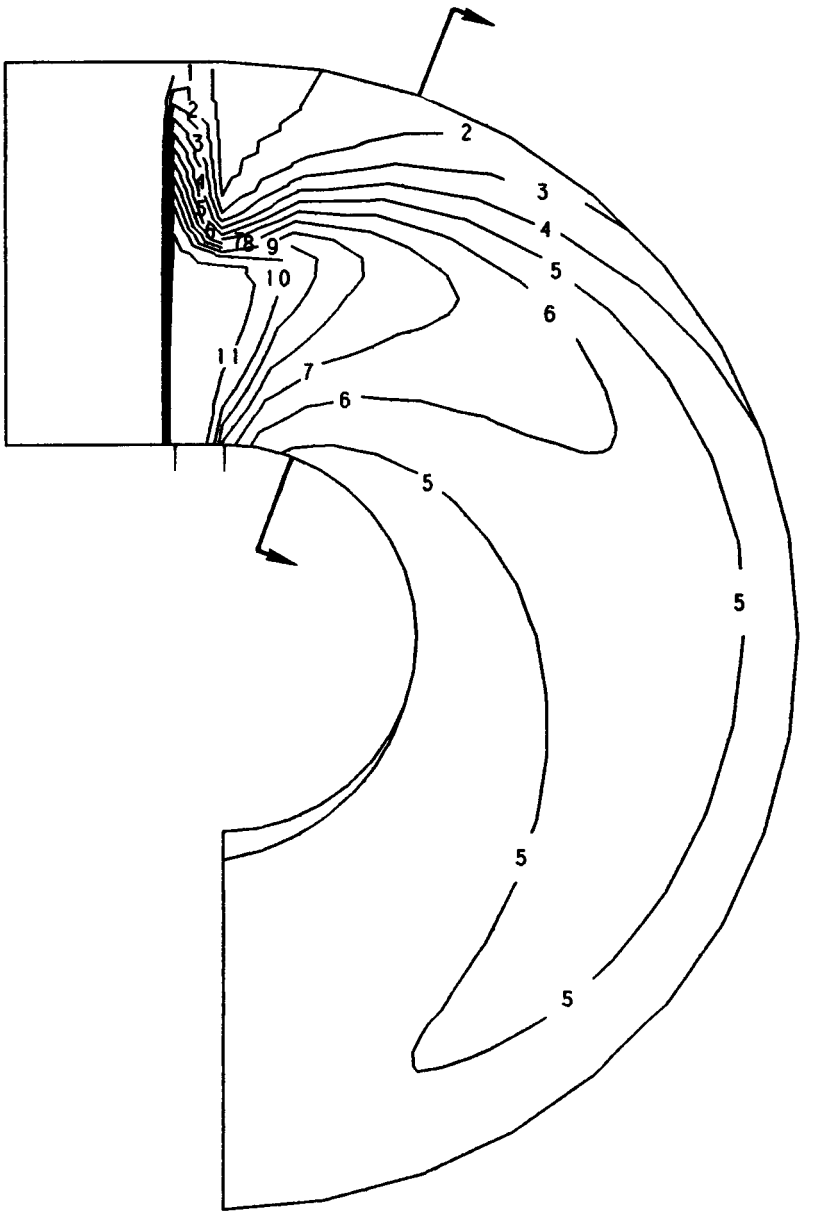

TMS CASE 20-ID JETS, J=105.6, S/HO=0.50, D/HO=0.125, RCI/HO=0.5, AR=1.0

Figure 3-19a. Streamwise Theta Contours for Case 20.

CONTOUR	VALUE
1	0.0500
2	0.1000
3	0.1500
4	0.2000
5	0.2500
6	0.3000
7	0.3500
8	0.4000
9	0.4500
10	0.5000
11	0.6000

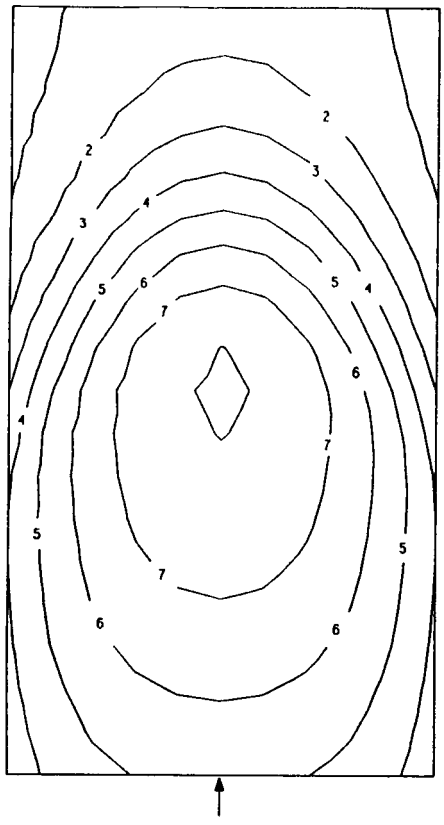

TMS CASE 20-ID JETS, J=105.6, S/HO=0.5, D/HO=0.125, RCI/HO=0.5, AR=1.0

Figure 3-19b. Cross-Stream Theta Contours at Phi = 20 Degrees for Case 20.

CONTOUR	VALUE
1	0.0500
2	0.1000
3	0.1500
4	0.2000
5	0.2500
6	0.3000
7	0.3500
8	0.4000
9	0.4500
10	0.5000
11	0.6000

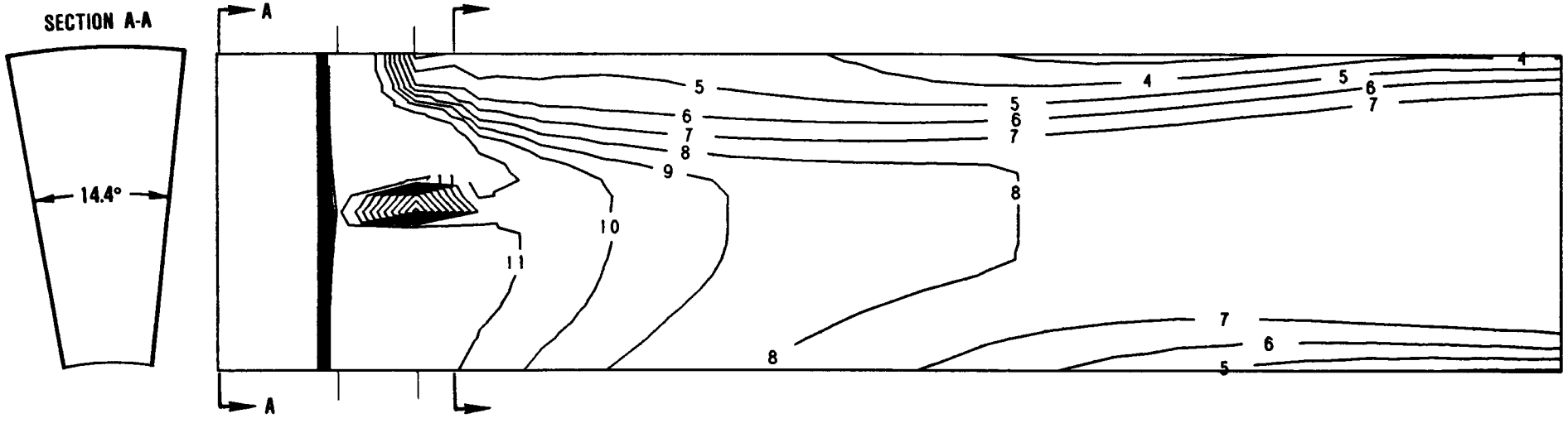

TMS CASE 21-0D/ID JETS (ANNULUS), J=6.6, S/H0=0.50, D/H0=.25, AR=1.00

Figure 3-20a. Streamwise Theta Contours for Case 21.

CONTOUR	VALUE
1	0.0500
2	0.1000
3	0.1500
4	0.2000
5	0.2500
6	0.3000
7	0.3500
8	0.4000
9	0.4500
10	0.5000
11	0.6000

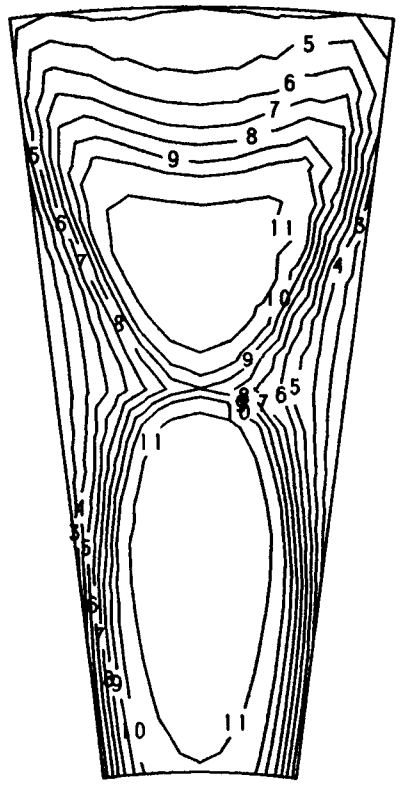

TMS CASE 21-OD/ID JETS (ANNULUS), J=6.6, S/HO=.5, D/HO=.25, AR=1.0

Figure 3-20b. Cross-Stream Theta Contours at x/H_0 = 0.25 for Case 21.

TMS CASE 22-OD JETS (ANNULUS), J=26.4, S/HO=.3535, D/HO=.1768, AR=1.0

Figure 3-21a. Streamwise Theta Contours for Case 22.

CONTOUR	VALUE
1	0.0500
2	0.1000
3	0.1500
4	0.2000
5	0.2500
6	0.3000
7	0.3500
8	0.4000
9	0.4500
10	0.5000
11	0.6000

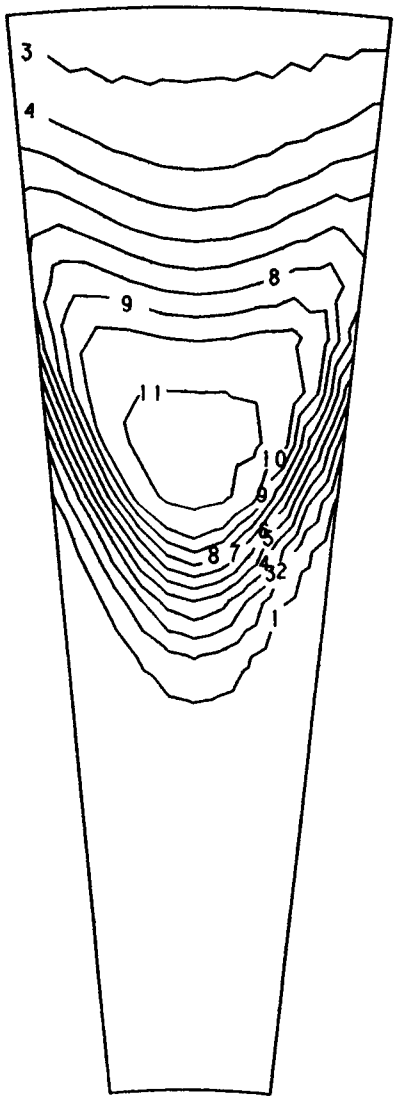

TMS CASE 22-0D JETS (ANNULUS), J=26.4, S/H0=.3535, D/H0=.1768, AR=1.0,X/H=.25

Figure 3-21b. Cross-Stream Theta Contours at x/H_0 = 0.25 for Case 22.

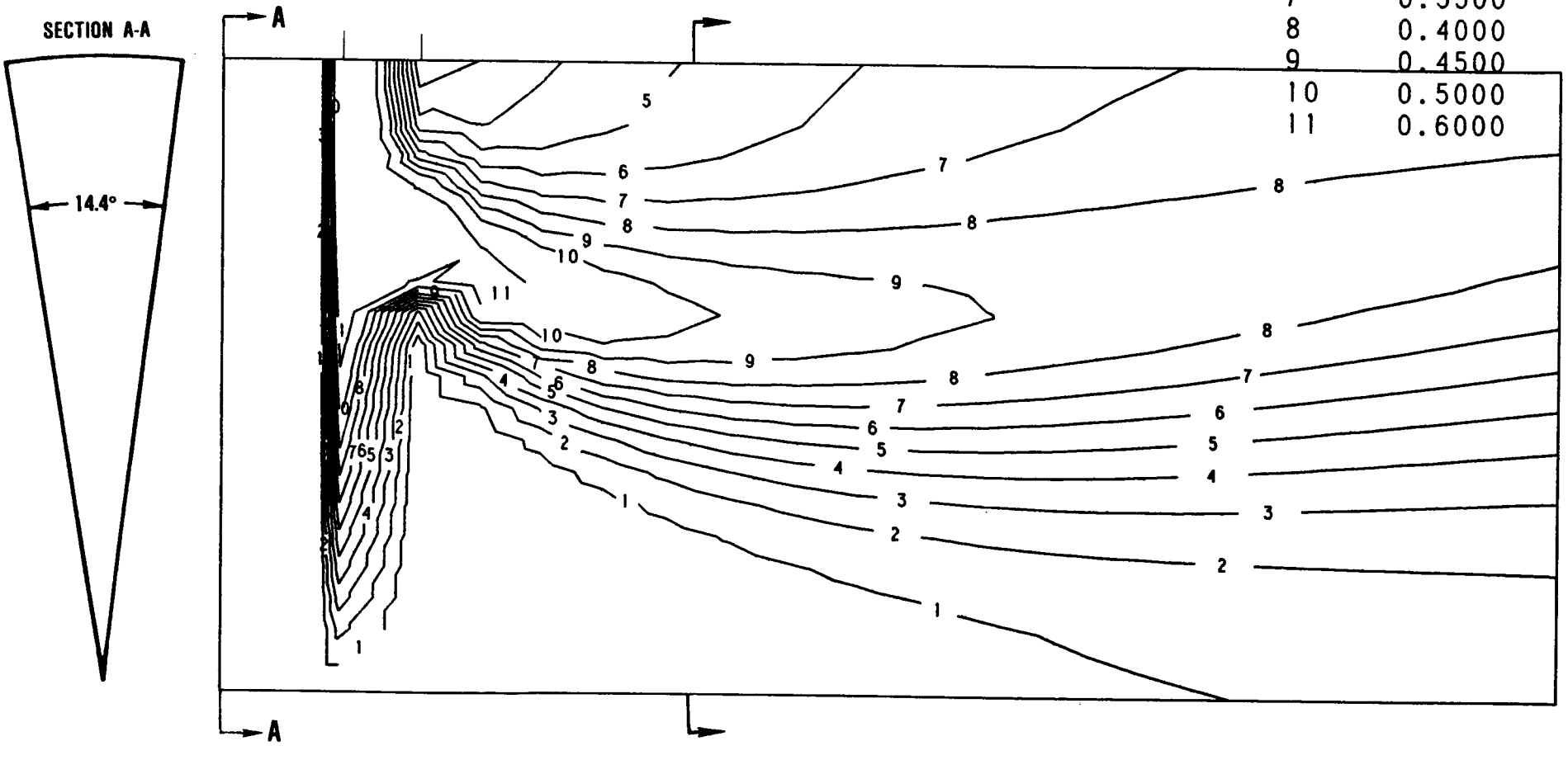

TMS CASE 23-0D JETS (16-IN. CAN), J=26.4, S/H0=0.25, D/H0=0.125, AR=1.0

Figure 3-22a. Streamwise Theta Contours for Case 23.

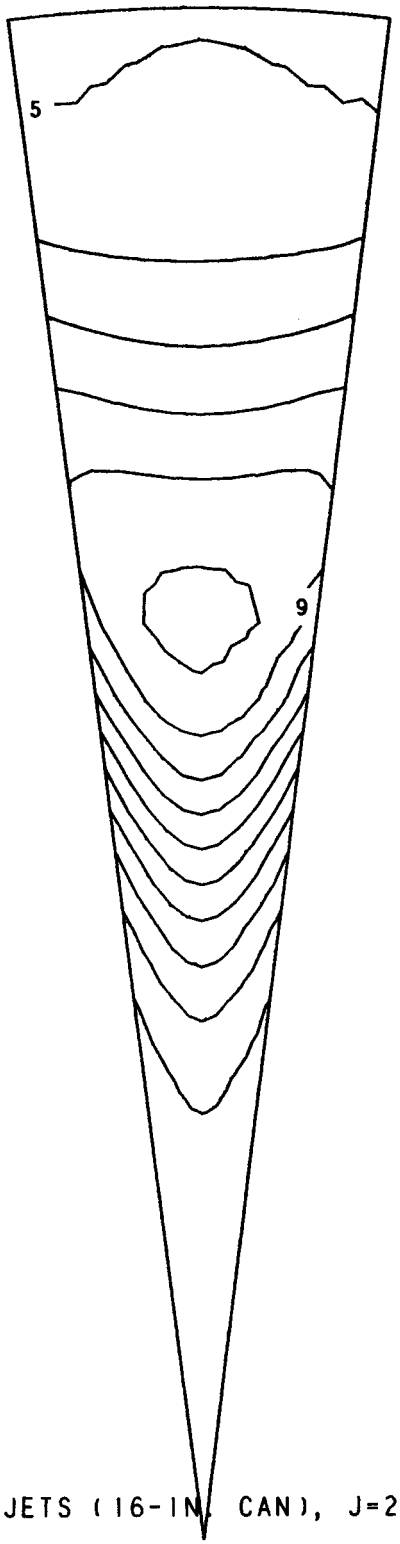

CONTOUR	VALUE
1	0.0500
2	0.1000
3	0.1500
4	0.2000
5	0.2500
6	0.3000
7	0.3500
8	0.4000
9	0.4500
10	0.5000
11	0.6000

TMS CASE 23-0D JETS (16-IN. CAN), J=26.4, S/H0=0.25, D/H0=0.125, AR=1.0

Figure 3-22b. Cross-Stream Theta Contours at x/H_0 = 0.50 for Case 23.

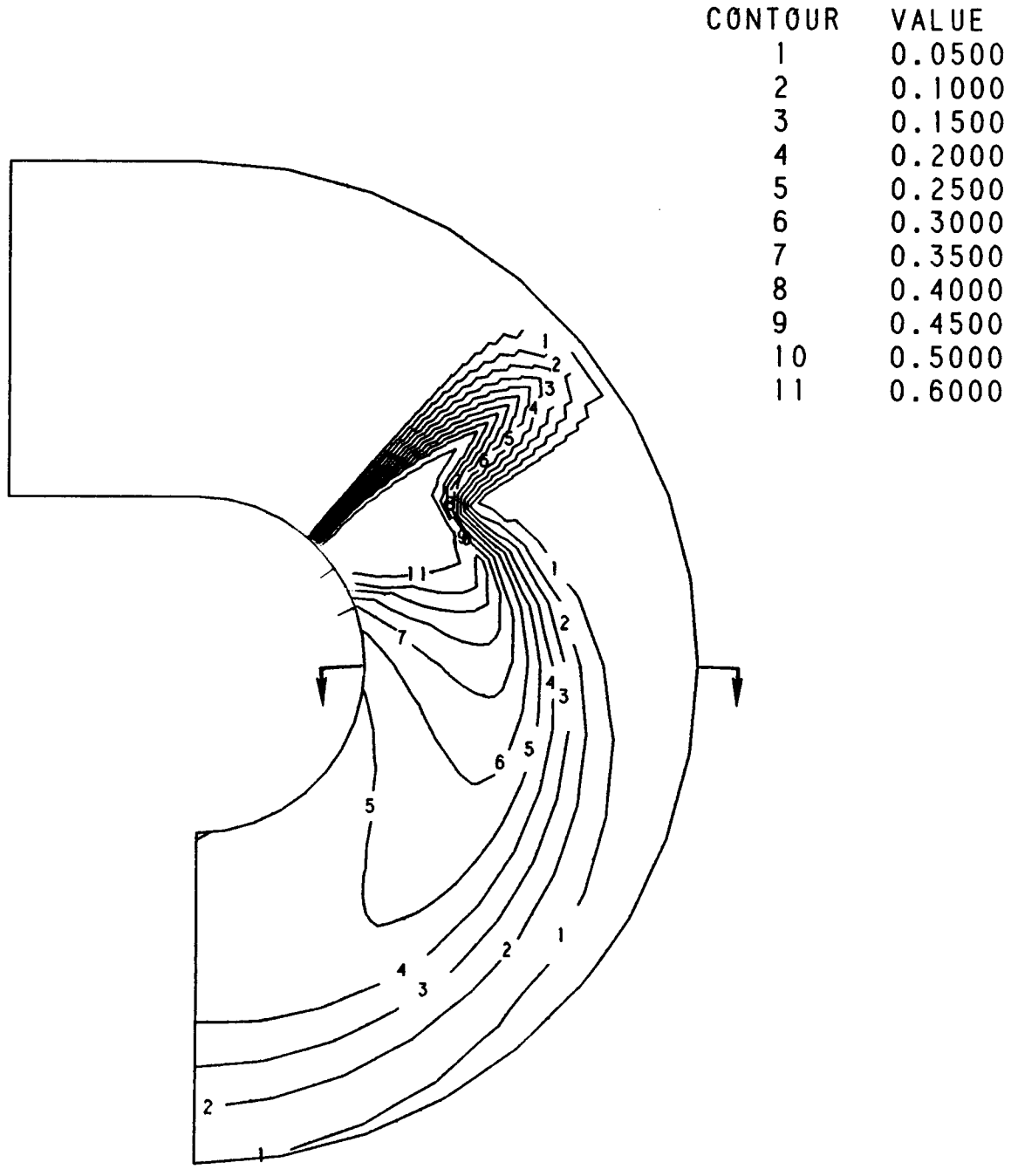

TMS CASE 24-ID JETS-60 DEG, J=26.4, S/HO=0.5, D/HO=0.125, RCI/HO=0.5, AR=1.0

Figure 3-23a. Streamwise Theta Contours for Case 24.

CONTOUR	VALUE
1	0.0500
2	0.1000
3	0.1500
4	0.2000
5	0.2500
6	0.3000
7	0.3500
8	0.4000
9	0.4500
10	0.5000
11	0.6000

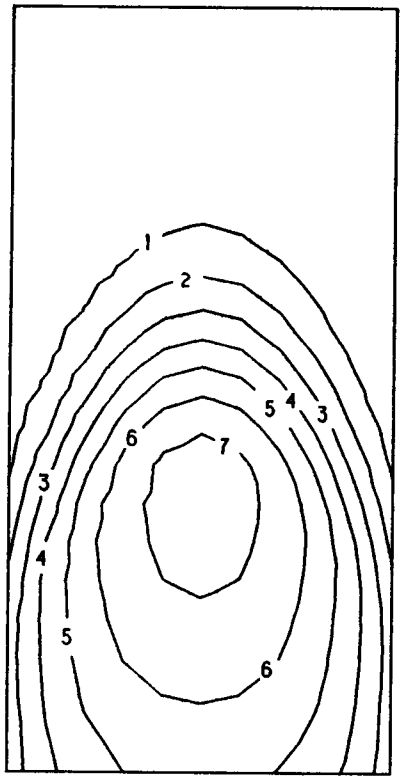

TMS CASE 24-ID JETS-60 DEG, J=26.4, S/HO=0.5,
D/HO=0.125, RCI/HO=0.5, AR=1.0

Figure 3-23b. Cross-Stream Theta Contours at Phi = 90 Degrees for Case 24.

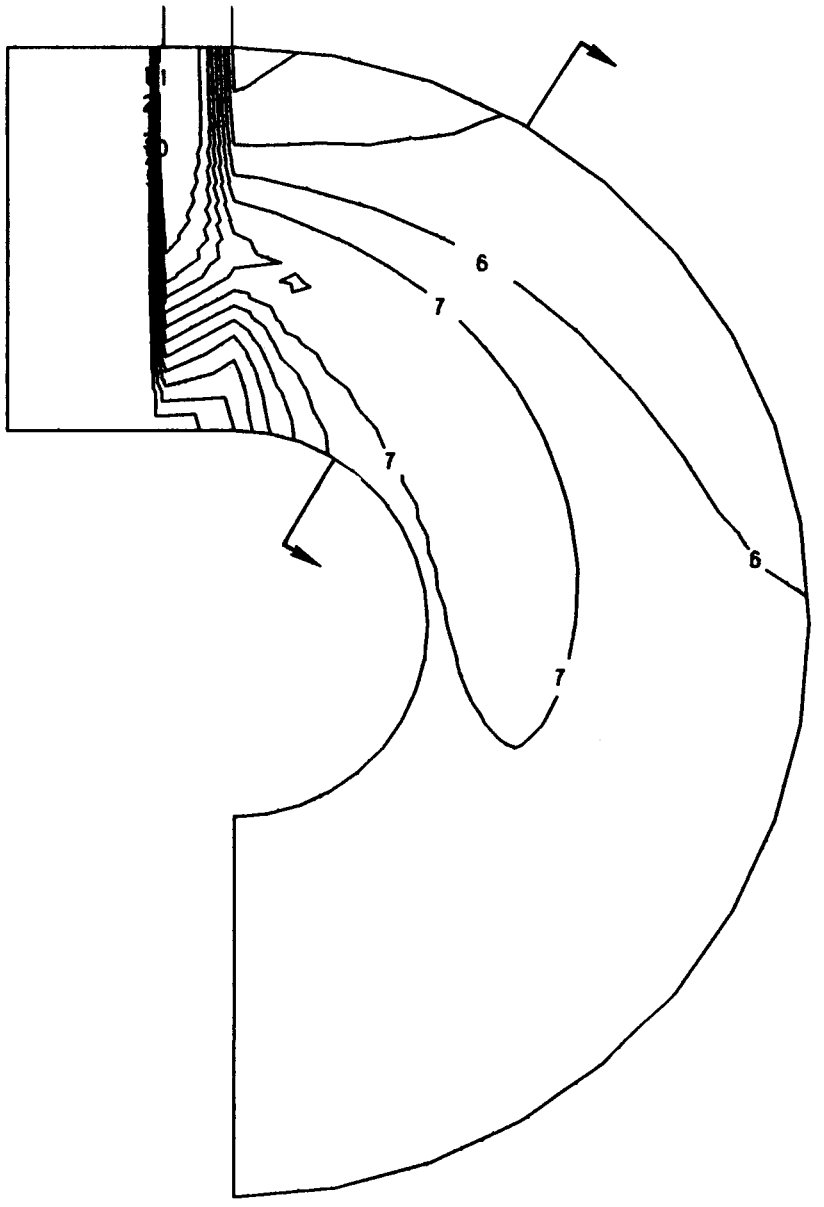

CONTOUR	VALUE
1	0.0500
2	0.1000
3	0.1500
4	0.2000
5	0.2500
6	0.3000
7	0.3500
8	0.4000
9	0.4500
10	0.5000
11	0.6000

TMS CASE 25-OD STAGED JETS(STG), J=26.4, S/HO=.5, D/HO=.1768, RCI/HO=.5,AR=1.0

Figure 3-24a. Streamwise Theta Contours Along the Lead Row Jet Centerplane for Case 25.

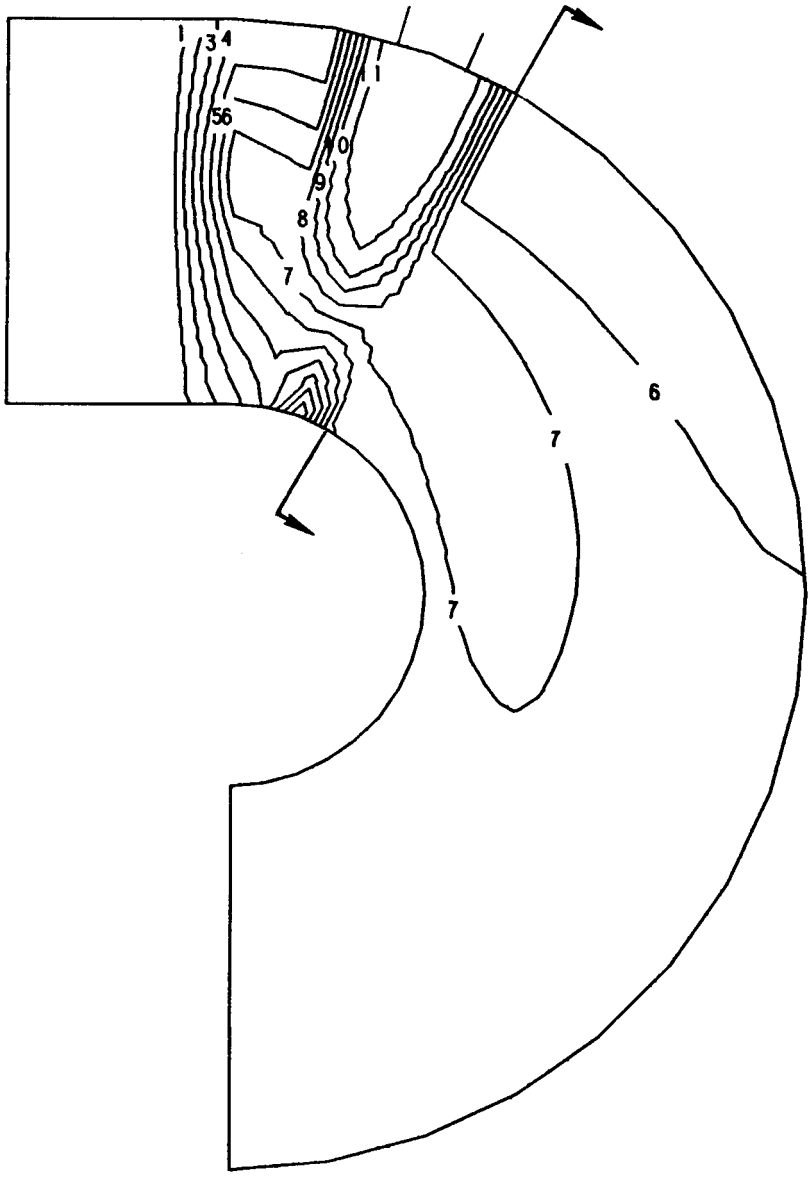

TMS CASE 25-OD STAGED JETS(STG), J=26.4, S/HO=.5, D/HO=.1768, RCI/HO=.5, AR=1.0

Figure 3-24b. Streamwise Theta Contours Along the Trailing Row Jet Centerplane for Case 25.

CONTOUR	VALUE
1	0.0500
2	0.1000
3	0.1500
4	0.2000
5	0.2500
6	0.3000
7	0.3500
8	0.4000
9	0.4500
10	0.5000
11	0.6000

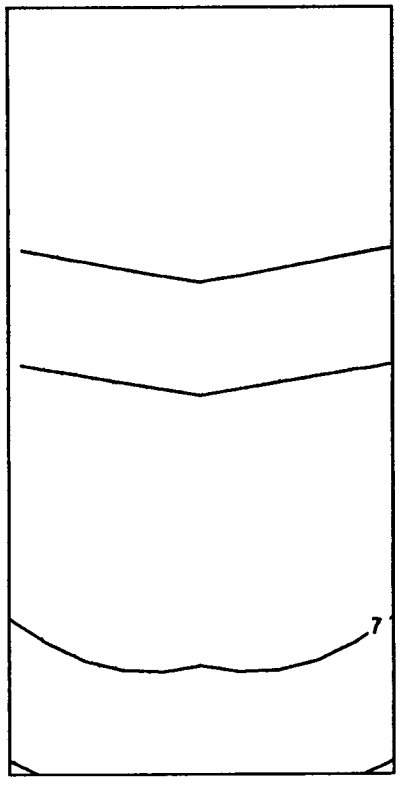

TMS CASE 25-0D STAGED JETS(STG), J=26.4, S/H0=.5, D/H0=.1768, RCI/H0=.5,AR=1.0

Figure 3-24c. Cross-Stream Theta Contours at Phi = 30 Degrees for Case 25.

CONTOUR	VALUE
1	0.0500
2	0.1000
3	0.1500
4	0.2000
5	0.2500
6	0.3000
7	0.3500
8	0.4000
9	0.4500
10	0.5000
11	0.6000

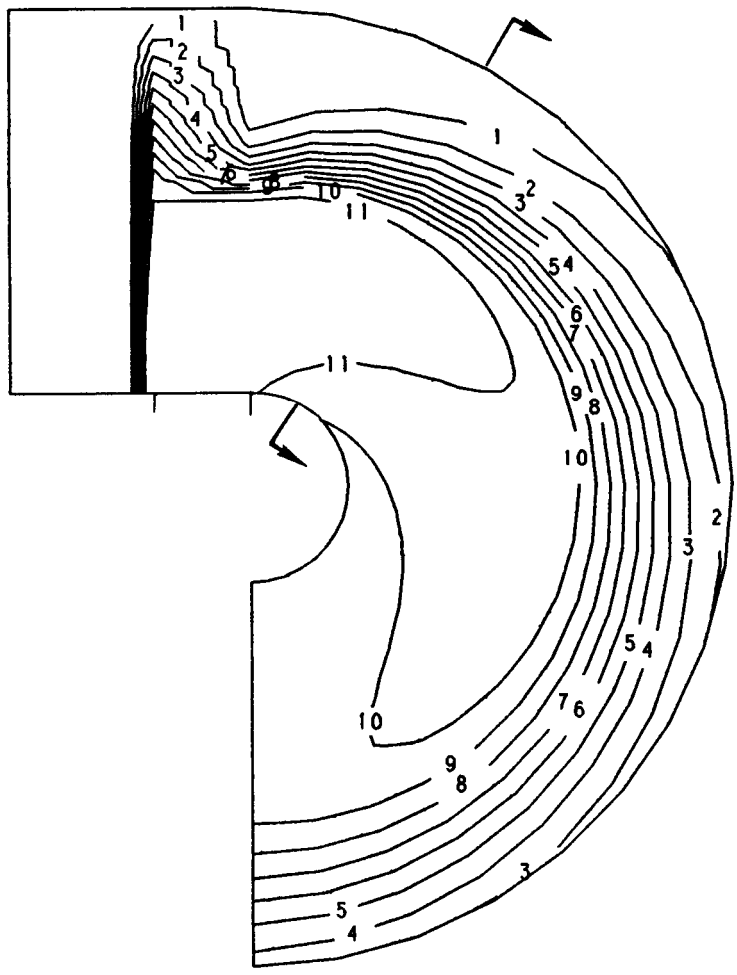

TMS CASE 26-ID JETS, J=26.4, S/HO=0.5, D/HO=0.25, RCI/HO=0.25, AR=1.0

Figure 3-25a. Streamwise Theta Contours for Case 26.

CONTOUR	VALUE
1	0.0500
2	0.1000
3	0.1500
4	0.2000
5	0.2500
6	0.3000
7	0.3500
8	0.4000
9	0.4500
10	0.5000
11	0.6000

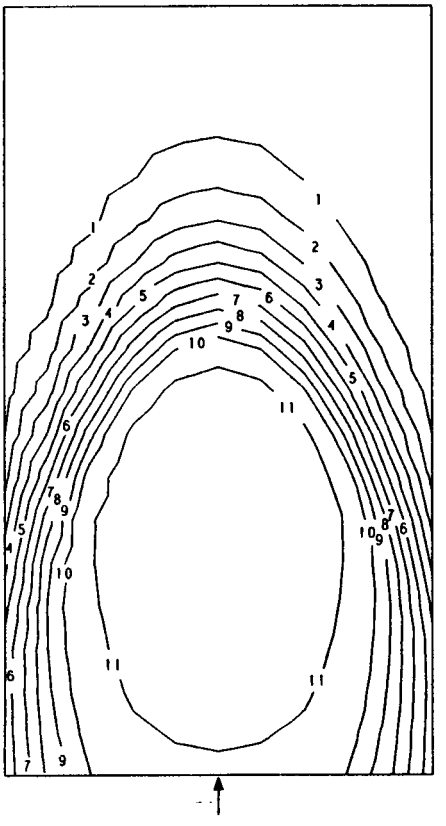

TMS CASE 26-ID JETS, J=26.4, S/HO=0.5, D/HO=0.25, RCI/HO=0.25, AR=1.0

Figure 3-25b. Cross-Stream Theta Contours at Phi = 30 Degrees for Case 26.

CONTOUR	VALUE
1	0.0500
2	0.1000
3	0.1500
4	0.2000
5	0.2500
6	0.3000
7	0.3500
8	0.4000
9	0.4500
10	0.5000
11	0.6000

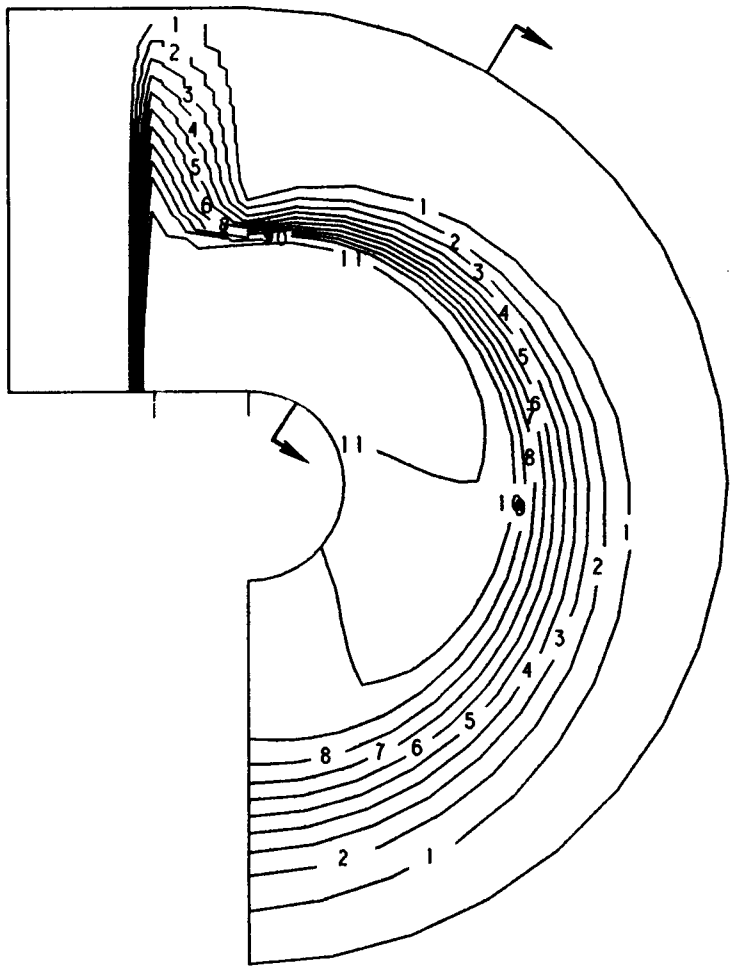

TMS CASE 27-ID JETS, J=6.6, S/H0=0.5, D/H0=0.25, RCI/H0=0.25, AR=1.0

Figure 3-26a. Streamwise Theta Contours for Case 27.

CONTOUR	VALUE
1	0.0500
2	0.1000
3	0.1500
4	0.2000
5	0.2500
6	0.3000
7	0.3500
8	0.4000
9	0.4500
10	0.5000
11	0.6000

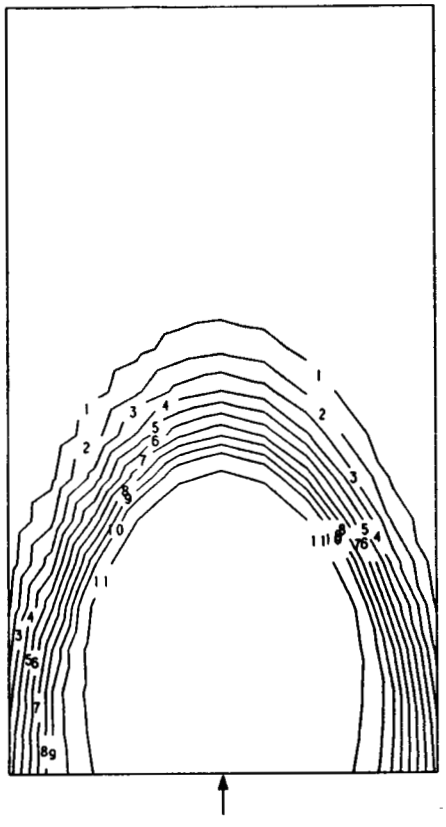

TMS CASE 27-ID JETS, J=6.6, S/HO=0.5, D/HO=0.25, RCI/HO=0.25, AR=1.0

Figure 3-26b. Cross-Stream Theta Contours at Phi = 30 Degrees for Case 27.

CONTOUR	VALUE
1	0.0500
2	0.1000
3	0.1500
4	0.2000
5	0.2500
6	0.3000
7	0.3500
8	0.4000
9	0.4500
10	0.5000
11	0.6000

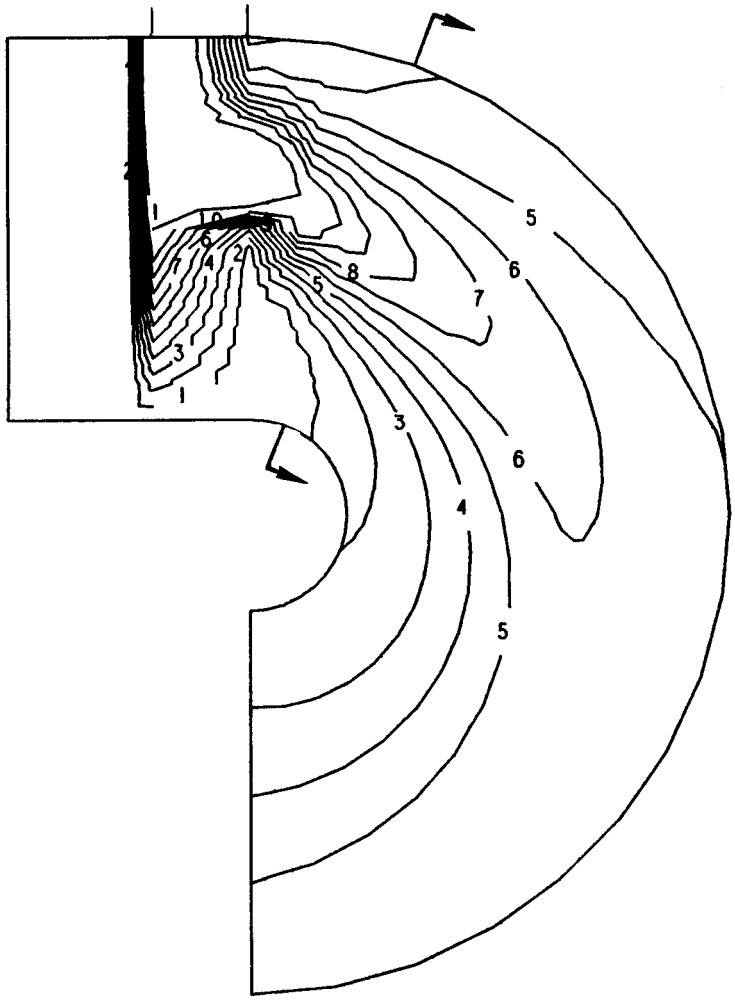

TMS CASE 28-0D JETS, J=6.6, S/H0=0.5, D/H0=0.25, RCI/H0=0.25, AR=1.0

Figure 3-27a. Streamwise Theta Contours for Case 28.

CONTOUR	VALUE
1	0.0500
2	0.1000
3	0.1500
4	0.2000
5	0.2500
6	0.3000
7	0.3500
8	0.4000
9	0.4500
10	0.5000
11	0.6000

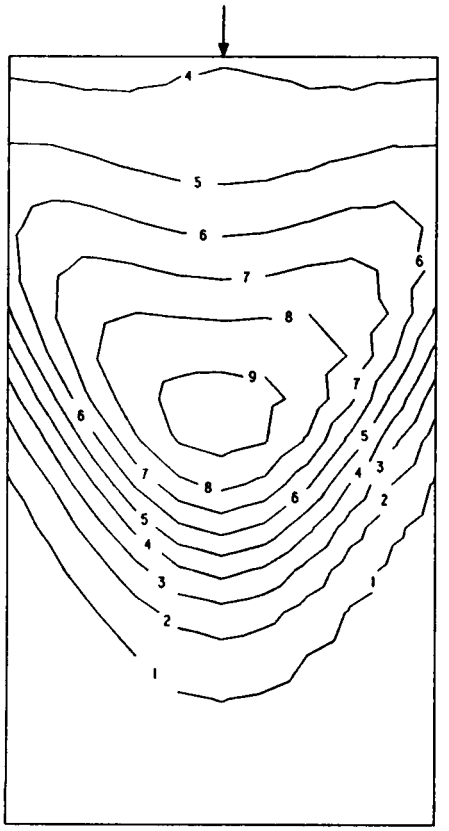

TMS CASE 28-0D JETS, J=6.6, S/H0=0.5, D/H0=0.25, RC1/H0=0.25, AR=1.0

Figure 3-27b. Cross-Stream Theta Contours at Phi = 20 Degrees for Case 28.

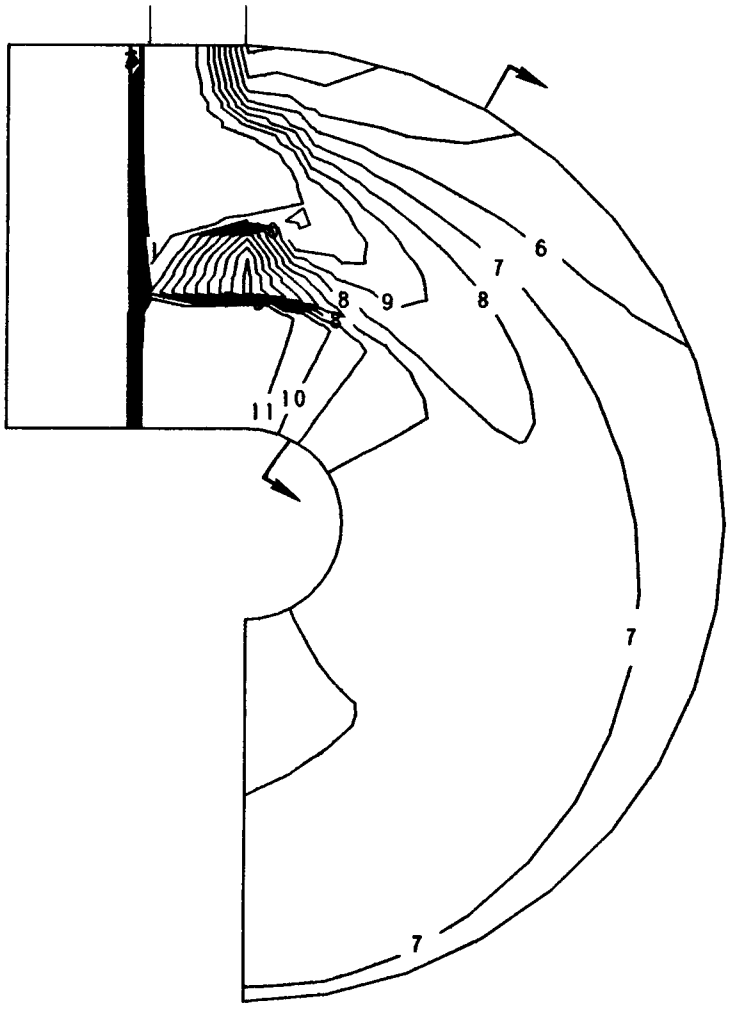

TMS CASE 29-0D/ID JETS (INL), J=6.6, S/H0=.50, RCI/H0=.25, D/H0=.25,AR=1.0

Figure 3-28a. Streamwise Theta Contours for Case 29.

CONTOUR	VALUE
1	0.0500
2	0.1000
3	0.1500
4	0.2000
5	0.2500
6	0.3000
7	0.3500
8	0.4000
9	0.4500
10	0.5000
11	0.6000

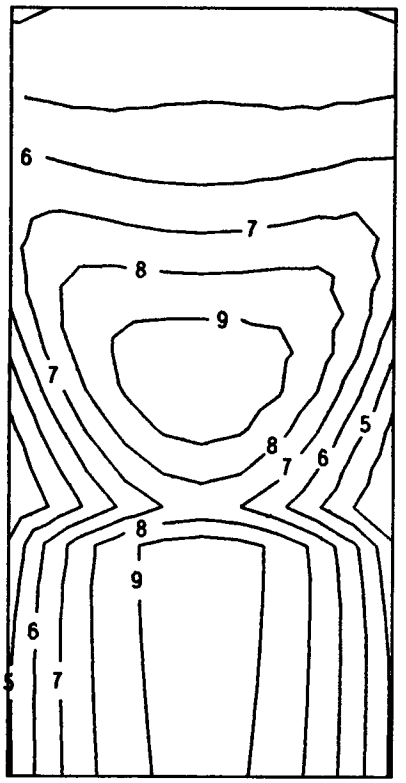

TMS CASE 29-0D/1D JETS (INL), J=6.6, S/H0=.5, RC1/H0=.25, D/H0=.25, AR=1.0

Figure 3-28b. Cross-Stream Theta Contours at Phi = 30 Degrees for Case 29.

CONTOUR	VALUE
1	0.0500
2	0.1000
3	0.1500
4	0.2000
5	0.2500
6	0.3000
7	0.3500
8	0.4000
9	0.4500
10	0.5000
11	0.6000

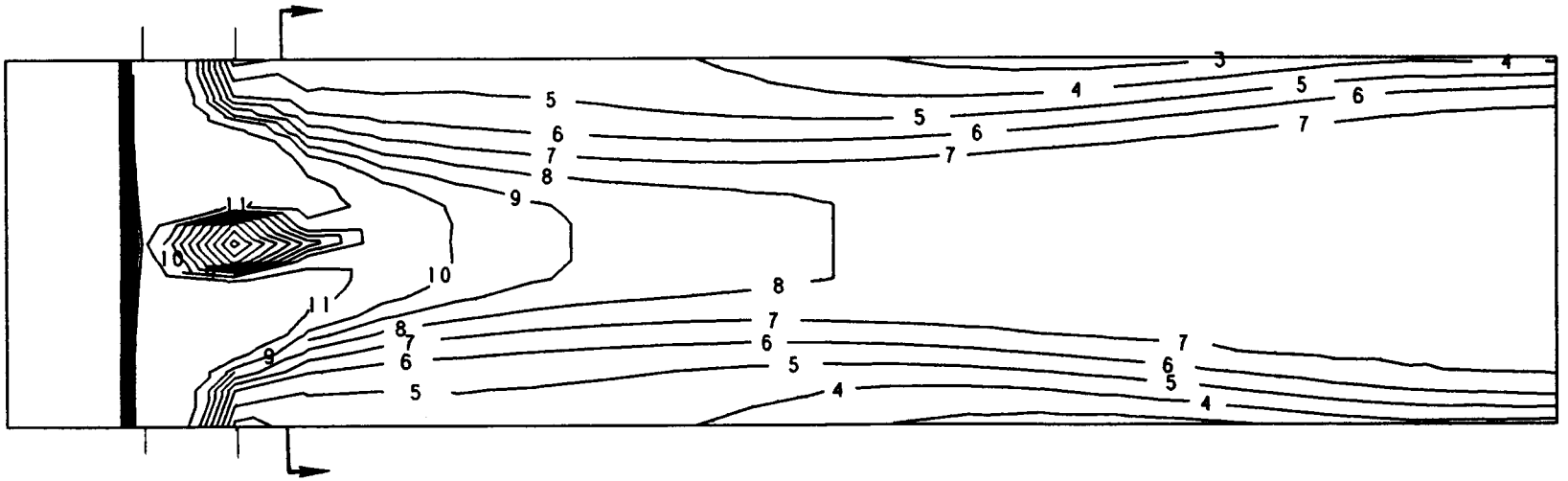

TMS CASE 30-0D/1D JETS (STRAIGHT DUCT), J=6.6, S/H0=0.50, D/H0=.25, AR=1.00

Figure 3-29a. Streamwise Theta Contours for Case 30.

CONTOUR	VALUE
1	0.0500
2	0.1000
3	0.1500
4	0.2000
5	0.2500
6	0.3000
7	0.3500
8	0.4000
9	0.4500
10	0.5000
11	0.6000

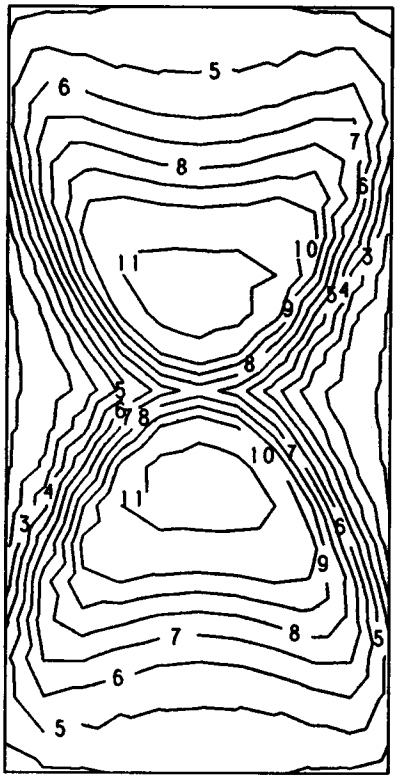

TMS CASE 30-0D/1D JETS (STRAIGHT DUCT), J=6.6, S/H0=.5, D/H0=.25,X/H=.25

Figure 3-29b. Cross-Stream Theta Contours at x/H_0 = 0.25 for Case 30.

CONTOUR	VALUE
1	0.0500
2	0.1000
3	0.1500
4	0.2000
5	0.2500
6	0.3000
7	0.3500
8	0.4000
9	0.4500
10	0.5000
11	0.6000

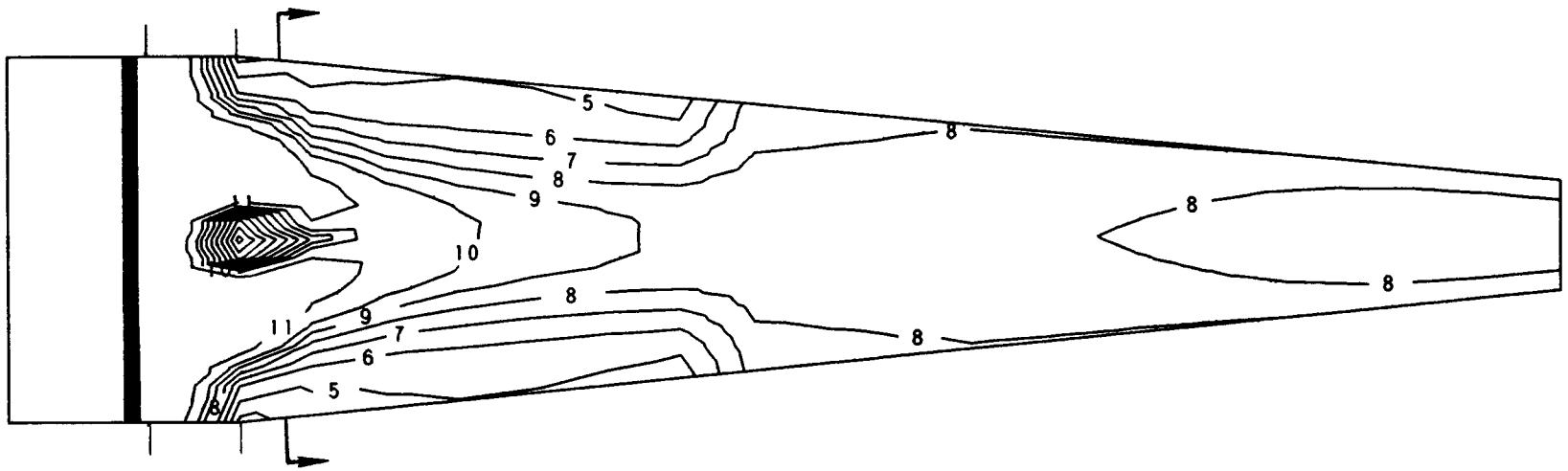

TMS CASE 31-OD/ID JETS (CONV. DUCT), J=6.6, S/HO=0.50, D/HO=.25, AR=2.566

Figure 3-30a. Streamwise Theta Contours for Case 31.

CONTOUR	VALUE
1	0.0500
2	0.1000
3	0.1500
4	0.2000
5	0.2500
6	0.3000
7	0.3500
8	0.4000
9	0.4500
10	0.5000
11	0.6000

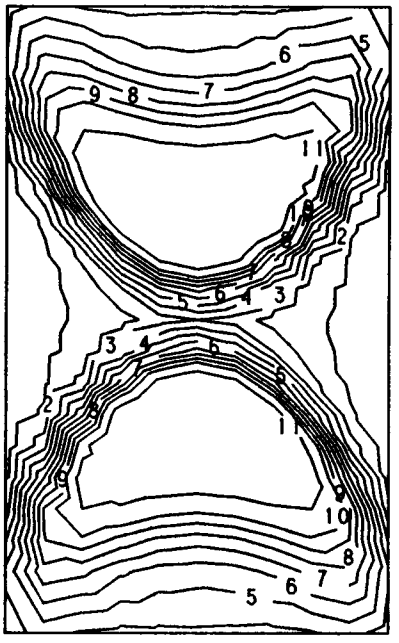

TMS CASE 31-OD/ID JETS (CONV. DUCT), J=6.6, S/HO=.5, AR=2.566, X/H=.25

Figure 3-30b. Cross-Stream Theta Contours at x/H_0 = 0.25 for Case 31.

CONTOUR	VALUE
1	0.0500
2	0.1000
3	0.1500
4	0.2000
5	0.2500
6	0.3000
7	0.3500
8	0.4000
9	0.4500
10	0.5000
11	0.6000

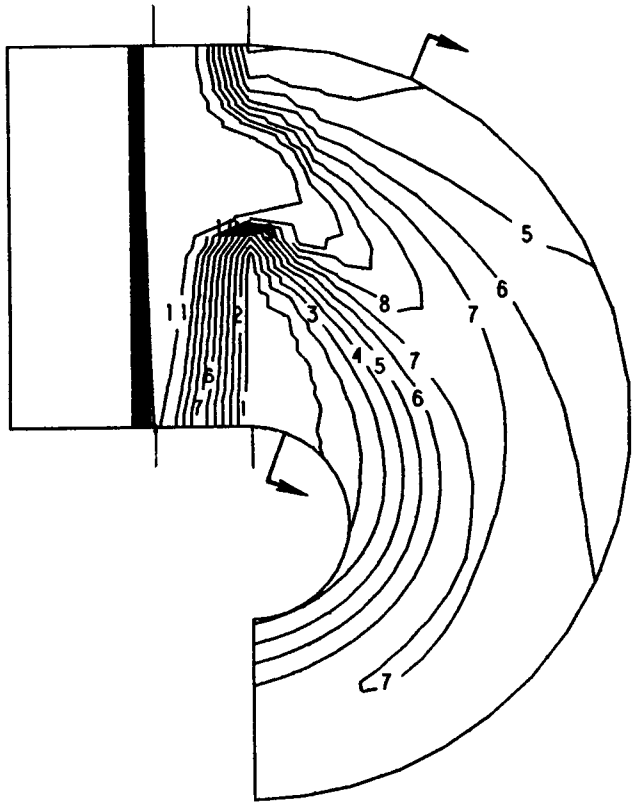

TMS CASE 32-OD JETS, J=6.6, S/HO=0.5, D/HO=0.25, RCI/HO=.25, AR=3.0

Figure 3-31a. Streamwise Theta Contours for Case 32.

CONTOUR	VALUE
1	0.0500
2	0.1000
3	0.1500
4	0.2000
5	0.2500
6	0.3000
7	0.3500
8	0.4000
9	0.4500
10	0.5000
11	0.6000

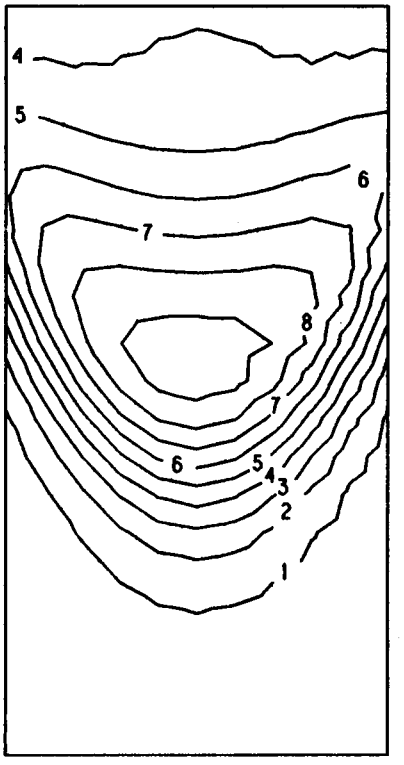

TMS CASE 32-0D JETS, J=6.6, S/H0=0.5, D/H0=0.25, RCI/H0=0.25, AR=3.0

Figure 3-31b. Cross-Stream Theta Contours at Phi = 20 Degrees for Case 32.

CONTOUR	VALUE
1	0.0500
2	0.1000
3	0.1500
4	0.2000
5	0.2500
6	0.3000
7	0.3500
8	0.4000
9	0.4500
10	0.5000
11	0.6000

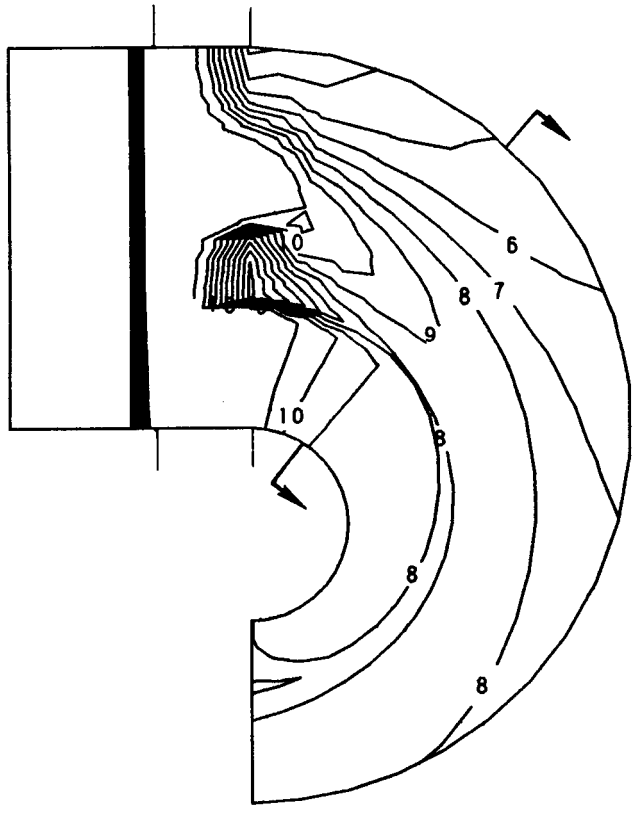

TMS CASE 33-OD/ID JETS (INL), J=6.6, S/HO=.5, RCI/HO=.25, D/HO=.25, AR=3.0

Figure 3-32a. Streamwise Theta Contours for Case 33.

CONTOUR	VALUE
1	0.0500
2	0.1000
3	0.1500
4	0.2000
5	0.2500
6	0.3000
7	0.3500
8	0.4000
9	0.4500
10	0.5000
11	0.6000

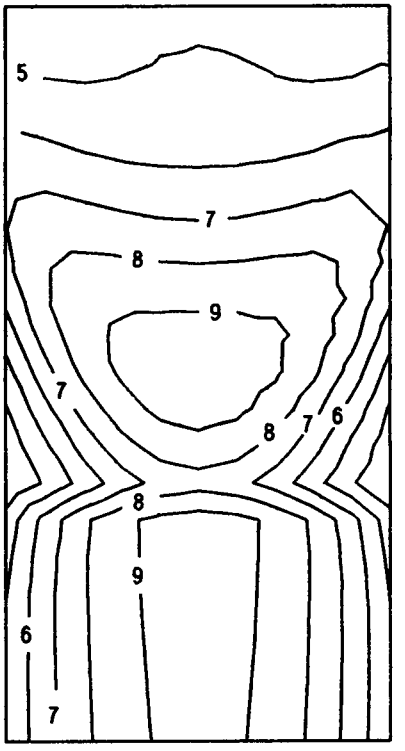

TMS CASE 33 OD/ID JETS (INL), J=6.6, S/HO=.5, RCI/HO=.25, D/HO=.25, AR=3.0

Figure 3-32b. Cross-Stream Theta Contours at Phi = 36 Degrees for Case 33.

CONTOUR	VALUE
1	0.0500
2	0.1000
3	0.1500
4	0.2000
5	0.2500
6	0.3000
7	0.3500
8	0.4000
9	0.4500
10	0.5000
11	0.6000

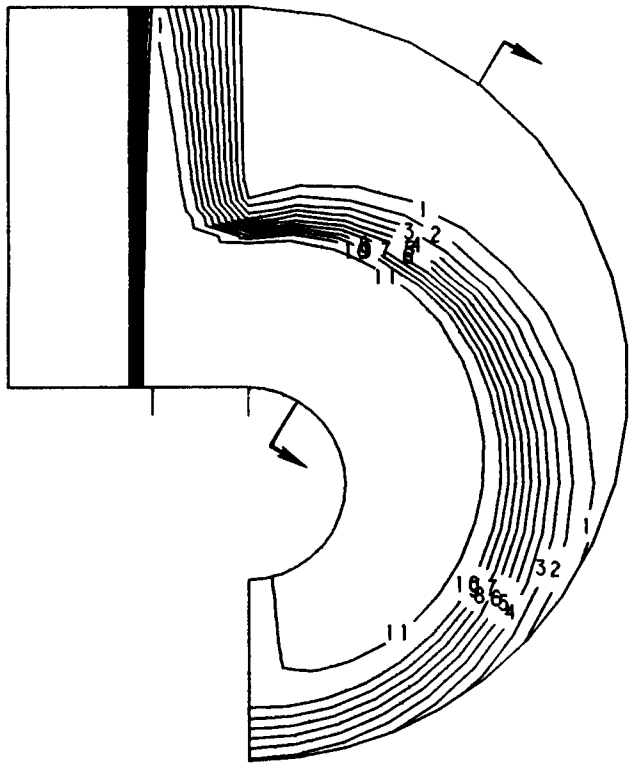

TMS CASE 34-ID JETS, J=6.6, S/HO=0.5, D/HO=0.25, RCI/HO=0.25, AR=3.0

Figure 3-33a. Streamwise Theta Contours for Case 34.

CONTOUR	VALUE
1	0.0500
2	0.1000
3	0.1500
4	0.2000
5	0.2500
6	0.3000
7	0.3500
8	0.4000
9	0.4500
10	0.5000
11	0.6000

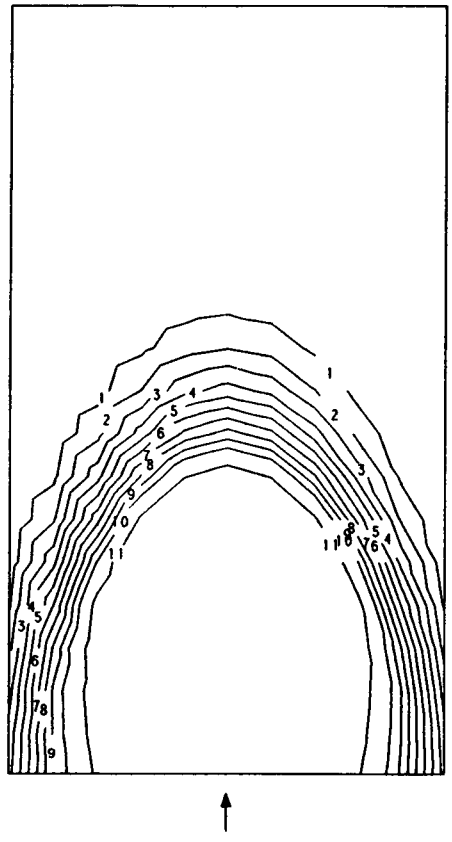

TMS CASE 34-ID JETS, J=6.6, S/HO=0.5, D/HO=0.25, RCI/HO=0.25, AR=3.0

Figure 3-33b. Cross-Stream Theta Contours at Phi = 30 Degrees for Case 34.

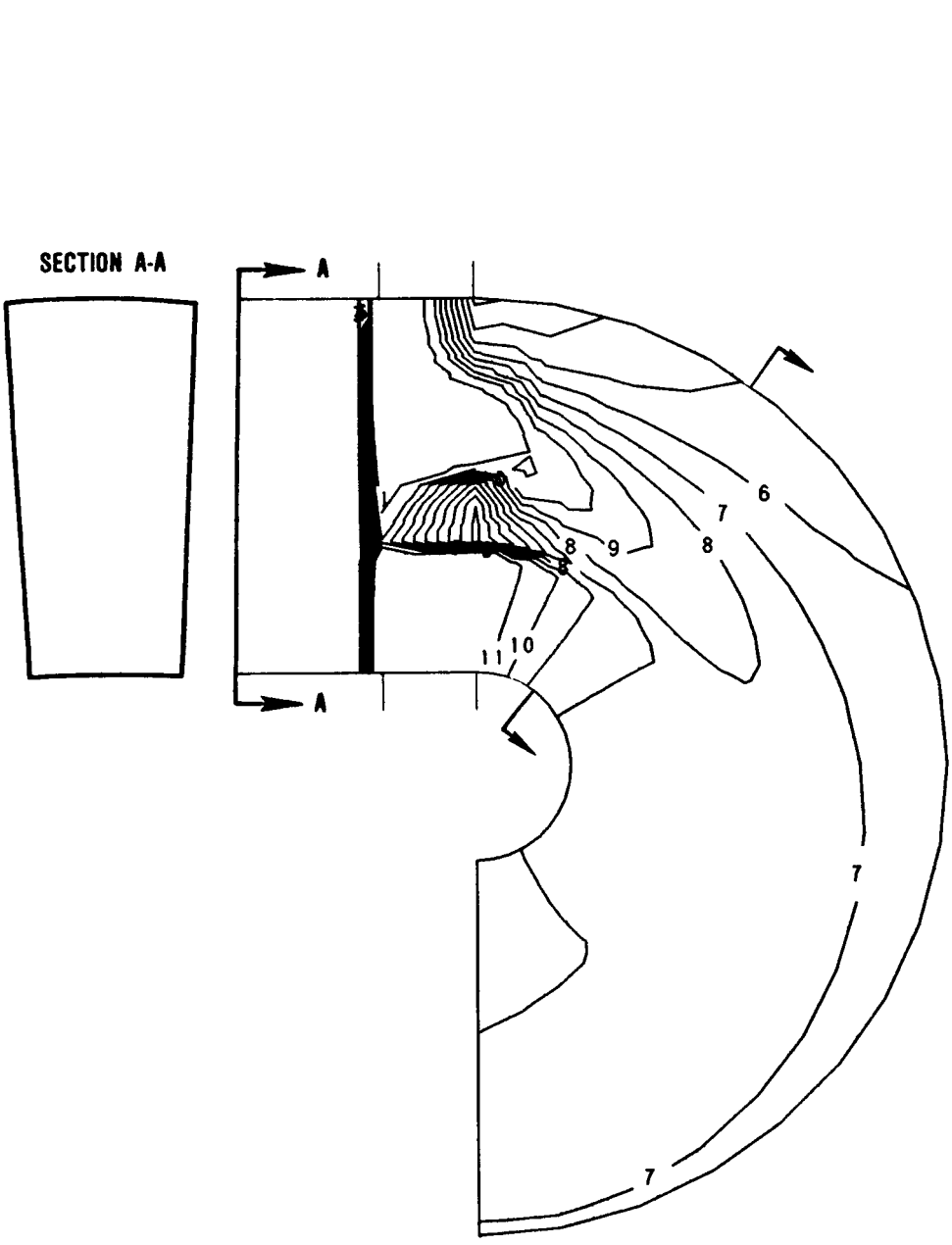

CONTOUR	VALUE
1	0.0500
2	0.1000
3	0.1500
4	0.2000
5	0.2500
6	0.3000
7	0.3500
8	0.4000
9	0.4500
10	0.5000
11	0.6000

TMS CASE 35 OD/ID JETS (INL), J=6.6, S/HO=.5, RCI/HO=.25, D/HO=.25, AR=3.0

Figure 3-34a. Streamwise Theta Contours for Case 35.

CONTOUR	VALUE
1	0.0500
2	0.1000
3	0.1500
4	0.2000
5	0.2500
6	0.3000
7	0.3500
8	0.4000
9	0.4500
10	0.5000
11	0.6000

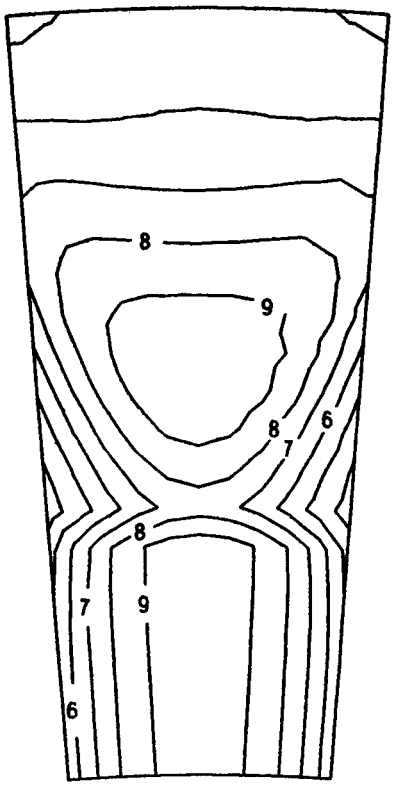

TMS CASE 35-OD/ID JETS (INL), J=6.6, S/HO=.5, D/HO=.25, RCI/HO=.25, AR=3.0

Figure 3-34b. Cross-Stream Theta Contours at Phi = 36 Degrees for Case 35.

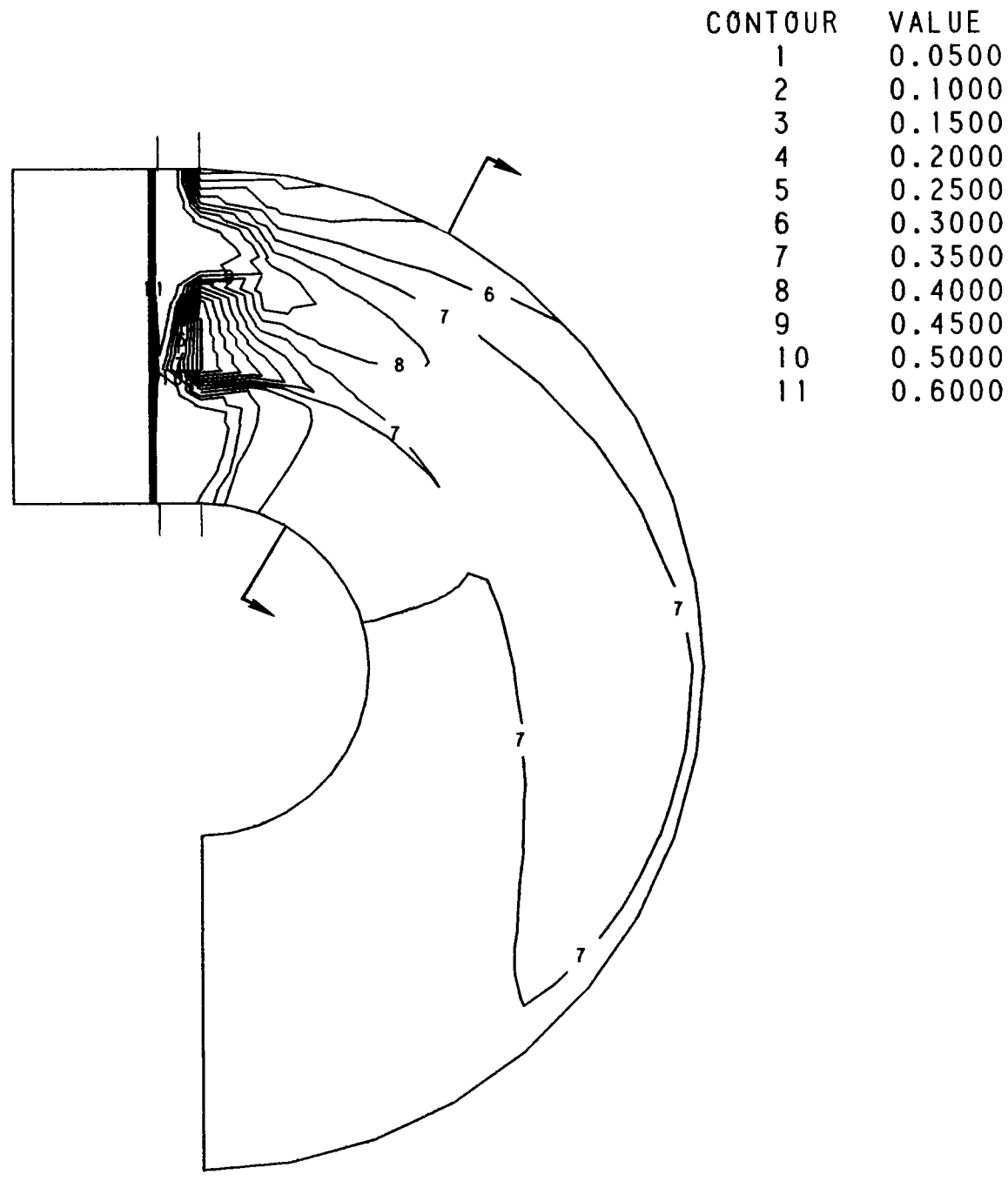

TMS CASE 37-0D/1D JETS(INL), J=26.4, S/H0=.25, D/H0=.125, RC1/H0=.5, AR=1.0

Figure 3-35a. Streamwise Theta Contours for Case 37.

CONTOUR	VALUE
1	0.0500
2	0.1000
3	0.1500
4	0.2000
5	0.2500
6	0.3000
7	0.3500
8	0.4000
9	0.4500
10	0.5000
11	0.6000

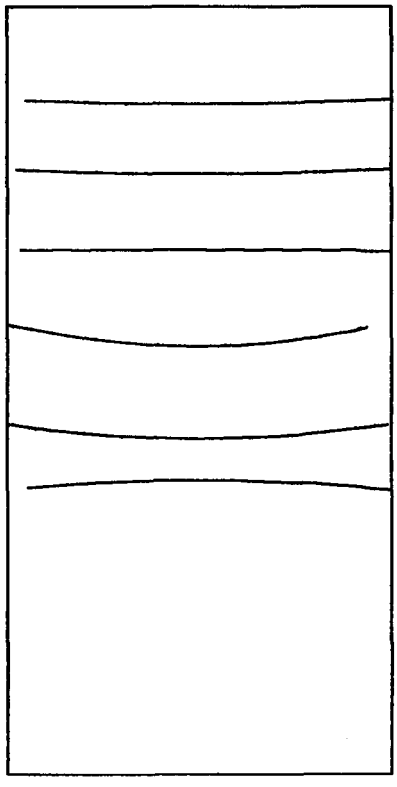

TMS CASE 37-0D/ID JETS(INL), J=26.4, S/H0=.25, D/H0=.125, RC1/H0=.5, AR=1.0

Figure 3-35b. Cross-Stream Theta Contours at Phi = 30 Degrees for Case 37.

CONTOUR	VALUE
1	0.0500
2	0.1000
3	0.1500
4	0.2000
5	0.2500
6	0.3000
7	0.3500
8	0.4000
9	0.4500
10	0.5000
11	0.6000

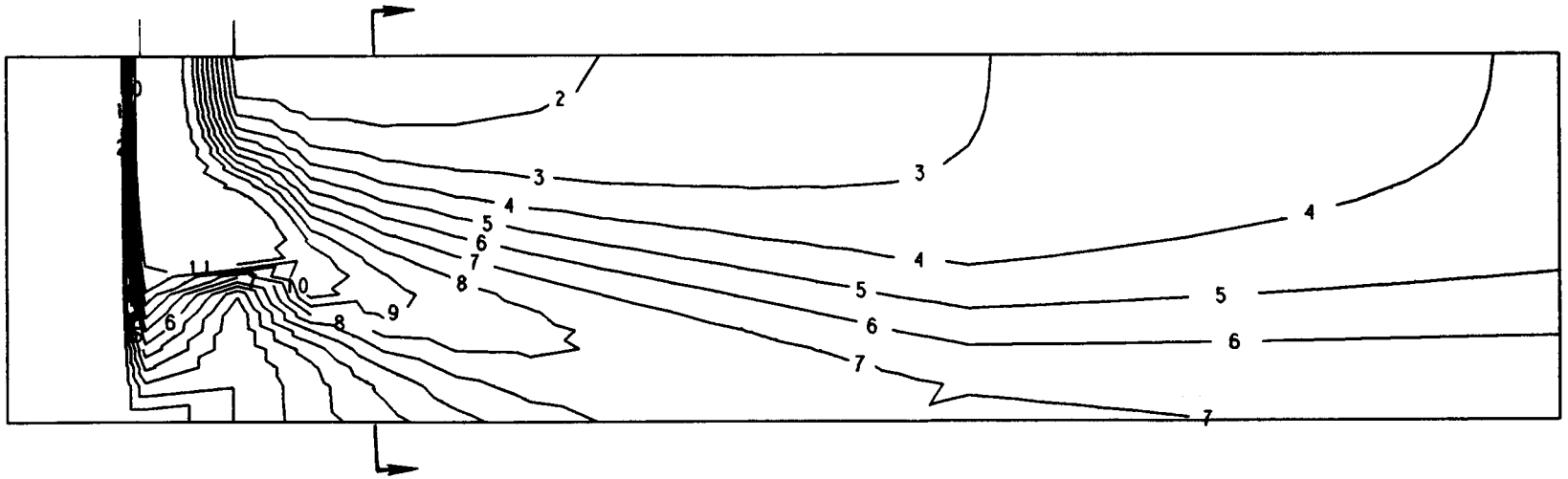

TMS CASE 40-0D JETS (8-IN. CAN), J=26.4, S/H0=1.00, D/H0=.25, AR=1.00

Figure 3-36a. Streamwise Theta Contours for Case 40.

CONTOUR	VALUE
1	0.0500
2	0.1000
3	0.1500
4	0.2000
5	0.2500
6	0.3000
7	0.3500
8	0.4000
9	0.4500
10	0.5000
11	0.6000

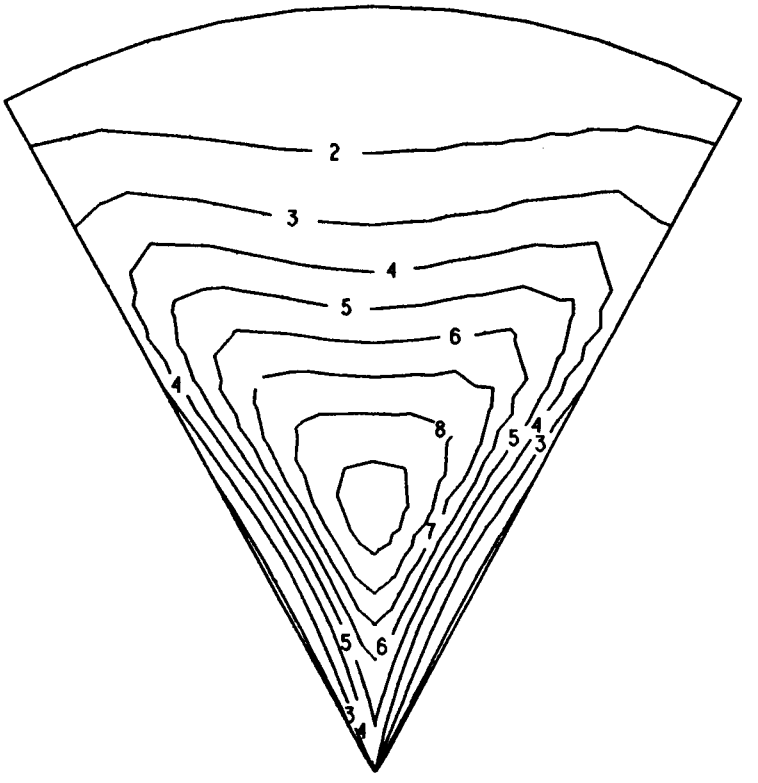

TMS CASE 40-0D JETS (8-IN. CAN), J=26.4, S/H0=1.000, D/H0=.25, AR=1.0

Figure 3-36b. Cross-Stream Theta Contours at x/H_0 = 0.25 for Case 40.

CONTOUR	VALUE
1	0.0500
2	0.1000
3	0.1500
4	0.2000
5	0.2500
6	0.3000
7	0.3500
8	0.4000
9	0.4500
10	0.5000
11	0.6000

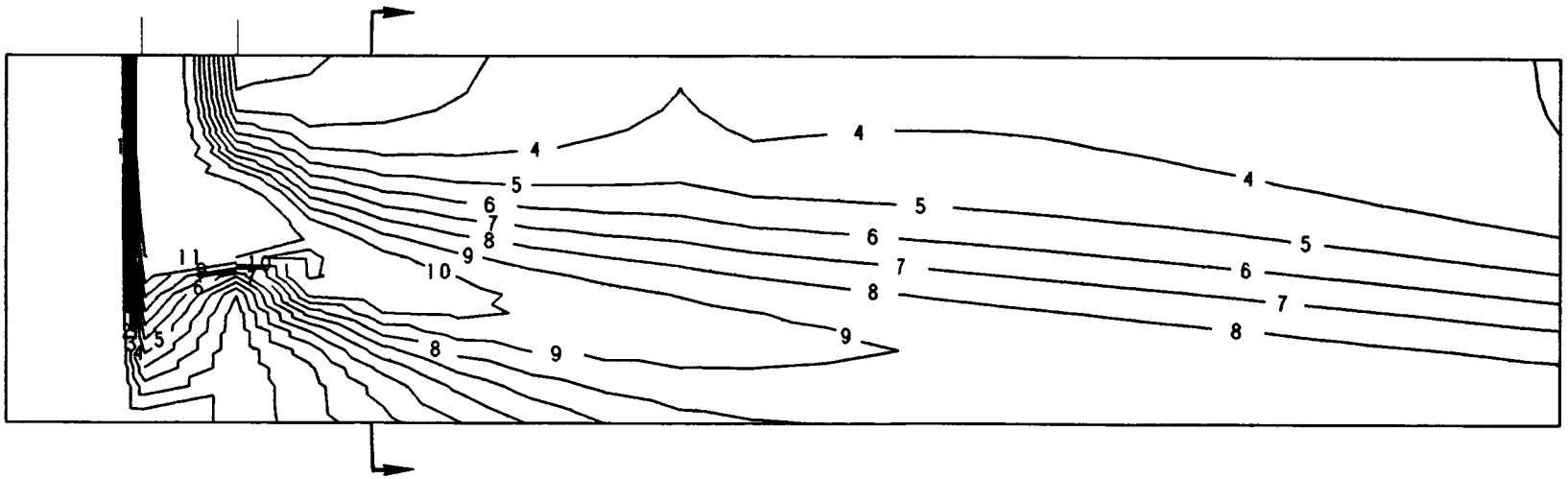

TMS CASE 41-0D JETS (8-IN. CAN), J=26.4, S/H0=0.707, D/H0=0.25, AR=1.0

Figure 3-37a. Streamwise Theta Contours for Case 41.

CONTOUR	VALUE
1	0.0500
2	0.1000
3	0.1500
4	0.2000
5	0.2500
6	0.3000
7	0.3500
8	0.4000
9	0.4500
10	0.5000
11	0.6000

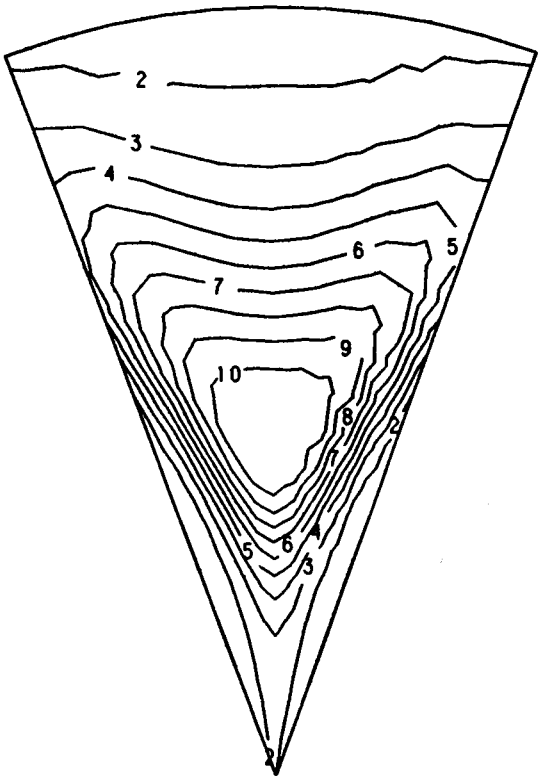

TMS CASE 41 OD JETS (8-IN. CAN), J=26.4, S/HO=.707, D/HO=.25, X/H=.25

Figure 3-37b. Cross-Stream Theta Contours at x/H_0 = 0.25 for Case 41.

CONTOUR	VALUE
1	0.0500
2	0.1000
3	0.1500
4	0.2000
5	0.2500
6	0.3000
7	0.3500
8	0.4000
9	0.4500
10	0.5000
11	0.6000

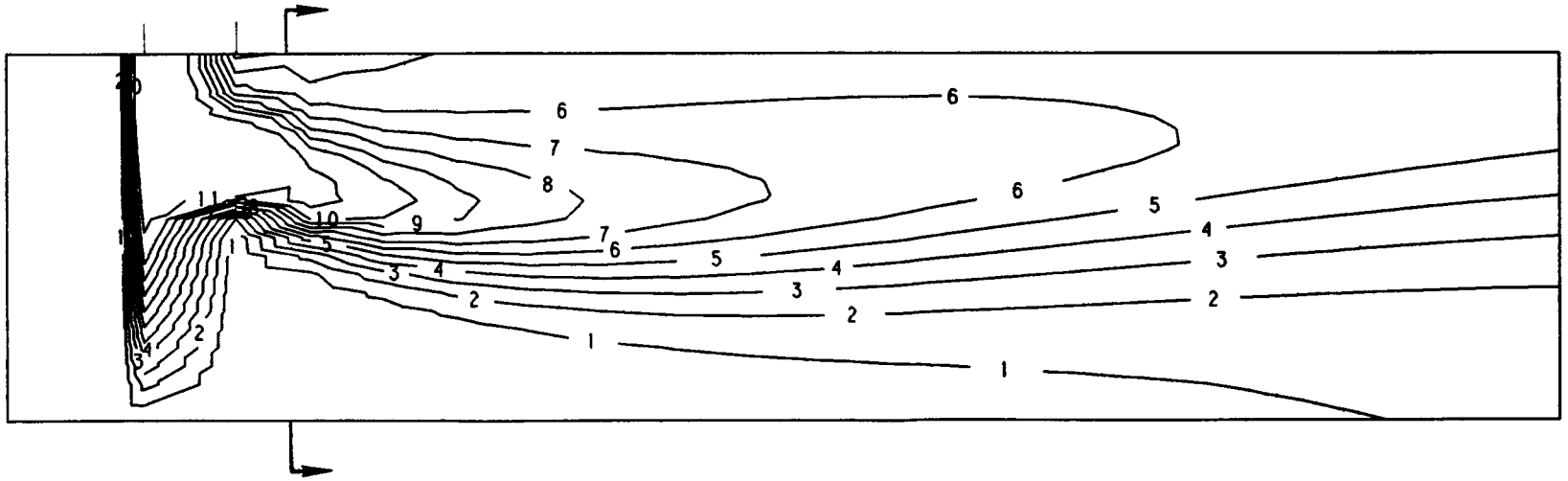

TMS CASE 42-0D JETS (STRAIGHT DUCT), J=6.6, S/H0=0.50, D/H0=.25, AR=1.00

Figure 3-38a. Streamwise Theta Contours for Case 42.

CONTOUR	VALUE
1	0.0500
2	0.1000
3	0.1500
4	0.2000
5	0.2500
6	0.3000
7	0.3500
8	0.4000
9	0.4500
10	0.5000
11	0.6000

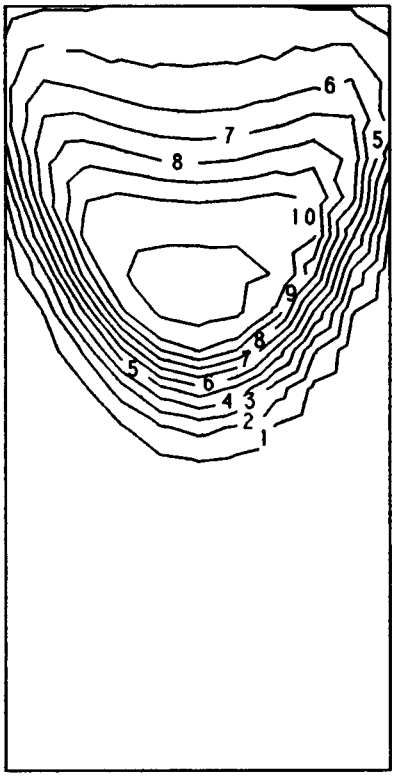

TMS CASE 42-OD JETS (STRAIGHT DUCT), J=6.6, S/HO=0.50, D/HO=.25, AR=1.00

Figure 3-38b. Cross-Stream Theta Contours at x/H_0 = 0.25 for Case 42.

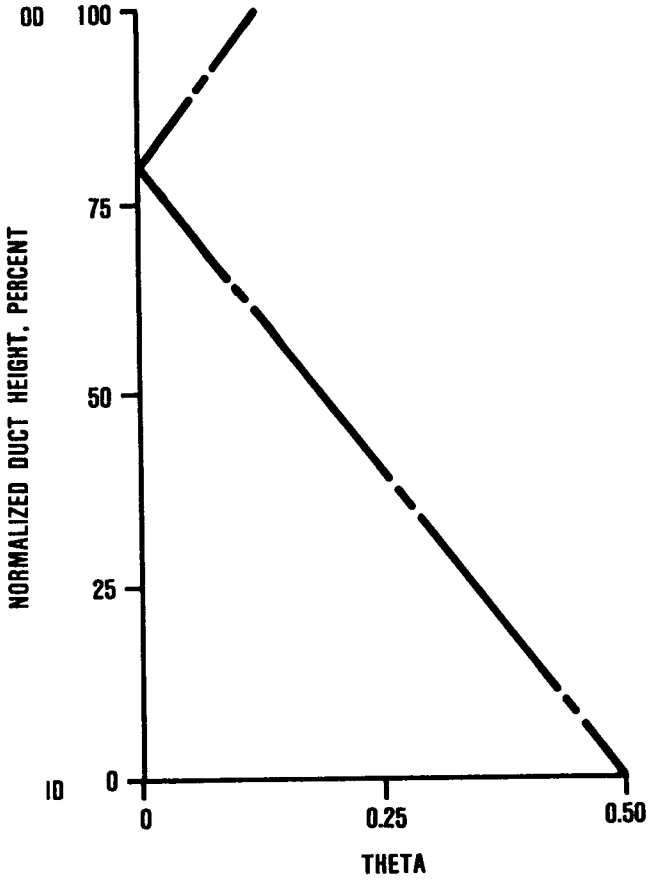

Figure 3-39. Inlet Theta Profile for Cases 14 and 16.

4.0 CONCLUSIONS AND RECOMMENDATIONS

4.1 Conclusions

The empirical model that was developed in the NASA Dilution Jet Mixing Program has been extended to be applicable to turn sections. The results obtained from 3-D numerical model predictions were used as a guide to extend the empirical model. The empirical model predictions were obtained for all the relevant test cases for which the 3-D numerical model results were available. The following conclusions are made from these results:

- Transition liner curvature causes the jets to drift toward the inner wall. The free vortex structure caused by the turn section of transition ducts enhances the entrainment of the mainstream by the jets from the outer wall. The same feature inhibits the entrainment process associated with the inner-wall jets. This interaction produces inner wall jet structures to be different from the familiar kidney shape.

- The optimum relationships between orifice spacing and momentum flux ratio, $(S/H_0)\sqrt{J} = C$, remains unchanged in a turning duct when compared with straight ducts.

- Mixing is not inhibited by convergence, whether the area reduction is achieved in radial or circumferential direction.

- Jet trajectories in a can (or annulus) are similar to those in a rectangular duct for the same values of J and S/H_0 if the orifice spacing is specified at the radius that divides the can (or annulus) into equal areas.

- Jets injected from the inner wall of an annular duct exhibit structures similar to those observed in turn sections.

- The TMS empirical model assumption of mainstream velocity ($V_m = C/r$) produces results that agree well with the 3-D numerical model.

- The TMS empirical model predicts higher mixing rates than the numerical model results. Similar observations were made in Reference 13.

- The TMS empirical model results are expected to be accurate enough as a useful tool in the preliminary design of dilution zones for reverse-flow combustion systems.

4.2 Recommendations

The TMS empirical model is derived from a model based on the experimental data obtained in the NASA Dilution Jet Mixing Program. The empirical model has been shown to provide good correlation with the data for values of parameters within the range of the generating experiments, as shown in Table 4-1. Caution must be exercised when using the model outside of this range. Use of the empirical model in regions close to the jet injection plane ($x/H_0 < 0.25$) is not recommended since the validity of the assumptions used in the model are questionable in regions close to the jet injection location. Furthermore, this model is not valid for predicting the mixing of a single jet in a confined flow or for semi-confined flows (large values of H_0/D or S/D).

Although the TMS empirical model results agree well with those of the 3-D numerical model, they have not been compared with experimental results because of the lack of available test data. Limited validation of the model with data from reverse-flow combustors is recommended.

Table 4-1. Ranges of Flow and Geometric Variables On Which Model Is Based.

Independent Variables	Values
Density ratio, DR	0.5 to 2.2
Momentum flux ratio, J	5 to 105
Orifice spacing, S/H_0	0.125 to 1
Orifice row offset, S_x/H_0	0.25 to 0.5
Orifice aspect ratio	0.36 to 2.8
Orifice diameter, D/H_0	0.0625 to 0.25
Area ratio (exit/inlet)	1 to 1/3
Radius of Curvature in x-r plane, R_{ci}/H_0	0.25 to infinity
Radius of Curvature in r-z plane, R_t/H_0	0.25 to infinity
Variable mainstream θ	0 to 0.5
Derived Variables	
A_j/A_m	0.025 to 0.1
w_j/w_T	0.075 to 0.36
$C = (S/H_0)$ [SQRT (J)]	0.5 to 10

REFERENCES

1. Reynolds, R., and C. White, (1987) Transition Mixing Study Final Report. Garrett 21-5723, Garrett Turbine Engine Company, Phoenix, Arizona, NASA CR-175062.

2. Srinivasan, R., A. Berenfeld, and H.C. Mongia, (1982) Dilution Jet Mixing Program Phase I Report. Garrett 21-4302, Garrett Turbine Engine Company, Phoenix, Arizona, NASA CR-168031.

3. Srinivasan, R., E. Coleman, and K. Johnson, (1984) Dilution Jet Mixing Program Phase II Report. Garrett 21-4804, Garrett Turbine Engine Company, Phoenix, Arizona, NASA CR-1174624.

4. Srinivasan, R., G. Meyers, E. Coleman, and C. White, (1985) Dilution Jet Mixing Phase III Report. Garrett Turbine Engine Company, Phoenix, Arizona, Garrett 21-5418, NASA CR-174884.

5. Zizelman, James (1985) Dilution Jet Configurations in a Reverse Flow Combustor. M.S. Thesis, Case Western Reserve University, Cleveland, Ohio, NASA CR-174888.

6. Lipshitz, and I. Greber, (1984) Dilution Jets In Accelerated Crossflows. Case Western Reserve University, Cleveland, Ohio, NASA CR-174714.

7. Srinivasan, R., R. Reynolds, I. Ball, R. Berry, K. Johnson, and H. Mongia, (1983) Aerothermal Modeling Program: Phase I Final Report - Vol. 2. Garrett 21-4742-2, Garrett Turbine Engine Company, Phoenix, Arizona, NASA CR-168243.

8. Sturgess, Geoffrey J. (1983) Aerothermal Modeling Phase I Final Report. PWA-5907-19, Pratt & Whitney Aircraft, E. Hartford, Conn., NASA CR-168202.

9. Kenworthy, M.J., S.M. Correa, and D.L. Burrus, (1983) Aerothermal Modeling Phase I - Final Report: Volume I - Model Assessment, General Electric Company, Cincinnati, Ohio, NASA CR-168297-Vol-1.

10. Claus, R.W. (1983) Analytical Calculation of a Single Jet in Crossflow and Comparision with Experiment. AIAA Paper 83-0238, NASA TM-83027.

11. Holdeman, J.D., and R.E. Walker, (1977) Mixing of a Row of Jets with a Confined Crossflow. AIAA Journal, Vol. 15, No. 2. pp. 243-249 (see also AIAA Paper 76-48, NASA TM-71821).

12. Wittig, S.L.K., D.M.F. Elbahar, and B.E. Noll, (1984) Temperature Profile Development in Turbulent Mixing of Coolant Jets with a Confined Hot Cross-Flow. Journal of Engineering for Gas Turbines and Power, Vol. 106, p. 193 (see also ASME Paper No. 83-GT-39).

13. Srinivasan, R., and C. White, (1986) Dilution Jet Mixing Supplementary Report. Garrett Turbine Engine Company, Phoenix, Arizona, Garrett 21-5705, NASA CR-175043.

14. Holdeman, J.D., R. Srinivasan, and A. Berenfeld, (1984) Experiments in Dilution Jet Mixing. AIAA Journal, vol. 27, no. 10, pp. 1436-1443 (see also AIAA Paper 83-1201, NASA TM 83457).

15. Holdeman, J.D., R. Srinivasan, E.B. Coleman, G.D. Meyers, and C.D. White, (1987) Effects of Multiple Rows and Non-circular Orifices on Dilution Jet Mixing. J. of Propulsion and Power, vol. 3 no. 2, pp. 219-226 (see also AIAA Paper 85-1104, NASA TM 86996).

16. Holdeman, J.D., and R. Srinivasan, (1986) Modeling Dilution Jet Flowfields. J. Propulsion and Power, vol. 2, no. 1, pp 4-10 (see also AIAA Paper 84-1379, NASA TM 83708).

NOMENCLATURE

C	=	$(S/H_0)\ \sqrt{J}$
C_d	=	Jet discharge coefficient
D	=	Orifice diameter
Dc	=	Offset Spacing
DR	=	Density ratio = (T_m/T_j)
H	=	Local duct height
H_0	=	Duct height at injection plane
J	=	Momentum flux ratio = $(DR)\ (R)^2$
J_{ID}	=	Effective momentum flux ratio for inner wall injections
J_{OD}	=	Effective momentum flux ratio for outer wall injections
n	=	Number of holes around can
r	=	Radial coordinate
R	=	Velocity ratio = (V_j/U_m)
R_{ci}, r_i	=	Inner radius of curvature in x-r plane
R_{co}, r_o	=	Outer wall radius of curvature in the x-r plane
r_c	=	Mid-channel radius of curvature = $(r_i + r_o)/2$
R_t	=	Inner radius of curvature at inlet in r-z plane
S	=	Spacing between orifices
T	=	Temperature
T_j	=	Jet temperature
T_0	=	Mainstream temperature
Theta	=	$(T_m - T)/(T_0 - T_j)$
U_m	=	Inlet mainstream velocity
V_j	=	Jet velocity
x	=	Axial coordinate (0 at orifice centerline)
y	=	Cross stream (radial) coordinate (0 at injection wall)
z	=	Circumferential coordinate (0 at jet centerline)

APPENDIX I

Deviation of equations 30 and 31 in paragraph 2.2.

This appendix presents the deviation of equations 30 and 31 in paragraph 2.2 for the effective momentum flux ratios for inner and outer wall injections.

Let r_i and r_o be the radii of curvature for the inner and outer walls, respectively. Note that r_i= RCI and r_o = RCO, as shown in Figure 3-1. The mean radius, r_c, is given by $r_c = (r_i+r_o)/2$.

The flow in a curved duct develops a free vortex structure caused by flow turning. In such a structure, the local mainstream velocity, V_m, can be expressed in the form $V_m = C/r$, where $C = 2\bar{U}_m/(r_o + r_i)$, and $\bar{U}_m$ is the average velocity in the duct at the jet injection plane. The free vortex structure results in higher mainstream velocity near the inner wall than near the outer wall. The momentum flux ratio, J, of a jet injected into a curved duct becomes:

$$J = \rho_j V_j^2/(\rho_m \bar{U}_m^2) \cdot r^2/r_c^2 \qquad \text{(A-1)}$$

In an equivalent straight duct, the average mainstream velocity, $J_m = V_c$, where V_c is the velocity in the center of the curved duct, and the corresponding momentum flux ratio, J_o, becomes

$$J_o = \rho_j V_j^2/(\rho_m U_m^2) \qquad \text{(A-2)}$$

The effective momentum flux ratio of the outer wall injection, J_{OD}, is defined as the integrated value of Equation (A-1) over the upper half of the duct.

$$\text{Thus, } J_{OD} = \rho_j V_j^2/(\rho_m U_m^2)\ 1/(r_o-r_c) \int_{r_c}^{r_o} r^2 dr/r_c^2 \qquad \text{(A-3)}$$

$$\text{or, } J_{OD} = J_o\ (r_o^3-r_c^3)/[3r_c^2(r_o-r_c)]$$

Simplifying further,

$$J_{OD}/J_O = [r_o^2/r_c^2 + r_o/r_c + 1]/3 \qquad \text{(A-4)}$$

From Figure 3-1, it is seen that at the injection plane,

$$r_o/r_i = 1+H_0/r_i;\ r_c = (r_o+r_i)/2$$

and $r_o/r_c = 2\ (1+H_0/r_i)/(2+H_0/r_i)$

Using these, equation (A-4) is simplified as:

$$J_{OD} = J_O\ [1 + 2\ C_{OD} + 4\ (C_{OD})^2]/3 \qquad \text{(A-5)}$$

where:

$$C_{OD} = (1 + H_0/RCI)/2 + H_0/RCI) \qquad \text{(A-6)}$$

In a similar manner, the effective momentum flux ratio, J_{ID}, is defined as:

$$J_{ID} = \rho_j V_j^2/(\rho_m U_m^2) \cdot 1/(r_c-r_i) \int_{r_i}^{r_c} r^2/r_c^2\ dr \qquad \text{(A-7)}$$

or, $J_{ID} = J_o \cdot (1+r_i/r_c + r_i^2/r_c^2)/3$ (A-8)

Using $r_o/r_i = (1+H_0/r_i)$, and $r_i/r_c = 2/(2+H_0/r_i)$, equation A-8 simplifies to the form:

$$J_{ID} = J_O\ [1 + 2\ C_{ID} + 4\ (C_{ID})^2]/3 \qquad \text{(A-9)}$$

$$C_{ID} = 1/(2 + H_0/RCI) \qquad \text{(A-10)}$$

1. Report No.	2. Government Accession No.	3. Recipient's Catalog No.
NASA CR-182139		

4. Title and Subtitle	5. Report Date
Transition Mixing Study Empirical Model Report	February 1988
	6. Performing Organization Code

7. Author(s)	8. Performing Organization Report No.
R. Srinivasan C. White	Garrett 21-6689
	10. Work Unit No.
9. Performing Organization Name and Address Garrett Engine Division Allied-Signal Aerospace Company P.O. Box 5217 Phoenix, Arizona 85010	11. Contract or Grant No. NAS3-24340
	13. Type of Report and Period Covered 9-86 through 1-88
12. Sponsoring Agency Name and Address National Aeronautics and Space Administration Washington, D.C. 20546	14. Sponsoring Agency Code

15. Supplementary Notes
Project Manager: Dr. J.D. Holdeman
NASA-Lewis Research Center
Cleveland, Ohio

16. Abstract
The empirical model developed in the NASA Dilution Jet Mixing Program has been extended to include the curvature effects of transition liners. This extension is based on the results of 3-D numerical model results generated under this contract.

The empirical model results agree well with the numerical model results for all the test cases evaluated. The empirical model shows faster mixing rates compared to the numerical model. Both models show drift of jets toward the inner wall of a turning duct. The structure of the jets from the inner wall does not exhibit the familiar kidney-shaped structures observed for the outer wall jets or for jets injected in rectangular ducts.

17. Key Words (Suggested by Author(s))	18. Distribution Statement
Combustor Transition-Mixing Computer-Model Empirical-Model	

19. Security Classif. (of this report)	20. Security Classif. (of this page)	21. No. of Pages	22. Price*
Unclassified	Unclassified		

* For sale by the National Technical Information Service, Springfield, Virginia 22161